ASSESSMENT OF RESTRAINED SHRINKAGE CRACKING OF CONCRETE THROUGH ELLIPTICAL RINGS

Department of Civil Engineering

School of Engineering and Design

Brunel University

MARCH 2014

CERTIFICATE OF AUTHORSHIP

"I certify that:

Each and every quotation, diagram or other piece of exposition which is copied from or based upon the work of others has its source clearly acknowledged in the text at the place where it appears.

All practical work has been carried out by me with no more assistance from members of the department than has been specified.

All additional assistance which I have received is indicated and referenced in the report."

DEDICATION

I will like to dedicate this thesis to my dear wife Julia Natacha Oladiran for her unwavering support through the thick times of my study. She has been faithful to a fault, thank you.

I will also want to dedicate this work to my parents Prof and Mrs J.A. Oladiran, my brothers and sisters (Ajibola (Mr and Mrs Oladiran and family), Olayiwola, Olamide and Temilola). I appreciate you all.

ABSTRACT

An elliptical ring test method is presented to replace the circular ring test method for assessing cracking potential of concrete and other cement-based materials under restrained condition. The latter is recommended by both ASTM (American Society of Testing Materials (C1581/C 1581M-09a) and AASHTO (American Association of State Highway and Transportation Officials (PP34–39, 2004) as a standard test method for such purpose. However, there is no research published so far on comparing circular and elliptical ring test for assessing the relative likelihood of cracking of concrete and other cement-based materials as proposed in this study. Besides, ASTM proposes to use thin concrete rings with the wall thickness of 1.5 inches while AASHTO to use thick concrete rings with the wall thickness of 3 inches. The implication of these two ring wall thicknesses has not been well studied. The elliptical ring geometry employed here was used to facilitate unique ways of analysing cracking sensitivity of concrete. In line with this, the test program and numerical model developed was focused on investigating the mechanism of the elliptical ring test, irrespective of the concrete materials used which is also novel in this research as efforts towards this assessment are still yet to be published.

The new experimental method investigated the use of elliptical rings for assessing the potential of concrete cracking under restrained condition to enable a faster and more reliable assessment of cracking tendency of concrete and other cement-based materials. A series of thin and thick elliptical concrete rings were tested alongside circular ones until cracking. Cracking age, position and propagation in various rings were carefully examined. It was found that thin elliptical rings with appropriate geometry can initiate crack quicker than circular ones which is desirable for accelerating the ring test. There were multiple visible cracks that occurred in elliptical rings and some cracks initiated but did not propagate through the ring wall, an interesting finding reported as the first time by this study. The features of multiple cracks in restrained elliptical rings were examined and their impact on interpreting elliptical ring test results was discussed. In addition, in restrained thin concrete rings, cracks initiated at their inner circumference and propagated towards their outer one while cracks initiated at the outer circumference and propagated towards their inner one for thick rings. To explore the mechanism of this new test method, a numerical model was developed to simulate stress development and crack initiation in concrete ring specimens under restrained shrinkage

in which the effect of concrete shrinkage was simulated by an artificial temperature field externally applied on concrete causing the same strain as shrinkage does.

A uniform artificial temperature field across the concrete ring wall generated good results and works well for simulating shrinkage cracking of thin concrete rings while an artificial temperature field with linear gradient across the concrete ring wall should be employed in order to predict cracking behaviour of thick concrete rings under restrained shrinkage reasonably well. Stress developed in concrete rings in the restrained shrinkage test was thus obtained through a combined thermal and structural analysis. Based on the maximum tensile stress cracking criterion, cracking age and position of a series of circular and elliptical, thin and thick rings were obtained from numerical analyses. It was found that numerical results match the experimental results in terms of initial cracking ages and position for a number of circular and elliptical concrete rings subject to restrained shrinkage.

The effects of ring geometry on cracking in concrete were equally investigated by comparing the behaviour of the elliptical and the circular rings under restrained shrinkage. Both experimental and numerical results indicated that the ratio between the major and the minor semi-axes of an elliptical ring emerges as the main factor which affects the maximum circumferential tensile stress in concrete when subjected to restrained shrinkage. Thin elliptical rings with appropriate geometry can enable crack initiating earlier than circular rings, which is able to accelerate the ring test for assessing the potential of cracking of concrete mixtures. On the other hand, thick elliptical concrete rings do not to possess a favourable geometry effect over circular ones in accelerating ring test due to a relatively weaker restraining effect provided by the central steel ring. The results on crack position and stress development in concrete rings based on numerical analysis were examined to further explore the mechanism of the proposed elliptical ring test for assessing cracking potential of concrete. It was also found that the drying direction of the concrete ring has a substantial influence on the cracking age when thin concrete rings are considered.

KEYWORDS

The keywords that will come across ever so often in the course of this study are listed thus, they are:

Concrete; Cracking; Crack Detection; Drying; Finite Element Analyses; Fracture; Geometry; Geometry Effect; Modeling; Numerical Models; Rings; Ring Test; Shrinkage; Stress Concentration; Structural Analysis; Thermal Analysis

ACKNOWLEDGEMENTS

A mighty long way to have come and to realise that it is done, for this reason, it is just right to give unhindered thanks and praise to God Almighty for life, health and strength through it all. I am indeed grateful to all those who have been supportive through this process, hence the acknowledgement.

Special and unreserved thanks to my Supervisor Dr Xiangming Zhou for all of his support both in moral and financial terms, and also for his time and technical support throughout my time of study. I am most grateful for the constant drive you continued to put on me to achieve success, your advice on my work and continuous support in challenging times. Thank you for your contributions to my written work, and your input is highly appreciated. I will also want to give my sincere appreciation to Prof. Mizi Fan for his technical advice, and contribution to my research project. Similarly, I will like to acknowledge the Civil Engineering lab technicians, and express my special thanks to Malcolm Austen for your ever sincere support through the tough times of constructing equipment used for testing for this project and also for your technical assessment of challenging situations. Further thanks go to Chris Alan, Paul Szadorski and Jeremy Edwardson for all their unselfish contributions in all areas of my research.

I will like to give profound thanks and acknowledgement to EPSRC UK for their financial support through my time of study without their support, this achievement would not have been possible And special thanks for the EPSRC Doctoral training account allocation to Brunel University is greatly appreciated.

In the same vein, I will like to give profound thanks and gratitude to my parents Prof and Mrs J A Oladiran for their support in moral and financial terms. I appreciate the prayers offered for my success and your continuous communication through my time of study, you have been very special parents and I am proud of you. Special appreciation to my brother Ajibola Oladiran and wife Tofunmi Oladiran, their children, Seun, Ase and Denzel Oladiran for their continuous support in all areas and for always there to lend a helping hand, I am unreservedly grateful. Likewise, my sincere thanks is extended to my Sisters Olamide Oladiran and

Temilola Oladiran, for their prayers and unending support and also for always keeping in touch, I appreciate you. Special thanks to my brother Olayiwola Oladiran, who was always ready to help out and was also in constant communication, as well as supportive in words and laughter all the way.

I will also like to extend special and unreserved thanks and appreciation to my wife Julia Oladiran for her support, mentally and spiritually, without her unselfish input in all areas, this research would have been a daunting journey altogether, thank you for your strength.

Special thanks to Patrick Aigbomain and Seyed Ghaffer for their contributions in every way to making working situations easier to handle. Very special thanks to Dr Dong Wei for his technical and unending support towards my research all the way. With great regards and gratitude, I want to extend special thanks to my church family in Milton Keynes. Special thanks to Pastor Augustus and Barbara Lawrence and family for their encouragement, still appreciation to Amos and Gloria Onchiri and family. And then again, a special thanks goes to Cathleen Best for her continuous prayers for me and my family. Gratitude and still special thanks goes to Alicia Gage for helping out in reading my thesis and their advice in my writing up phase. To all those that have contributed to my success, I just want to say a big thank you.

Table of contents

LIST OF FIGURES

LIST OF TABLES

LIST OF ABBREVIATIONS

AASTHO	American Association of State Highway and Transportation Officials
ASTM	American Society of Testing Materials
DAS	Data Acquisition System
ECM	Effective Crack Model
EN	European Standard
EDX	Energy-Dispersive X-ray Spectroscopy
FCM	Fictitious Crack Model
ISO	International Organisation for Standardisation
LEFM	Linear elastic fracture model
RB	Restrained at the base
RBE	Restrained at based and end
RE	Restrained at one end
RELIM	International Union of Laboratories and Experts in Construction Materials, Systems and Structures
PCC	Portland Concrete Cement
SCC	Self Consolidating Concrete
SDA	Strong discontinuity approach
SEM	Size Effective Model
TPFM	Two parameter fracture model
USD	United States Dollar
XRD	X-ray Diffraction

FeO	Iron oxide
SiO_2	Silicon dioxide
Al_2O_3	Aluminium oxide
CaO	Calcium oxide
MgO	Magnesium oxide
SO_3	Sulphur trioxide
Na_2O	Sodium oxide
K_2O	Potassium oxide

LIST OF SYMBOLS

$CTOD_c$	Critical tip opening displacement
CMOD	Crack mouth opening displacement
C_i	Initial flexibility
C_u	Unloading flexibility
$K_{IC}s$	Critical stress intensity
E	Modulus of elasticity
S	Span length
b	Depth
t	Thickness of specimen (beam)
a_o	Depth of the notch
P_{max}	Ultimate load
a_c	Critical effective crack length
β_o	Ratio of the length of the Initial crack to the critical effective crack
g (α)	Geometrical function about α
COD	Crack opening displacement
W	Self-weight of beam
f_c	Compressive strength
f_t	Tensile strength
HO	Height of knife edge

CHAPTER 1: INTRODUCTION

1.1 Background of the Research

The complexities of early-age cracking of concrete and other cement-based materials are not yet fully understood. Cracking can lead to premature deterioration, which shortens the service life of concrete structures and present a potential hazard. It is estimated that the total cost of repair, rehabilitation, strengthening, and protection (including waterproofing) of concrete structures in the U.S. alone is between 18 and 21 billion (USD) a year of which at least around 6 to 8 billion (USD) are crack related repairs (Emmons and Sordyl, 2004). Recent advances in rapid construction, high early-strength concrete technology, and new cement and admixture development have renewed worldwide concerns on cracking of concrete. However, the shrinkage induced cracking in concrete is presented as a unique challenge to engineers as many engineering materials do not possess shrinkage as concrete does. The extent of shrinkage is indeed the driving force for early-age cracking of concrete, but whether cracking will occur or not is also dependent on the restraint provided in the structure and the stress relaxation, which may be particularly high in early-age concrete (Bentur and Kovler, 2003).

Early-age cracking of concrete due to restrained shrinkage has been mainly evaluated by qualitative means through a variety of cracking tests, such as the ring, the bar, and the plate/slab tests, among which the ring test has become a standard method as recommended by the American Association of State Highway and Transportation Officials (AASHTO PP34-99(2004) which is a standard for estimating the cracking tendency of concrete and the American Society of Testing Materials (ASTM C1581/C1581M-09a) for quantifying the potential of shrinkage/cracking of concrete and other cement based materials. Over the years, these test methods have been developed to assess how susceptible a given concrete mixture may be to cracking. Although free shrinkage measurements are useful in comparing different mixture proportions, they do not provide sufficient information to determine how concrete will crack in service (Shah et al., 1998). Rather, cracking potential of concrete and other cement-based materials is mainly assessed under restrained condition.

Documented reviews have also been done by researchers (Kraai, 1985; Paillere et al., 1989; Grzybowski and Shah, 1990; Bentur, 1995; and Weiss et al., 1998; Loser and

Leeman, 2008). Some of these studies employed linear specimen geometries (mainly used for uniaxial testing) because of its simplicity in interpreting logged data (Springenschmidt et al., 1985; Kovler 1994, Weiss et al., 1998; Toma et al., 1999; Van Breugel and Lokhorst, 2001; Altoubat and Lange, 2002). The experiments employed in these studies utilised either *passive restraint*, allowing the test frame to provide a restraint, or *active restraint* which used either a hydraulic or electrical actuator to apply a force to counteract the change in length as a result of shrinkage. While the studies that employed active restraint provide complete restraint along with accurate stress and stiffness history, their cost may effectively limit their use in common quality control testing and large-scale parametric evaluations.

On the other hand, studies utilising passive restraint are typically designed to be either too rigid or are too flexible to allow strain development in the steel to be measured, in that they provide information on the state of the stress of the concrete (Hossain, 2004). According to Altoubat and Lange (2002), it has been shown that movements may occur at the end grips that would make it possible to further reduce the stress level in a passive restraint test. Nevertheless, the ring specimen geometry is frequently preferred for quality control testing and material evaluation as the difficulties associated with providing adequate end restraint is now removed as a step to eliminate the limitations posed by previous test methods. In line with this, the restrained circular ring test has become a standard method (AASHTO, PP34–39, 2004) using a ring with an inner diameter of 305mm, around 75mm thickness of concrete wall, a height of 152mm and a 12.7mm ± 0.4mm thickness of steel ring wall with inner and outer surfaces machined smooth, round and true and polished.

Conversely, ASTM have used a standard test method for determining age at cracking and induced tensile stress characteristics of mortar and concrete under restrained shrinkage. They used thin circular ring specimens with a concrete wall thickness of around 37.5mm in order to shorten its ring test duration. These test methods make use of strain gauges which are placed mid-height and equidistant on the inner circumferential surface of the steel ring. The strain is subsequently measured over a specified period and an abrupt jump in the steel strain indicates crack initiation (i.e. the age of cracking), (Grzybowski and Shah, 1990; Krauss et al., 1995). The ring test highlights the relative comparison of concrete materials for the purpose of selecting those with less cracking sensitivity (i.e. cement-based materials that are less likely to crack under restrained shrinkage), and is not intended to determine the age of the cracking of concrete or any specific type of structure, configuration or

exposure. The actual cracking tendency in service depends on many variables, including the type of structure, degree of restraint, rate of property development, construction and curing methods or environmental conditions.

The ring test method can also be used to determine the relative effects of material variations on induced tensile stresses and cracking potential. These variations can include, but not be limited to, aggregate source, aggregate gradation, cement type, cement content, water content, supplementary cementing materials and chemical admixtures. While the ring test methods recommended by AASHTO and ASTM represent a benchmark for continuous testing, since it can be used to compare the age of cracking or crack width that develops in different mixtures, it has some limitations which include a very low cracking sensitivity, and making it very time-consuming, (He et al., 2004). Besides, initial cracking may appear anywhere along the circumference of the ring due to the geometric effect of the circular ring which provides uniform stress throughout this region. Sometimes, a visible crack may not be generated if the restraining core is not stiff enough, which makes it very difficult to detect cracking (He et al., 2004). In retrospect, the bar test was originally used to provide a relatively uniform uniaxial restraint for specimens when they are relatively thin to assess shrinkage cracking of concrete. Albeit, the major disadvantage of this test method is that, specimens will always rupture as a result of dead load because of its vertical positioning (Paillere et al., 1989). Following, the plate test used plate specimens to investigate the behaviour of concrete and the effects of material composition on plastic shrinkage cracking under restraint. The main drawback however, is the inadequate restraint provided on the specimen by the steel plate (Kraai, 1985). Generally, the end condition for the bar test and the difficulty in providing a constant restraint in the plate test, greatly limits their application. Hence, a new, faster and more reliable test method for assessing cracking sensitivity of concrete is greatly needed by academia and industry.

1.2 Research Scope

In this research, a new test method is developed by using elliptical ring specimens to assess the cracking tendency of a concrete mixture and also explore the mechanisms of the elliptical ring test. Compared to circular ring geometries, it is believed that elliptical ring geometries have the ability to generate a higher stress concentration and hence can amount to an increased cracking sensitivity, making the elliptical ring test method less time-consuming and more efficient. Besides, due to the stress concentration, the location of

cracking will be highlighted at predictable positions along the circumference of an elliptical ring specimen, thus making it more detectable, with its propagation also easier to trace. The elliptical ring test is therefore helpful in determining the relative likelihood of the cracking of concrete mixtures in a much shorter period and for aiding in the selection of concrete mixtures that are less likely to crack before they are used for construction projects.

A numerical model is established to provide design engineers with a tool to predict when and where a crack will occur in a concrete elliptical ring specimen under restrained shrinkage. The effects of specimen size/geometry and the degree of restraint on the shrinkage cracking of concrete is explored to provide the guidance required to choose the geometries of both the elliptical concrete ring specimen and the central restraining steel ring for estimating the cracking tendency of concrete in the field. Findings obtained from this project will be subsequently recommended to relevant standard organisations as a possible standard test method, to replace the circular ring test method, for estimating the cracking tendency of concrete mixtures.

In line with this, the test program is focused on investigating the mechanism of the elliptical ring test, without emphasis on the concrete materials used. Rather a normal strength formulation is adopted for all circular and elliptical, thin and thick concrete rings tested in this project. It is therefore necessary to quantify how the geometry or shape of the central steel ring changes the degree of restraint to the concrete surrounding it, and consequently its cracking age during the ring test. This is achieved by testing a series of circular and elliptical concrete rings, thin and thick with different geometries in parallel, which are subjected to the same curing environment, under restrained shrinkage. A series of circular and elliptical concrete ring specimens, with nominal ring thickness of 37.5mm and 75mm denoted as thin and thick respectively, and a height of 75mm will be made for experimental purpose. One thing that is worthy of noting here is that the two concrete ring thicknesses aforesaid were selected deliberately to be consistent with the AASHTO and ASTM recommendations with the former adopting thick rings with the concrete ring wall thickness of 3 inches (75mm) and the latter thin rings with the concrete ring wall thickness of 1.5 inches (37.5mm). Both ring thickness adopted are assembled with the restraining cores and outer moulds made of stainless steel and wood respectively, which are much stiffer than hardening concrete. In addition, the steel ring annulus used was 12.5mm to

assess how the steel core by providing restraint to shrinking concrete can influence the cracking behaviour, by age and position, of the concrete surrounding it.

Moreover, it is believed that the thickness of a concrete ring wall has a significant effect on the stress development in concrete under restrained shrinkage. AASHTO (PP34–99) recommends thick rings with a concrete wall thickness of 3 inches (75mm) while ASTM C1581/C1581M-09a recommends thin rings with a concrete wall thickness of 1.5 inches (37.5mm). Therefore, it is valuable to investigate and evaluate how the elliptical ring may exhibit different cracking behaviours in thick ring specimens as compared to thin ring specimens (AASHTO, PP34-99 and ASTM C1581/C1581M-09a) which may yield different results in assessing the cracking potential of concrete under restraint.

Experiments have indicated that thicker concrete sections exhibited higher resistance to cracking than thinner ones, which suggests that the age of the cracking of concrete is different in structures of different thicknesses (Weiss, 1999). This implies that thin concrete rings may exhibit different cracking behaviour from thick ones made of the same concrete formulation under the same restrained condition. Due to the increase in wall thickness, a complex stress field appears across the wall thickness of a concrete ring specimen during the drying process, from the outer circumferential cylindrical surface. It is believed that the assumption that shrinkage strain, and thus the resulting stress, is uniform across the ring wall adopted for analysing thin rings may not be appropriate for analysing thick rings. Besides, experiments have indicated that cracks initiate at the outer circumference and propagate toward to the inner circumference in thick rings when drying from their outer circumferential surface in restrained shrinkage tests (Hossain, 2004), while on the contrary, a crack would initiate at the inner circumference of a thin ring and propagate toward the outer circumference if based on the assumption of uniform strain across the ring wall. In order to characterise stress development with the consideration of the effect of ring geometry and drying direction, analytical models were developed to assess residual stress in restrained ring specimens (Moon and Weiss, 2006; Moon et al., 2006; Hossain and Weiss, 2006; Weiss, 1999; Hossain, 2004). But it should be noted that those analytical models were developed and suited for circular ring specimens only rather than for elliptical ones. Subsequently, the influence of the drying direction was also considered (i.e. sealed concrete rings at the top and bottom, leaving the circumferential surface exposed to drying, was compared to sealed concrete rings at the outer

circumferential surface with the top and bottom exposed to drying) and the effect on its crack age presented.

In line with this, numerical analysis is used in this study to simulate cracking behaviour of concrete in restrained ring specimens drying from their outer circumferential cylindrical surface, which agrees with the exposure condition in the ring tests recommended by AASHTO and ASTM.

Generally, mechanical properties of concrete are more difficult to be measured at early ages compared to later ages, because they are so often continuously changing during the course of the physical measurement. So understanding the development of mechanical properties during this early age of concrete maturity is a key to fundamental materials science-based prediction of early age cracking (Grasley et al., 2005 and Lura, (2003). These time-dependent material test results are significant to the numerical model developed in this research. The following mechanical tests were performed to provide time-dependent material parameters for hardening concrete; in addition restrained shrinkage test is was carried out alongside. These include:

(1) Compressive and tensile strengths which were evaluated using 100mm×200mm cylinders at five different ages (1, 3, 7, 14, and 28 days), by using a VJT6000 concrete compression machine conforming to the relevant EN standards.

(2) Fracture properties which were tested following a fracture model (i.e. two-parameter fracture model- (TPFM) proposed by Jenq and Shah (1985), which was developed to account for pre-critical crack growth for cement-based materials using an Instron 5580 series testing system. Notched beam specimens, 100mm×100mm×500mm, with notch lengths of one-third the specimen depth were tested at five different ages (1, 3, 7, 14, and 28 days). The specimens were loaded using crack mouth opening displacement (CMOD) control with a rate of 0.0075 mm/min; The elastic Modulus was evaluated from results of fracture testing;

(3) Free shrinkage was tested in accordance with ISO 1920-8 on a series of 285mm-long prismatic specimens with 75 mm^2 cross section by a shrinkage measuring device (55-C0115/3, Controls) for a period of 28 days.

(4) Restrained shrinkage test was performed by using the circular and elliptical ring specimens proposed in this study.

A combined thermo-mechanical 3-D numerical model, based on the ANSYS FE code, were developed for predicting early-age shrinkage cracking initiation, in a series of circular and elliptical concrete rings with various geometries. The numerical model took into account the effects of restraint from central restraining steel core, and the development of strength, and stiffness, and of hardening concrete with time. Thermo analysis will be performed first, which generates 'temperature-load' as the input for mechanical analysis. The mechanical analysis will predict the position and time of the first major cracking in the elliptical ring test. The ANSYS code both allows a smooth transfer of elements and mesh from thermo to mechanical analyses. Finally, the numerical model will be calibrated by experimental results obtained. Once it is verified, parametric studies will be carried out to:

1. Investigate the effect of ring geometry, drying direction, restraining stiffness and how these factors influence cracking age and cracking position.

2. Further explore the mechanism of the proposed elliptical ring test for assessing the cracking potential of concrete, which can lead to the recommendation of choosing an appropriate concrete and steel ring geometry for simulation of restrained concrete in the field (i.e. in service).

1.3 Research Objectives

In this research project, the elliptical ring test will be investigated for assessing concrete cracking due to restrained shrinkage at early ages. It is expected that, due to stress concentration which is ascribed to the elliptical shape of the specimen and restraint, the position of initial cracking can be predicted, making it much easier for detecting cracking. Besides, the first major cracking is expected to appear earlier than that in the traditional circular ring test, enabling it to be a faster method for assessing the cracking sensitivity of concrete and other cement-based materials. As a result, this study underscores these specific objectives which are:

- To investigate the appropriateness of using elliptical ring specimens in assessing the cracking potential of concrete and other cement-based materials under restrained condition.
- To develop and verify a numerical model to predict the position and time of initial cracking in elliptical concrete ring specimens, in a restrained shrinkage test.

- To investigate the effects of ring geometry, degree of restraint, drying direction on cracking of concrete in restrained rings, to provide guidance on choosing ring geometry, and using the elliptical ring test in assessing the cracking of concrete in service.

1.4 Research Significance

This research presents an inclusive study in developing a faster and more reliable test method by using elliptical ring specimens for assessing the cracking potential of concrete and other cement-based materials under restrained shrinkage, by comparing this with the conventional circular ring test methods described in ASTM C1581/C1581M-09a and AASHTO PP34–99. Elliptical ring specimens with various geometries, as well as circular ring specimens, will be tested under different drying techniques. The initial cracking age and position of concrete, as well as the cracking features in various circular and elliptical ring specimens observed from the experiment will be extensively discussed.

The new elliptical ring test method is to overcome the main drawbacks, such as time consumption, of the circular ring test, in assessing the likelihood of the cracking of concrete and other cement-based materials. Besides, due to geometry effect, the first cracking is likely to be concentrated at certain positions on elliptical concrete rings so that resources required for detecting their cracking initiation and propagation in ring specimens can be largely reduced. The effects of elliptical ring geometry on the initial cracking age and position of concrete will be investigated in order to recommend the best elliptical ring geometry for assessing the cracking tendency of concrete and other cement-based materials. Retrospectively, the disadvantages outlined for the circular rings have paved the way for an innovative method of assessing restrained shrinkage cracking by using the elliptical rings. The experimental efforts employed in this research will therefore underpin the performance and mechanism of the elliptical ring test. Hence in a bid to achieve this fit, a series of elliptical rings will be tested in parallel with the circular rings. And then again, it is not clear where crack initiates, whether from the inner surface to the outside of the concrete ring specimen or from the outer surface to the inner surface. By carrying out this research, the ring test will clearly demonstrate at what position crack will initiate and subsequently propagate whether it is from the inner or outer surface. Thus, the ring test employed herein will parallel those recommended by AASTHO (for thick rings) and ASTM (for thin rings). As this comparison has not been investigated with elliptical ring

geometries before, this research will probe further the generation of different cracking potential for concrete when using thin and thick ring specimens. In line with this, a study is carried out to investigate the size of the restraining steel ring, in this case 12.5mm; observations will be made on how this steel ring size will affect cracking age of concrete. At this juncture, a numerical model will be developed to simulate the abovementioned ring test with verification made possible by the series of test results obtained. A significant part of this research is carrying out a parametric study by using the numerical model to analyse several other rings specimens in order to further investigate the mechanism of the elliptical ring test, as testing several samples physically in the lab at the same time will be challenging to carry out given the time frame for the project. This study will help provide a base understanding on the mechanism of the elliptical ring test and hence a recommendation can be made by choosing geometries of concrete and steel elliptical rings for assessing cracking potential of concrete. In conclusion, the overall goal of this research is to suggest elliptical ring geometries for faster and more reliable assessment of the cracking tendency of concrete under a restrained condition in the field.

1.5 Organisation of Contents

Chapter 2 provides a review of the existing literature dealing with assessing early-age shrinkage cracking mainly test methods with a focus on AASHTO and ASTM circular ring test as well as relevant analytical/numerical models for analysing circular rings under restrained shrinkage. The typical behaviour of restrained concrete and shrinkage cracking is also presented. A review of the shrinkage mechanism is provided. Furthermore, a brief description of concrete fracture mechanics is provided.

Chapter 3 provides a general description of the typical material properties and various test methods used in this investigation. Details of the testing procedures, material composition, and experimental results are also presented. The early-age time dependent engineering properties of the concrete used in this study are also presented.

Chapter 4 explores the use of thin elliptical rings by experimental procedure to assess the cracking potential of concrete in a restrained ring test, the effect of ring geometry considering the concrete wall thickness on the cracking behaviour of ring specimens under restrained shrinkage.

Chapter 5 follows up Chapter 4 that presents a numerical model developed for predicting stress and the cracking initiation in thin concrete ring specimens with the wall thickness of 37.5mm and subjected to restrained shrinkage. The use of the proposed method will involve free shrinkage tests to be carried out to obtain the time-dependent relationship between fictitious temperature drop, which represents the effect of concrete shrinkage, and the exposed drying surface area-to-volume ratio of a concrete element. A constant temperature profile across a thin concrete ring wall is assumed in this mode. The numerical model will be verified using the experimental results of the circular and elliptical thin concrete rings tested and discussed in Chapter 4. The proposed method will then be applied to simulate the evolution of maximum circumferential tensile stress in circular and elliptical ring specimens, respectively.

Chapter 6 investigates stresses in thick elliptical ring specimens with wall thickness of 75mm, by introducing artificial temperature fields to represent the mechanical effect of the shrinkage of concrete, for predicting stress development and cracking initiation in thick concrete rings, subject to restrained shrinkage. Different temperature fields will be derived to take into account the effect of concrete wall thickness on moisture gradient, thus shrinkage strain, across a ring wall. The numerical model will be verified using the experimental results of circular and elliptical thin concrete rings tested and then be used for simulating the evolution of maximum circumferential tensile stress in thick rings to further explore the mechanism of the elliptical ring test.

Chapter 7 contains the summary and points out future research. Conclusively, this chapter will point out how the restrained ring test can be made more useful so that it provides valuable information using the numerical model developed in this research. On this platform, further research can then be carried out on material and geometry variation.

CHAPTER 2: LITERATURE REVIEW

This chapter provides a summary of the main investigations carried out so far by other researchers on assessing cracking of concrete and other cement-based materials under restrained condition including experimental, theoretical and numerical approaches. Cracking potential of concrete and other cement-based materials under restrained condition depend on many factors such as, shrinkage, mechanical properties and fracture resistance of concrete as well as restrained conditions enforced on concrete. The chapter reviews previous work within the scope of this topic that has been carried out by various researchers.

2.1 Introduction

Shrinkage is a reduction of volume of concrete which is mainly caused by losing moisture from a concrete member. Water is lost either through evaporation (i.e. drying shrinkage) or internal reactions (i.e. autogenous shrinkage), and consequently concrete volume decreases with age. Tensile stresses are generated if decreasing in concrete volume is restrained. These stresses pull the cement paste closer together which registers as a volume reduction. During early ages, shrinkage is even more critical to concrete since the strength of concrete is considered to be low. Even the smallest tensile stress during early ages can have large resulting shrinkage strains (Holt 2001). The exact definition of "early age" changes depends on the context and time frame of the measurements. Still according to Holt (2001) early-age shrinkage is defined as the volume changes occurring immediately after placing concrete up to the age of about 24hours. This includes the time when the concrete is fluid or liquid, then the transition period when it undergoes early stiffening by the information of a skeletal frame, and finally the initial hardening when the concrete is rigid and the formworks can be removed. Concrete shrinks when it is subjected to a drying environment. Shrinkage in restrained concrete elements develops tensile stresses, and since concrete has a low tensile strength, the development of even small tensile stresses due to shrinkage may often result in cracking within restrained concrete members. Cracking reduces load carrying capacity of concrete members, results in corrosion of steel reinforcement, increase the probability of alkali silica reaction and sulphate attack, and causes other durability problems, resulting in increased maintenance cost and reduced service-life. For decades, efforts have been made in concrete science and engineering community for appropriate methods to assess the susceptibility of a concrete element to cracking.

2.2 Shrinkage

According to Kovler and Zhutovsky (2006), shrinkage of concrete is the time-dependent strain measured in an unloaded and unrestrained specimen at constant temperature. Shrinkage is usually measured by monitoring the longitudinal strain on standard concrete prisms. When the tensile stresses due to restrained volume contraction exceed the tensile strength of concrete, the shrinkage leads to cracking which is referred to as shrinkage cracking. Shrinkage can be classified based on the causes of volume change and state of concrete. The volume of concrete change have become an unavoidable phenomenon resulting from the materials drying in their exposed environment as well as their autogenous, or internal, reactions. Shrinkage is most often evaluated over a long time period of months or years, though recent observations have also focused on early age or plastic drying problem. Meanwhile, this problem aforementioned has hindered comprehensive physical testing and understanding of factors influencing plastic shrinkage (Holt 2000). Furthermore, the driving forces affecting early-age shrinkage can be strongly influenced not only by material properties but also by concrete's surrounding environment. For both autogenous and drying cases however, the environment should be monitored to account for shrinkage variations due to temperature, wind and relative humidity. Although, when drying is considered, all these factors mentioned can severely alter the amount of water evaporating from the concrete surface and thus the ultimate shrinkage amount (Holt 2001). In practice, long-term shrinkage has been measured by using standardised prismatic specimens as a length change over a time period; some of such substantiated test methods are; Standard test method for length change of hardened hydraulic-cement mortar and concrete (ASTM C157) and Measurement of shrinkage and swelling in concrete (RELIM CPC 9). In addition, the duration of shrinkage is dependent on the concrete's size and its shape since these two factors literally controls the rate of moisture loss. In conventional terms, they are often considered and known together as surface area-to-volume ratio (A/V). Still, larger specimens will shrink for longer periods but the ultimate magnitude may be lower (Mindess and Young 1981). According to their investigation, they compared a T-beam to a solid beam with a different A/V. If both beams have the same widths and heights, the T-beam will dry more rapidly and will exhibit slightly less ultimate shrinkage since it has a lower A/V. The faster drying is however attributed to the shorter diffusion path for water to travel to reach an equivalent humidity through the cross section. From

results, it was concluded that a high volume-to-surface ratio will usually result in lower shrinkage magnitude (Mindess and Young 1981); this is illustrated in Figure 2.1.

Similarly, in situations such as curing conditions and rapid drying, the first day's shrinkage can easily exceed the long-term measurements after day 1. As shown in Figure 2.2, the illustration highlights various environmental conditions beyond the first day. It was observed that the long-term shrinkage due to drying was equivalent in all cases, although readings from the first day (1^{st}) showed a significant change in the magnitude of "total shrinkage" and hence affect the cracking expected. (Holt 2001). In the next sub-sections, thermal expansion and carbonation will be briefly addressed in relation to early-age shrinkage, before getting into more details on the mechanisms of drying and autogenous shrinkage.

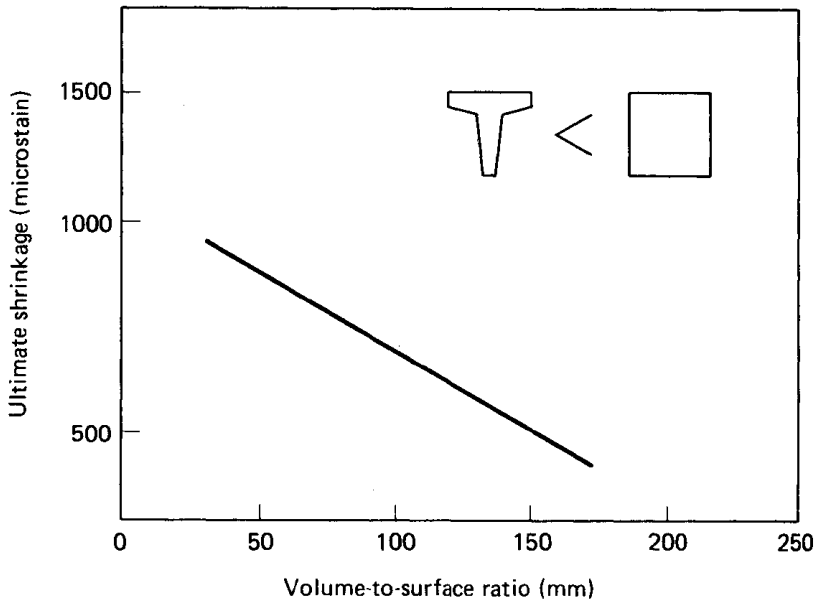

Figure 2.1—Effect of volume-to-surface ratio and the drying shrinkage of concrete (Mindess & Young 1981)

2.2.1 Thermal Dilation

Thermal dilation refers to the volume changes that occur when concrete undergoes temperature fluctuations (Hedlund 1996; and Holt 2001). It is often referred to as thermal expansion i.e. the portion resulting when the concrete temperature is rising. Dilation can occur due to heating or cooling, in both the early and late ages. When the temperature is increasing, the concrete will expand, followed by contraction with cooling.

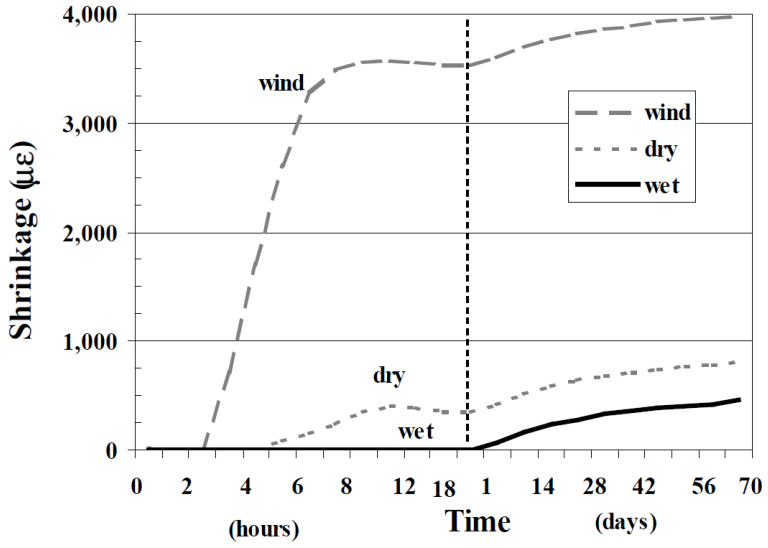

Figure 2.2—Accumulation of early age and long term shrinkage, with various curing environments during the first day; Wind = 2 m/s (4.5 mph), dry = 40% RH, wet = 100% RH . (Holt 2001)

Thermal expansion causes problems when the rate of temperature change is too severe and when gradients exists over the concrete's cross-section. During early ages, the concrete temperature is changing due to cement hydration. As a general rule, this early heat of hydration is about 5 to 8°C (10-15°F) of adiabatic temperature rise per 45kg of cement. (Kosmatka and Panarese, 1988). The argument followed that a mortar mixture will have much higher amount of heat generated compared to concrete mixture since it is richer in cement. The heat rise typically occurs in the first 12 hours as long as no extreme retarding conditions exist. The next stage where the concrete is cooling results in contraction or shrinkage. It was observed that some of the thermal expansion is elastic since the concrete will return to its original dimensions upon cooling. But any non-elastic portion will result in early age shrinkage (Holt 2001). The gradient resulting from the uneven temperatures will cause strains and may result in cracking. During the early ages, differential temperatures within the concrete specimen cause thermal strains as the exterior surface will have a different temperature (due to environmental exchanges) than the interior. The gradient develops when temperature equilibrium cannot be reached, thus generating stresses if concrete is restrained and risking cracking. This becomes even more of a risk with massive concrete structures (i.e. >1 meter thick) since it takes much longer to obtain a temperature equilibrium. Each concrete has a "thermal dilation coefficient" which is dependent on the individual material properties (such as aggregate and w/c). During early

ages, thermal dilation coefficient changes very rapidly as the concrete gains strength (Hedlund 1996). In this research, Hedlund provided early-age measurements of thermal coefficients of concrete with time, illustrated in Figure 2.3. Measurements showed that thermal dilation coefficient reaches a platform of approximately 12με/°C (i.e. 12 $\times 10^{-6}$/°C) after 24 hours. Thermal expansions can be a problem if the concrete is restrained in any manner and there is no space for the volume change to occur, such as a large restrained slab without joints (Mehta and Monterio 1993).

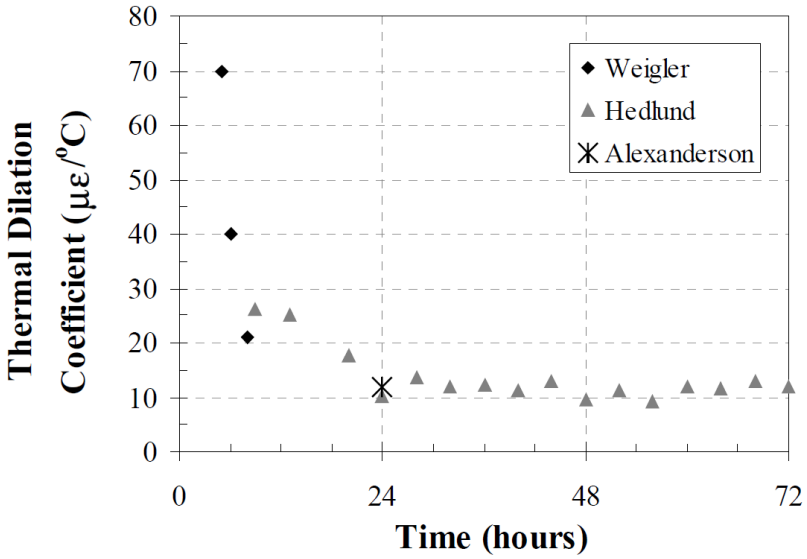

Figure 2.3—Early age thermal dilation coefficients for concrete (Hedlund 1996)

2.2.2 Drying Shrinkage

Drying shrinkage refers to the reduction in concrete volume resulting from a loss of water from concrete (Ropke 1982). As water is lost, the concrete will shrink. Initially, free water escapes to the concrete surface as bleed water, as the heavier aggregate particles settle. This bleed water can evapourate off the surface to the surrounding environment (Holt 2001). Once the bleed water has disappeared, the concrete will still be subjected to drying and excess water will be pulled from the interior of the shrinkage mass.

The most common situation resulting from drying shrinkage at early ages is the appearance of surface cracking (Mindess & Young, 1981). There can also be a problem with internal

stresses or cracking due to water suction into the framework and/or sub-base material. However, according to Hewlett (1998), a finer microstructure can also result from altering the concrete ingredients, such as including silica fume. In effect, silica fume, or microsilica, refines the pore structure by subdividing the larger pores but maintaining nearly the same total pore volume.

On the other hand, Koenders (1997) demonstrated that when drying of concrete is concerned, the larger pores are the first to lose their internal water as seen in Figure 2.4. During drying of fresh concrete, the evaporation rate can exceed the amount of bleed water rising to the concrete surface (Holt 2001). With further observation, it was seen that the free surface from which extra water is lost will then migrate into the concrete body as evaporation continues. The loss of internal water through the concrete surface is the main cause of the drying shrinkage. Janz (2000), discussed further by combining both Laplace and Kelvin's equations to show the relationship between the relative humidity and the pressure which is depicted in Figure 2.5. In this case, the pressure drastically increases with a decrease in humidity, pointing out how useful this is in the understanding of how a change in internal humidity of the concrete will create greater stresses within the system. It is these stresses however, that subsequently lead to the eventual shrinkage. On the other hand, Mehta (1994) states that drying shrinkage tends to increase when admixtures that increase water requirement of a mix are used. However, drying shrinkage is not reduced by using water-reducing admixtures that reduce the water content. Brooks and Neville (1992) reported that shrinkage has been found to increase by 10 to 20% with the use of superplaticisers. Air entrainment is also believed to have no influence on shrinkage (Neville 1996).

2.2.3 Autogenous Shrinkage

Autogenous shrinkage of cement paste and concrete is defined as the macroscopic volume change occurring with no moisture transferred to the exterior surrounding environment (Japan 1999); it is a result of chemical shrinkage affiliated with the hydration of cement particles. A graphic depiction of a sealed concrete's composition change due to the cement hydration reactions is shown in (Figure 2.6). The bar graph relates how the autogenous shrinkage is a portion of chemical shrinkage. While chemical shrinkage is an internal volume reduction, the autogenous shrinkage is an external volume change. It is therefore

possible to measure autogenous shrinkage as a linear change on a concrete slab or other similar arrangement.

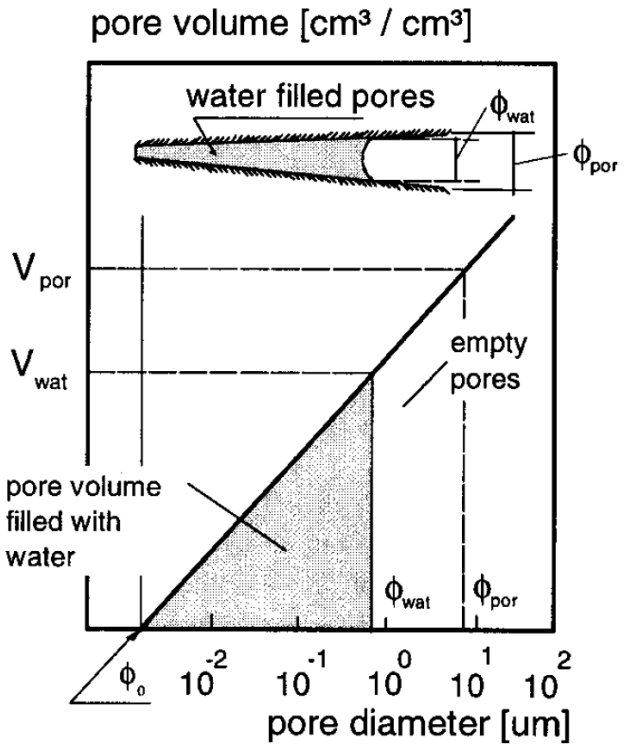

Figure 2.4—Schematic representation of the pore size distribution with emphasis on the state of the pore water within the total pore volume (Koenders 1997)

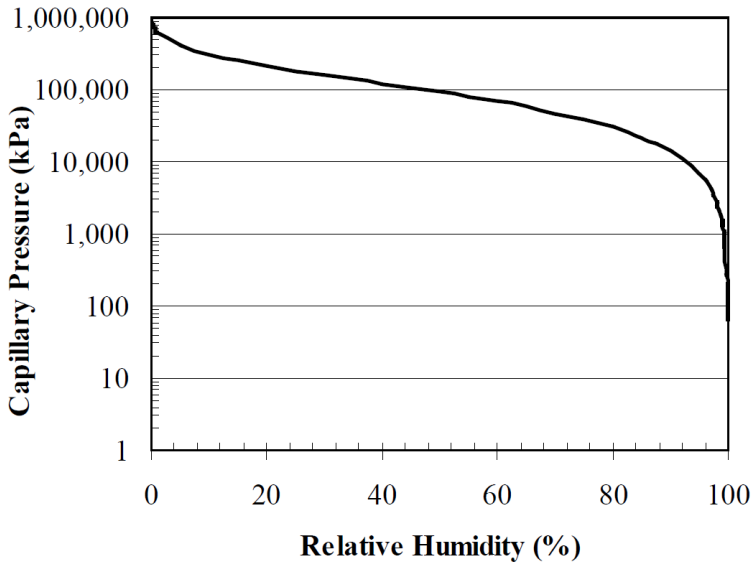

Figure 2.5—Relationship of relative humidity and pressure (suction) based on the combination of Laplace and Kelvin equations (Janz 2000)

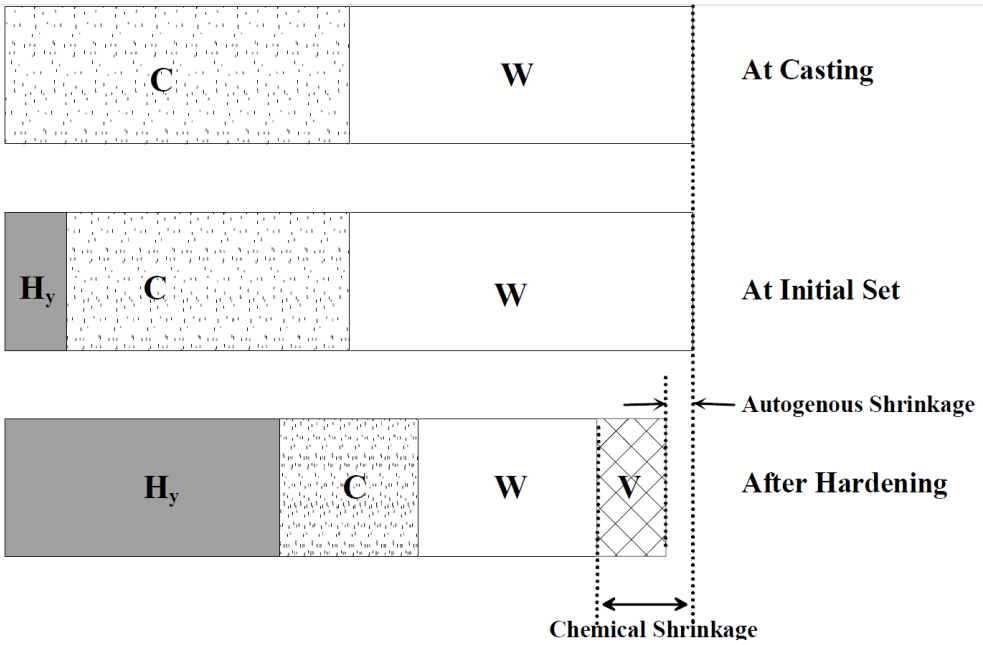

Figure 2.6—Reactions causing autogenous and chemical shrinkage (Japan, 1999)

The factors influencing the magnitude of autogenous shrinkage are often disputed. It is agreed that autogenous shrinkage cannot be prevented by casting, placing or curing methods, but must be addressed when proportioning the concrete mixture. It appears that the internal components or ingredients have the most significant influence (Justnes et al., 1996).

Autogenous shrinkage has only recently been documented and accurately measured. It was first described in the 1930's by Lyman (1934), as a factor contributing to total shrinkage, which was difficult to assess. In these earlier days, autogenous shrinkage was noted to occur only at very low water-to-cement ratios that were far beyond the practical range of concrete. But with the development and frequent use of modern admixtures, such as superplasticisers and silica fume, it is much more realistic to proportion that concrete is susceptible to autogenous shrinkage.

2.2.4 Plastic Shrinkage

Plastic shrinkage occurs only in fresh concrete. The most common mechanism is the evaporation of water from the surface of the plastic concrete. However, the loss of water through the sub-base or formwork can exacerbate the effects of surface evaporation. In the fresh concrete the particles are completely surrounded by water (Holt 2001). If water is removed from the system, menisci are formed between particles. These menisci generate

negative capillary pressure, which pulls the cement particles together. By pulling on the particles, the capillary stresses tend to reduce the volume of the cement paste. Capillary pressures continue to rise as water is lost at the surface of the concrete. When the pressure reaches a critical value, the water that remains in the concrete rearranges to form discrete zones with voids between them; plastic shrinkage cracking is said to occur at this point. In addition, plastic shrinkage cracks may form in a random manner or be roughly parallel to each other.

According to reports in CCAA (Cement Concrete and Aggregates Australia, 2005), they rarely occur near the edges and they can be up to 3mm wide at the surface. The cracks that develop are believed to form a weakness in the concrete and will be widened and/or extended by subsequent drying shrinkage of thermal movement (CCAA, 2005).

2.2.5 Carbonation Shrinkage

According to Mehta and Monteiro (1993), hardened cement paste will chemically react with carbon dioxide (CO_2). The amount present in the atmosphere is enough to cause considerable reaction over long periods of time. The extent to which concrete can react with the CO_2 is a function of relative humidity (Folliard K et al., 2004). At high relative humidity the concrete pores near the exposed surface are mostly filled with water; the water prevents the ingress of carbon dioxide and thus limits the reaction.

Concrete exposed to CO_2 loses water and behaves as though it were exposed to drying conditions, in other words, the concrete will behave as though it were exposed to a lower atmospheric relative humidity than actually exists (Folliard K et al., 2004). Carbonation has been observed to cause durability issues and in the long term, can severely affect a concrete structure (Holt 2001).

2.3 Factors Affecting Concrete Shrinkage

Concrete shrinkage cracking depends on several factors including free shrinkage, age dependent material properties, creep relaxation, shrinkage rate, and degree of restraint (Shah et al., 1998). Some other factors include, cement (Shoya 1979), water content (Neville 1996), cement fineness (Mehta 1994), length of curing (Powers 1959), aggregate (Neville 1996), and drying (Mehta 1994) amongst others. These factors are outlined and summarised in the following subsections.

2.3.1 Cement

Cement paste (i.e. water added with cementitious materials) is described as the portion of concrete that most commonly experiences volume changes (Tritseh et al., 2005). Therefore, the quantities of water and cementitious materials, and hence the water-cement ratio, have become important factors that influence the shrinkage behaviour. It is also known, that shrinkage increases with increasing water-cement ratio. In this light then, the water-cement ratio controls the evaporable water content per unit volume of paste and the rate at which water can reach the surface (Tritseh et al, 2005). However, for mixes with the same water-cement ratio, shrinkage increases with increment in cement content because the volume of hydrated cement or paste also increases (Shoya 1976).

2.3.2 Water Content

Water content on the other hand may not be as influential on shrinkage as cement content does. With constant water content, increasing the cement content may have no real effect or may even decrease shrinkage due to the reduced permeability caused by the now reduced water-cement ratio (Shoya 1979). However, the water content is significant, because of the fact that it affects the volume of the aggregate mix (Neville 1996). Similarly, according to Ödman (1968), shrinkage increases at a much greater rate with decreasing aggregate volumes than it does with increasing water-cement ratio. Similarly, Troxell (1996) backed the aforesaid observation by stating that, for a given w/c ratio, concretes of wet consistency have higher paste content and have a greater amount of shrinkage than stiffer mixture

2.3.3 Cement Fineness

Cement fineness can affect the drying shrinkage of concrete (Tritseh et al., 2005). Larger cement particles that do not undergo full hydration can provide a restraining effect similar to those provided by aggregates. For this reason, shrinkage values tend to be greater for finer cement (Mehta 1994). Following, Chariton and Weiss (2002) observed that mortar made with finer cement experienced lower weight loss due to drying than mortar made with coarser cement. They believed that the increased surface area of the finer cement increased the amount of pore water that was hydrated, and hence decreased the amount of evaporable water. However, they concluded that the finer cement resulted in a finer pore structure which caused capillary stresses and increased shrinkage.

2.3.4 Curing Duration

According to Powers (1959), an argument was made, that the length of curing is relatively unimportant with regards to the overall concrete shrinkage. He believed that longer curing times reduce the amount of unhydrated cement particles, which previously restrained the paste from shrinkage. Curing also increases the modulus of elasticity and reduces the rate of creep of the paste. These effects lead to a greater cracking potential when the paste is severely restrained. Microcracking of the paste around the aggregates however, can diminish the total shrinkage in the concrete.

2.3.5 Aggregates

Neville (1996) pointed out that, the most important influence on shrinkage is the aggregate. The aggregate is said to retain shrinkage of the cement paste, consequently, the use of more aggregate allows for a mix with less paste. Similarly, aggregates provide restraint because they do not undergo volume changes due to changes in moisture conditions. The amount, size, and stiffness of an aggregate determine how much restraint it provides (Mindess, Young, and Darwin 2003). On the other hand, Pickett (1956) stated that shrinkage was reduced by 20% for mixes with the same water-cement ratio in which the aggregate content was increased from 71% to 74%. The amount of restraint provided by the aggregate depends on its elastic properties. Similarly, Reichard (1964) observed that concrete shrinkage was directly related to the modulus of elasticity and compressibility of the aggregate. However, lightweight aggregates with low moduli of elasticity exhibit higher shrinkage (Mindess, Young, and Darwin 2003).

Several other researchers (Karagular and Shah (1990), Shah, Karaguler, and Sarigaphuti (1992), Folliard and Berke (1997), Shah, Weiss and Yang (1998), Weiss and Shah (2002), See, Attiogbe, and Miltenberger (2003)) observed improved shrinkage resistance and cracking behaviour by using shrinkage-reducing admixture (SRA) in concrete. It is well known that SRAs works by reducing the surface tension of the mix water, which in turn reduces the stresses in the capillary pores (Shah, Weiss and Yang 1998). Similarly, Shah et al. (1992) found that free shrinkage decreased with increasing amounts of SRA and that crack widths were reduced compared to mixes of plain concrete.

2.4 Heat of Hydration

The heat of hydration produces the first thermal load on a concrete member (i.e. a concrete deck). As the fresh concrete hydrates and gains strength, the exothermic chemical reaction produces heat within the concrete placement. The temperature of the concrete slowly drops to match ambient conditions as hydration proceeds. (Folliard K et al., 2004). This process is proportional to the size of the concrete member; larger members take longer to cool to ambient temperatures. The plastic concrete can accommodate thermal loads without developing thermal stresses; after hardening, any thermal load restrained against length change will induce stresses. Thermal stresses will be the highest if the concrete hardens when it is at its highest temperature by forcing the stress-free state to be at an elevated temperature. As a result, the average temperature that the deck experiences will be lower than the environment in which the deck hardened, causing a volume contraction throughout the life of the deck (Folliard. K et al., 2004).

2.5 Methods to Assess Shrinkage Cracking

Several methods have been used in the past to assess shrinkage of concrete and resulting cracking. While tests like ASTM C 157-04, are frequently used to measure the free shrinkage of a concrete mixture, it further highlights that free shrinkage by itself is insufficient to predict whether cracking will occur in concrete. Rather according to Weiss et al, 2000, it is believed that the potential for cracking is dependent on the combination of several factors including the magnitude of free shrinkage, the rate of shrinkage, elastic modulus, and degree of restraint, creep/stress relaxation and fracture toughness of a concrete element. Although, several of the tests methods employed by researchers such as Carlson and Reading (1998) and Weigrink et al., (1996) investigated how material properties influence the potential for shrinkage cracking, there are still limitations encountered in the course of testing. Some of these methods are discussed below.

2.5.1 Free Shrinkage

Tests to measure the unrestrained shrinkage of concrete are widely used and are often performed simultaneously with restrained shrinkage tests. Some standard test methods to examine the free shrinkage of concrete include ASTM C490 (Standard Practice for Use of Apparatus for the Determination of Length Change of Hardened Cement Paste, Mortar, and Concrete), EN1367-4 (Tests for Thermal and Weathering Properties of Aggregates;

Determination of Drying Shrinkage) and ASTM C157. The test method that is more commonly used by researchers is described in ASTM C157, this method requires a prismatic specimen 285-mm long and 75 × 75mm square in cross section. The procedure includes the measurement of the time dependent change in length of the sample. The information obtained from this method can be used for comparative studies, however it should be noted that shrinkage to be acceptable for a given structure, the specimen and structure should have similar surface area to volume ratio (Weiss 1999). Since this method is only suitable for measuring free shrinkage, researchers have developed different methods to measure shrinkage of concrete when undergoing restraint.

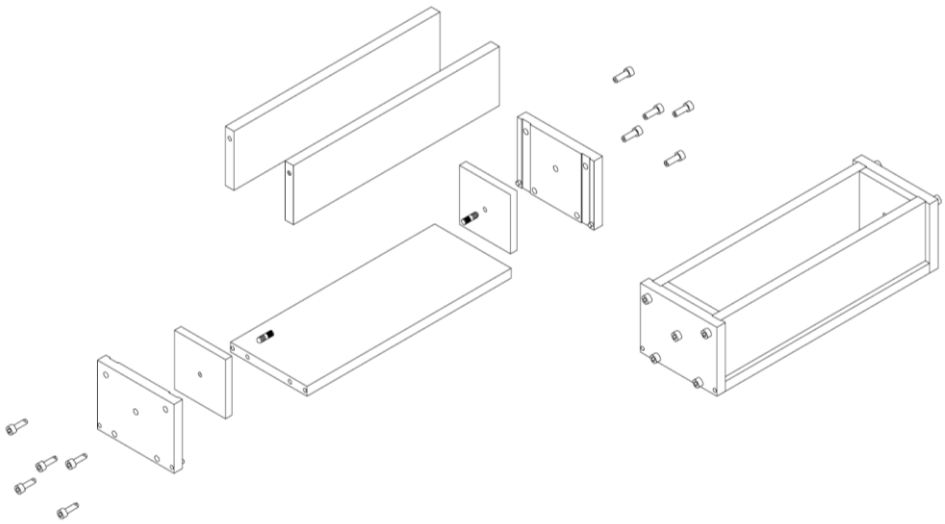

(a)

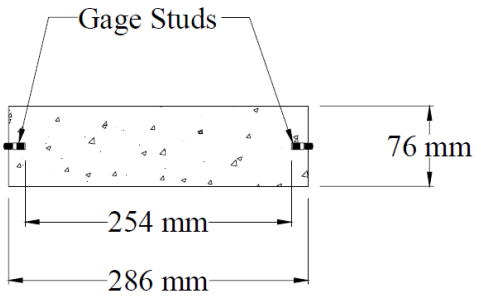

(b)

Figure 2.7—Prismatic mould coupled with a 286 mm long and 76×76 mm square cross section (Tritseh et al, 2005)

In a study conducted by Babaei and Purvis (1996) for the Pennsylvania Department of Transportation using the free shrinkage test 75×75×285mm (3×3×11in), a bridge deck cracking prediction procedure was developed. They observed that, thermal shrinkage in excess of 228 microstrains due to temperature differences between the concrete deck and steel girders can cause cracking at early ages. However, they could not really detect crack development; neither could they predict the exact position of crack. A more recent work by (Tritseh et al, 2005) used the free shrinkage test, with prism 76×76×286 mm (3×3×11(1/4) in) (see Figure 2.7) a slightly modified prism to evaluate the behaviour of shrinkage cracking in concrete. Previously, Attiogbe and colleagues (2003) had used the free shrinkage test to collect data by measuring 75×75×285 mm (3×3×11in) specimens that had the same surface area-to-volume ratio as the rings. The free shrinkage specimens were always monitored alongside the companion restraint ring test until cracking.

2.5.2 Bar Specimens

Restrained bar specimens were used to assess shrinkage cracking of concrete in the past. These specimens provide relatively uniform uniaxial state of stress when they are relatively thin (Bloom and Bentur 1995). Paillere at al. (1989) used bar specimen to test cracking of concrete at early age. In Paillere's research, the mould was placed horizontally during casting but the specimen was tested in a vertical position. In retrospect, the main disadvantage of the Paillere's method was the vertical positioning of the specimen, because the dead load was suspected to result in rupture of the specimen. On the other hand, Bloom and Bentur (1995) used a modified system of the same nature, but was rather used with the horizontal arrangement to investigate restrained and free shrinkage of concrete. Furthermore, Bloom and Bentur used a 1000 mm long concrete specimen with a 40 mm square cross section (Figure 2.8). The two ends of the specimen were wider than the rest of it to fit into grips. One grip was fixed while the other one was free to move. The movement of the grip was monitored by a special gauge. As concrete contracted as a result of shrinkage, the moveable grip could be returned to its original position (i.e. zero displacement) by a screw assembly. A load cell monitored the load required to move the grip to its original position. As a result of the above procedure, a complete restraint is believed to be obtained by returning the grip to its original position. Special arrangements were subsequently provided to avoid eccentricity and to reduce friction to an acceptable level. (Kovler, 1994) also used a similar testing method to assess the restrained shrinkage of concrete. Similarly, D'Ambrosia and Co (2004); and Tia et al, 2005), characterised

early-age behaviour of concrete by using a uniaxial test to measure the shrinkage strain and the restrained shrinkage stress (see Figure 2.9). The extent of stress relaxation by tensile creep was determined using simple superposition analysis. In addition, the experimental measurements were compared with some current creep and shrinkage models to assess their validity for early-age prediction.

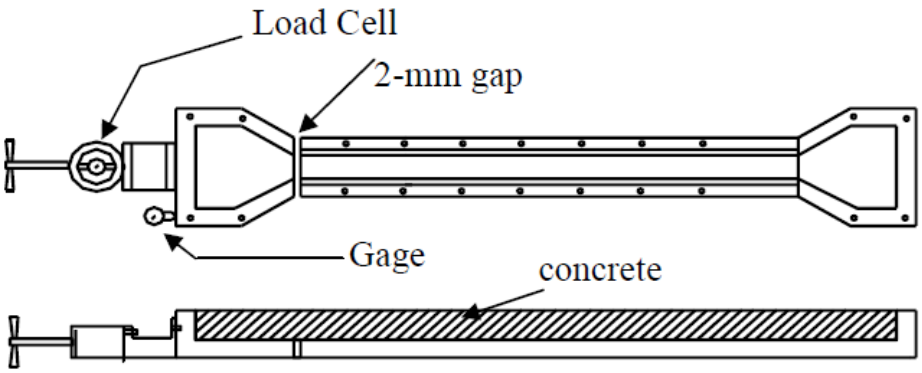

Figure 2.8—Restrained Bar Specimen (Bloom & Bentur 1995)

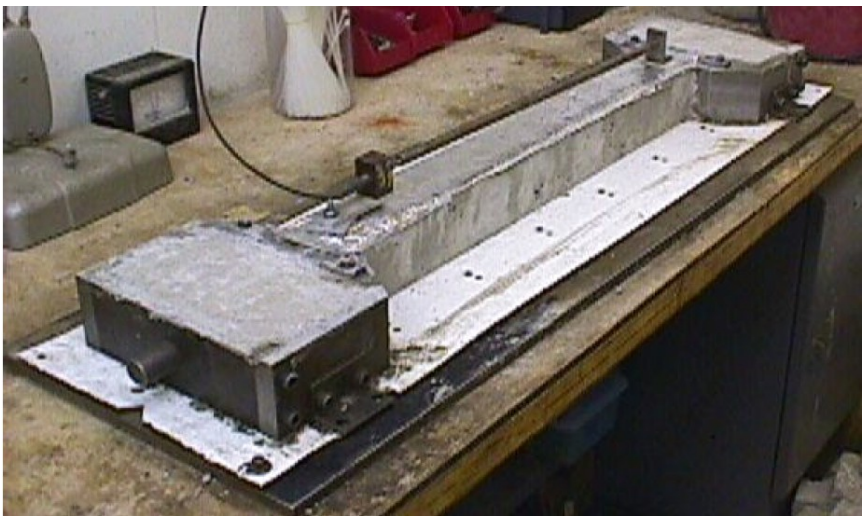

(a)

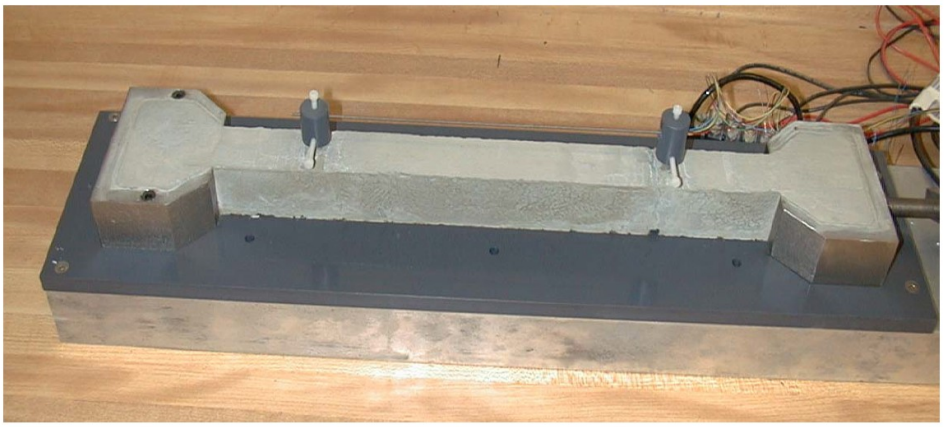

(b)

Figure 2.9—Unrestrained uniaxial test specimen (a) D'Ambrosia et al, (2004); (b) Tia et al, (2005)

2.5.3 Plate and Slab Specimens

Other research efforts have used thin plate specimens to investigate the behaviour of concrete under restrained shrinkage. The work of Kraai (1985), involved using plate specimens investigate the effects of material composition on plastic shrinkage cracking. The dimension of the concrete specimens was 0.9m × 0.6m × 0.02m. Since most of the structures are planer in nature, the information obtained from this method can be applied to a particular structure. The main limitation of this method is that it does not provide sufficient restraint to the specimen as expected. Since most of the structures are planer in nature, the information obtained from this method can be applied to a specific structure.

Subsequently, Weiss et al. (1998) developed a test method to simulate the restraint experienced in highway pavements and bridge decks. This method requires sufficiently thin concrete slab in an attempt to minimise moisture gradients. The researchers used two types of slab specimens (see Figure 2.10): slabs restrained at one end (RE) and slabs restrained at both the base and the end (RBE). The RE specimens were used to simulate slabs of finite length and RBE specimens were used to simulate the effects of sub-base friction. Initially (at first), the researchers considered slabs restrained at the base (RB) along with two other specimens (RE and RBE). Finally, they rejected the RB specimen since there was no appreciable difference that existed between RB and RBE cases. The two ensured sufficient resistance against bending, the researchers provided solid bases which consisted of 75mm×100mm steel tubes with wall thickness of 9.5mm. To provide

sufficient axial restraint, end plates were attached to the specimens by horizontal threaded rods. Additionally, clamping mechanisms were provided at both ends that consisted of end plates and vertical threaded rods. For RBE slabs, additional base restraint was provided by using 6.5mm×3mm steel strips welded to the base.

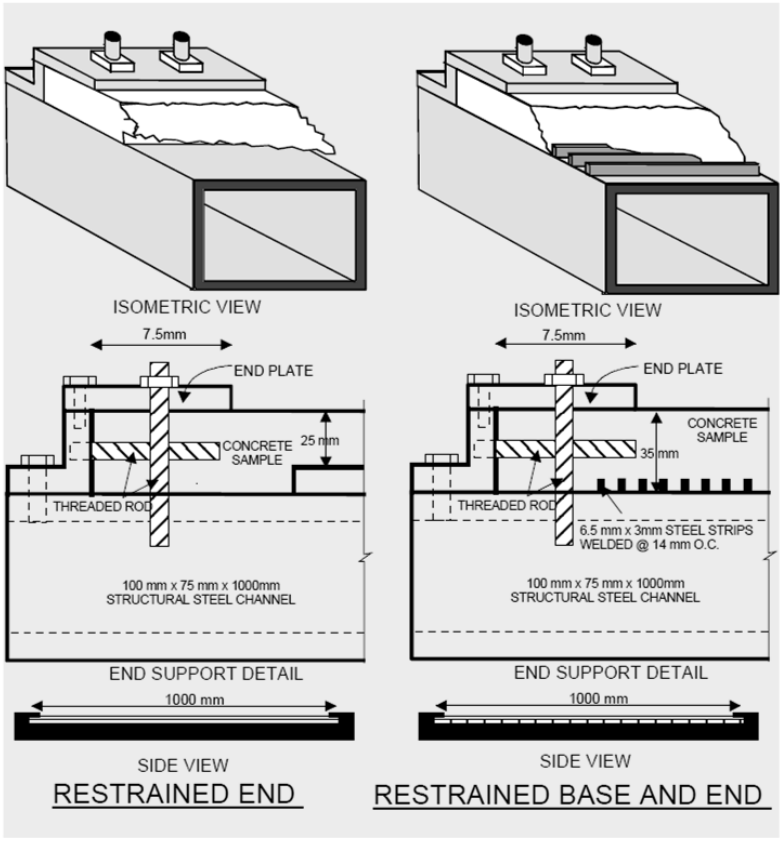

2.10— Restrained Slab Specimens (Weiss et al., 1998)

Loser and Leeman (2008) in recent times compared restrained shrinkage and free shrinkage of self consolidating concrete to that of conventional concrete. The test involved conducting compressive strength, flexural strength and modulus of elasticity on prisms 120mm×120mm× 360mm at the age of 28 days. Free shrinkage and creep were likewise tested, in the same vein; they investigated restrained shrinkage cracking using concrete with predetermined breaking points cast around a steel square as shown in Figure 2.11. The dimensions of the cross section are 100mm×100mm and reduced to 60mm×100mm in the predetermined breaking point. The corners of the concrete specimens were reinforced to avoid cracking at these points. After curing, the samples were kept at 20°C and 70% relative humidity for 12days and then kept at the same temperature but this time with 35% relative humidity. Results showed that SCC (Self Consolidating Concrete) at age 91 days is

about 10-40% greater with respect to drying shrinkage when compared to conventional concrete.

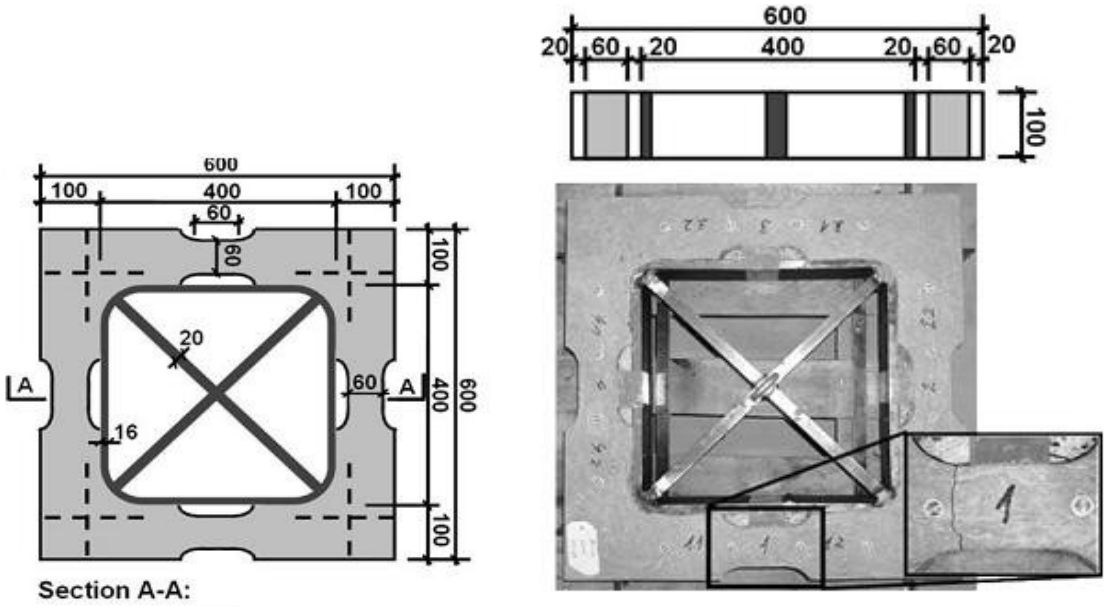

Figure 2.11— Restrained shrinkage setup by Loser and Leeman (2008)

2.5.4 Mechanics of Shrinkage Cracking

As concrete dries, it shrinks. When shrinkage is restrained in a concrete member, it can result in tensile stress. It should be noted however, that structural elements of hardened concrete are always under restraint, usually from sub-grade friction, end members, reinforcing steel, or even from differential strains between the exterior and interior of concrete. The magnitude of the stress that is generated due to restraint could be computed using Hooke's law based on the elastic modulus (E) of concrete and the difference between the free shrinkage and the restrained shrinkage displacement (Hossain 2003) and Moon 2006). Concrete may be expected to crack when the tensile stress exceeds the tensile strength of concrete (f_t), but it does not happen in practice due to the effects of creep (Hossain 2003).

In practice, fortunately, the tensile stress developed due to restrained shrinkage in concrete element is lower than that predicted by Hooke's law. This beneficial reduction in stress can be attributed to the fact that a concrete element which is subjected to a given displacement experiences a reduction in stress over time. This phenomenon is called stress relaxation. This is also similar to another phenomenon called creep. Creep can be defined as the

gradual change in length with time under sustained stress; creep and stress relaxations though, are typical of a viscoelastic material (Hossain 2003).

A concrete element cracks when the developed tensile stress exceeds tensile strength (i.e. crack resistance) of concrete. Similarly, it follows that if the strength of concrete is always greater than the developed stresses, no cracking will occur. Thus, under the restrained condition present in concrete, the interaction between strength of concrete, tensile stresses induced by shrinkage and stress relief due to creep relaxation is at the heart of deformations and cracking in most structures (Mahta and Monteiro, 1993).

2.6 Ring Test

The ring test has become the most popular method used in assessing or investigating the shrinkage cracking potential of concrete. In the ring test, a concrete ring is cast around a steel ring, as the concrete dries out, concrete tends to shrink but the steel reactively prevents the shrinkage that occurs. According to Hossain and Weiss (2002), as a result, the concrete ring develops tensile stresses in the circumferential direction. The relative dimensions of the specimens can be selected in such a way to approximate uniaxial tension as a result of restraint (i.e. thin wall). Because of the axis-symmetric nature of the ring specimens, it can be thought to approximate an infinitely long slab subjected to tensile stress. This ring test according to previous assessments has been found to be easy to conduct in the laboratory as a result of the removal of difficulties encountered with providing sufficient end restraint to the tensile specimens (Weiss 1999). Thus, as a result of the above mentioned advantages, the ring test has become a very useful method of assessing the shrinkage cracking potential concrete. Researchers have been using ring specimens to perform restrained shrinkage since 1939 (Grzybowski and Shah 1990).

This method has been primarily used to investigate concrete cracking and the effectiveness of different types of material additives and different types and volume fractions of fibres in controlling cracking of concrete mortars (Mahnberg and Skarendahl, 1978; Swamy and Stravrides 1979; Krenchel and Shah, 1987; Grzybowski and Shah 1990 and Sarigaphuti et al., 1993). In the last two and a half decades (See Table 2.1), researchers have used the circular ring test to investigate various aspects of restrained shrinkage cracking. Subsequently, Weiss and co-workers (Weiss and Fergeson 2001 and Hossain and Weiss 2002) have also developed analytical stress solutions to calculate residual stresses in the ring specimens based on fundamental elastic and viscoelastic properties and complete

restraint. Hossain and Weiss (2006) performed tests on the development of stress and the cracking of restrained shrinkage ring specimens of varying geometry and boundary conditions (See Figure 2.12). This time, the specimens were sealed either at the top and bottom or on the outer circumferential surface according to the author's discretion with a view to prevent moisture loss.

At the same time the degree of restraint was varied by keeping specimen thickness the same, while changing the thickness of the steel rings. The height of specimen remained at 75mm (3inches), and the other dimensions stayed the same according to AASTHO standard. However, the steel rings had varying thickness of 3.1mm (0.125inches), 9.5mm (0.375inches) and 19mm (0.75inches) respectively. The outcome of this test procedure showed that drying from top and bottom surfaces caused greater shrinkage strains to occur compared to drying from the outer circumference. The larger exposed surface area-to-volume ratio was believed to be a cause of this observed behaviour.

Furthermore, it was observed that the thicker the steel ring, the greater the stresses that developed in the concrete compared to the thinner ones; specimens with thinner steel rings either did not crack within the duration of the ring test or cracked at a later day. Four strain gages were connected to each ring at mid-height and interfaced with a data acquisition system in a half-bridge configuration. This was done to capture the early-age strains that developed during the first 24 hours. The specimens were sealed for the first 24 hours to prevent moisture loss. A similar work was conducted by Tritseh et al, (2005) as they evaluated four (4) concrete mixes that were simultaneously exposed to similar drying conditions. The rings were sealed on the top and bottom surfaces, exposing only the circumferential surface, similar to the ASTM (2003) and AASHTO (1998) recommendations and subsequently, outer circumferential surface was sealed exposing the top and bottom surfaces. Similarly, the drying regime for both the rings and free shrinkage prisms were the same. The geometries of the rings as well as their dimensions are shown in Figure (2.13), highlighting the different drying direction.

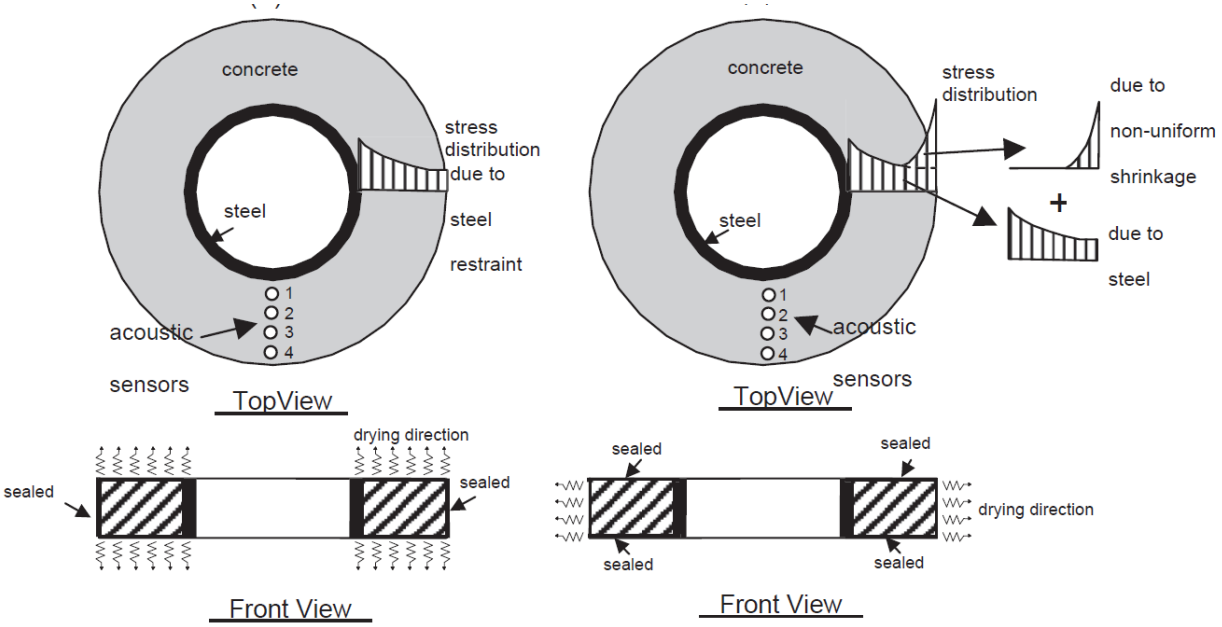

Figure 2.12—Restrained circular ring specimens (Hossain and Weiss 2006)

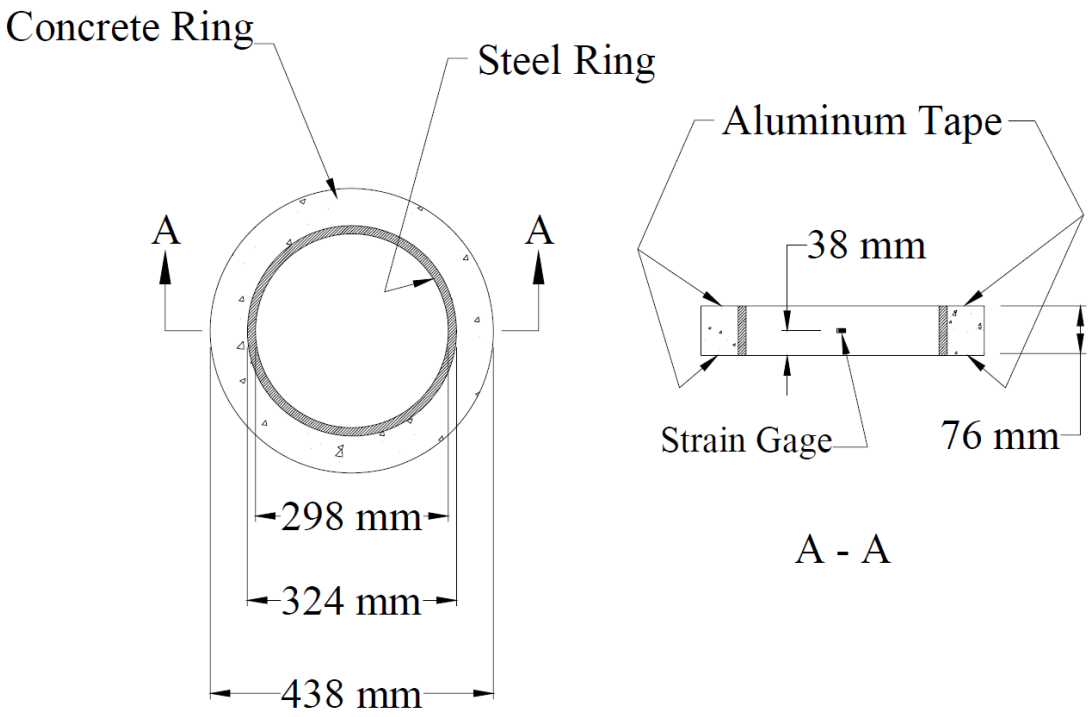

(a)

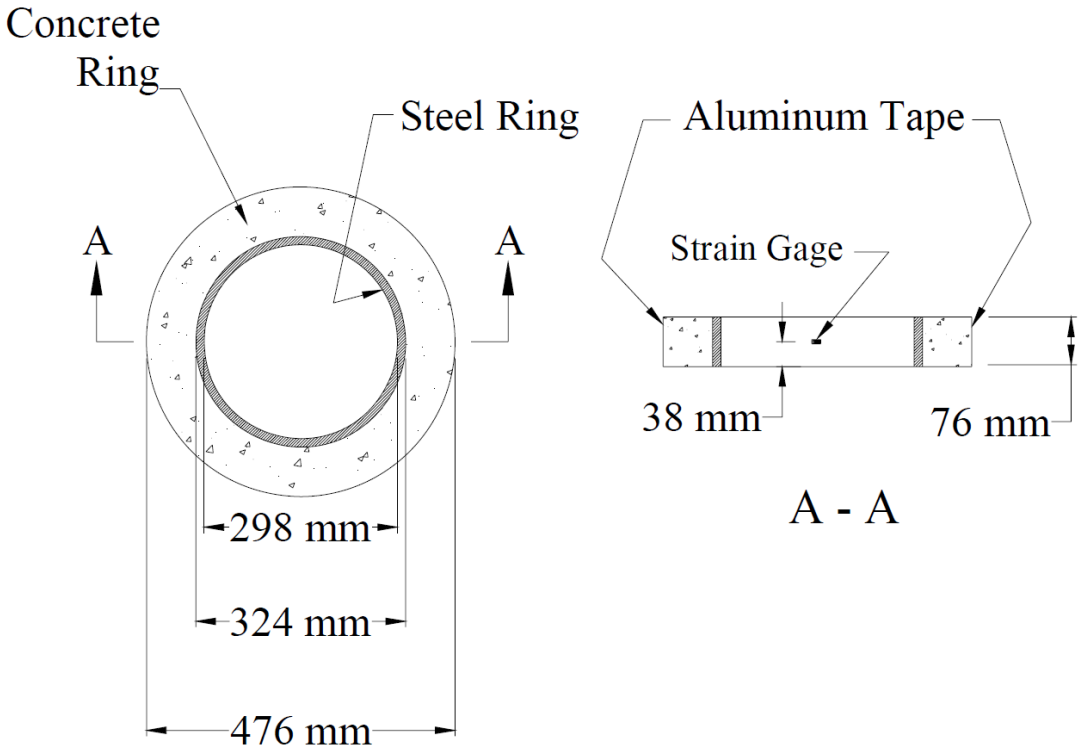

(b)

Figure 2.13—Ring set up when the (a) outer circumferential surface is exposed for drying; and (b) top and bottom surfaces are exposed for drying (Tritseh et al, 2005)

Table 2.1—Summary of previous Circular ring tests

Carlson R.W., and Reading T.J	The test performed using circular steel rings were used to examine the influence of cracking resistance on shrinkage cracking in concrete walls.	1988
Grzybowski M., and Shah S.P	Investigated shrinkage cracking of fibre reinforced concrete using a restrained ring test. In their case, the top surface of the concrete ring was sealed and the bottom surface remained on the form to permit drying only from the outer circumferential surface only. They assumed that uniform drying occurred along this surface since the concrete height was four times its thickness	1990
Krauss and Rogalla	Evaluated the geometry of both the steel and the concrete rings by subjecting concrete to either a uniform shrinkage stress or a shrinkage stress that increased linearly from the steel-concrete interface; simulating drying from either the top and bottom surfaces or the circumferential surface.	1996
Weiss W.J. and Shah S. P.	Highlights the fact that shrinkage cracking is also influenced by geometry. Influence of specimen size/geometry was apparent with smaller specimens cracking at an earlier age.	2001
See H.T., Attiogbe E.K., and Miltenberger M.A.	Ring specimens with height four times the radial thickness were used in this investigation and drying occurred at the outer circumferential surface. It was assumed that drying shrinkage was uniform along the height of the ring due to its geometry. They also assumed that the concrete rings were under uniaxial tensile stress due to the internal pressure applied to the concrete by the steel ring.	2003
Hossain, A.B., Pease B., and Weiss, W. J.	Describes a simple stress solution that can be used to quantify the results of the ring test. To better illustrate the microcracking and visible crack development process, acoustic emission testing was performed.	2003
Hossain A.B., Weiss, W.J.	Describes how the ring test may be used to provide quantitative information about stress development that may be used to assess the potential for cracking in concrete.	2004
Attiogbe E.K., Weiss W.J., and See H.T.	Determined that the time-to-cracking was related to the thickness of the concrete ring. Based on the rings dried from the outer circumferential surface, they established that the depth of drying increased proportionally with the square root of the drying time.	2004
Shah, S. P. and Weiss, W.J.	Describes the use of the 'ring-test' for assessing the performance of a fiber reinforced concrete. An equation is presented that enables the residual stress that develops in the concrete ring specimen to be estimated.	2006
Moon J.H, Rajabipour F., Pease B, and Weiss, W.J	Focused primarily on assessing two aspects of the restrained ring test: the influence of the drying direction and the influence of steel ring thickness.	2006

2.6.1 AASHTO PP34-99

The main purpose of this ring test is to determine the cracking potential of a proportioned concrete mix under restrained conditions. It has become of great use to compare the influence of changing certain parameters in concrete mix proportions. The variations of

interest include, type of aggregate used, the cement type, the w/c ratio and the sand to gravel ratio. Effectively, the restrained circular ring test has become a standard method recommended by American Association of State Highway and Transportation Officials (AASHTO) PP34-99 (2005): *A Standard Practice for Estimating the Cracking Tendency of Concrete* using circular thick ring specimens with the concrete wall thickness of 75mm as shown in Figure 2.14.

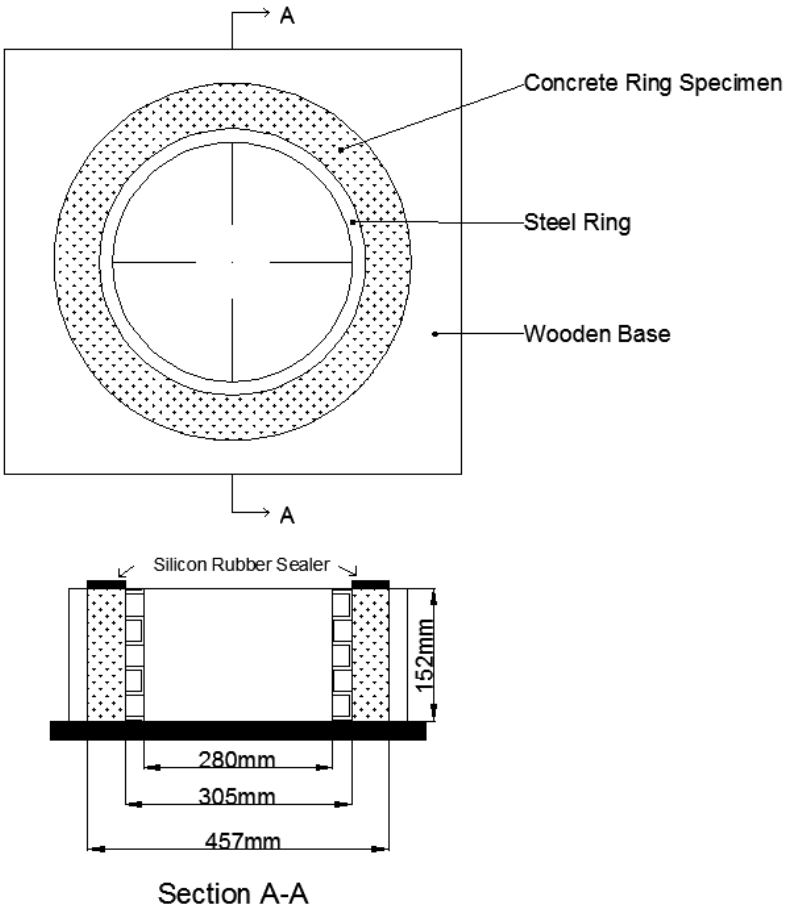

Figure 2.14—Cracking Tendency Test Apparatus with dimensions used in AASHTO

The AASHTO ring test is conducted by casting concrete of thickness of 76mm (3inches) around a steel ring with thickness of 12.7mm (1/2 ± 1/64inches). The steel ring has an outside diameter of 12 inches and height of 6 inches. Four strain gauges are placed on the inner surface of the steel ring equal-distant to one another at mid-height to account for crack initiation the occurs in concrete by measuring the compressive stain drop experienced by the steel ring via a data acquisition system (DAS), taking the strain readings every other minute. Afterwards, the strain profiles are checked and the rings are also visually inspected for any crack propagation through the concrete wall thickness.

2.6.2 ASTM C1581/C1581M-09a

This test is used to determine cracking age of mortar and concrete under restrained shrinkage and also to investigate the effect of changes in mix proportions on the cracking of concrete. The mix proportions that can be varied include the aggregate, cement type, water content, cementitious material, water and cement ratio and sand to gravel ratio etc. Albeit, the ASTM (American Society of Testing and Materials (ASTM) C1581/C1581M-09a: A Standard Test Method for Determining Age at Cracking and Induced Tensile Stress Characteristics of Mortar and Concrete under Restrained Shrinkage using circular thin ring specimens with the concrete wall thickness reduced to 37.5mm (1.5 inches) in order to shorten ring test duration. The ring test (see Figure 2.15), follows the general procedure of the AASHTO ring test but with slight variations. The steel ring's wall thickness labelled as (A) is 13±1 mm (0.5±0.05 inches) with an outer diameter labelled as (B) is 330±3 mm (13±0.12 inches). The outer diameter labelled as (C) stayed at 405±3 mm (16±0.12 inches). The height of the ring labelled as (D) is 150±6 mm (6±0.25 inches). In both standards, strain gauges are used to measure the strain of the central restraining steel core to provide a more accurate assessment of cracking age as compared to simple visual observation of the time-to-first-cracking, which may also be useful but maybe less reliable than strain monitoring.

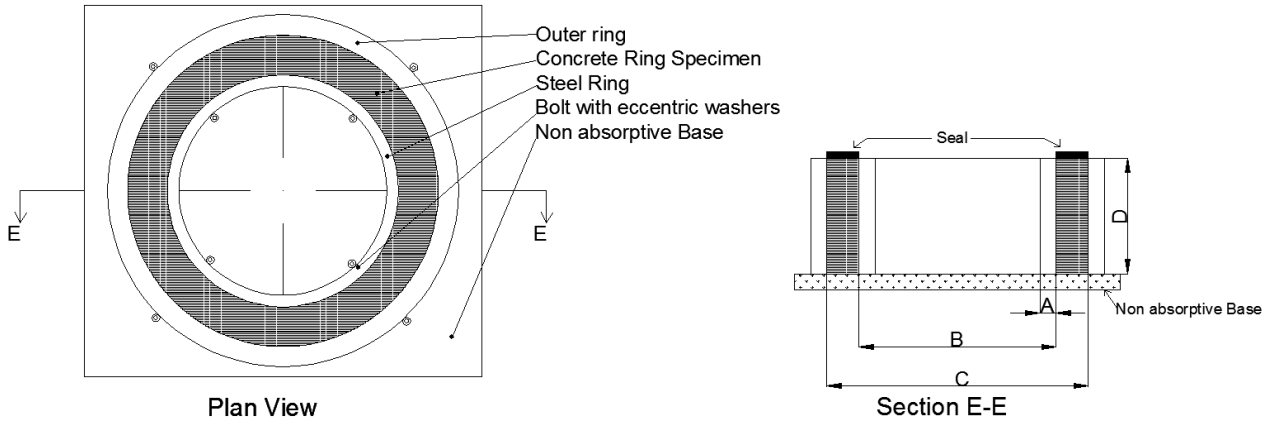

Figure 2.15—Test Specimen Dimension used in ASTM

In practice, the circular ring test is also widely used to determine the effects of material variations on induced tensile stresses in restrained concrete and cracking potential of concrete mixture. These variations may include, aggregate source, aggregate gradation, cement type, cement content, water content, fibre reinforcement, supplementary cementing materials or chemical admixtures. However, the test methods recommended by ASTM and

AASHTO, both using circular ring specimens, have been noted to have a low degree of restraint, resulting in a fairly long time before the first crack initiates (Bentur and Kovler (2003);Moon et al, (2006)). It is also regarded to have a low cracking sensitivity and not efficient for large amounts of material evaluation (See et al, 2003). In addition, because the degree of restraint is largely dependent on stiffness and geometry of the central restraining steel ring, concrete in a circular ring test may not develop a visible crack if the steel ring is not thick enough, i.e., the restraining stiffness of the steel core is not big enough. Meanwhile, due to geometric effect, there is an equal opportunity of the crack occurring along the circumference of circular concrete ring, so that it is not possible to predict the exact position of the crack.

2.7 Elliptical Ring

With a view to investigate the potential of cement-based materials, especially those with varying alkali content, He, Zhou and Li (2004) developed a novel method. With the prospects of the circular rings being the main test method, they otherwise fabricated an ellipse-shaped ring to provide restraint, having the same function as the circular steel ring to the concrete ring specimen. It was generally believed by them and other researchers (He et al., 2004, He et al., 2005 He et al., 2006 and Ma et al., 2007), that because of stress concentration due to the effect of the steel ring geometry, cracks will initiate earlier in the elliptical ring specimens compared to the circular ones; however, this comparison was not validated in their investigations. Due to the fact that a crack may initiate anywhere in the circular ring specimen further exposed its limitations. Hence, in comparison, the elliptical ring seemed to have an advantage in this area, since cracks will tend to initiate at certain predictable positions in the elliptical ring specimen for a given ring geometry. Thus, the elliptical ring specimens were used to assess the cracking tendency of cement-based materials as an improved ring test by these researchers (He et al., 2004, He et al., 2005 He et al., 2006 and Ma et al., 2007). According to He and colleagues (2004), the inner steel ellipse and the outer PVC mould has the form to place freshly mixed concrete. The height of the specimens used were 50mm (2 inches) and the concrete thickness varied between 18.75 and 20 mm (0.74 and 0.79 inches) around the elliptical ring. The details of the elliptical ring setup are shown in Figure 2.19 under section 2.11. In addition, the mould base was covered with Teflon in order to reduce friction through the course of place concrete mix in the mould. The specimens were subsequently cured for 18 hours at 28±1°C (84.4±1.8°F) and over 95% relative humidity. After the curing period (18 hours), the outer

moulds of the ring specimens were stripped off, and then the top surface of concrete in the mould was covered with epoxy (without hardener). This was to allow drying only from the outer circumferential surface as the bottom surface was already in full contact with the mould base. The specimens were placed in a testing room with 28 ± 1°C (84.4 ± 1.8°F) and 50% ± 5% relative humidity. In their case, an electroconductive material (see Figure 2.16) was used to monitor the elliptical rings for cracking; a loop of zero-strength materials was also attached on the outer circumferential surface of the specimens.

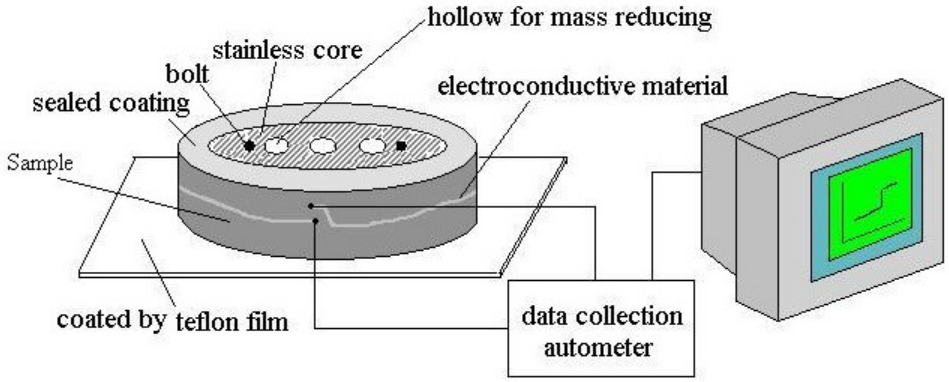

Figure 2.16—Experimental setup of the elliptical ring test (He et al., 2004)

Following, electrodes from a universal meter were connected to each end to close the circuit and then provide a voltage source likewise. In the course of the test however, the material's resistance was monitored and recorded by a noncontact resistance meter as shown in Figure 2.17a. A broken conductive loop as well as the resistance abrupt jump was indicative of crack initiation, under observation. The experimental results obtained for elliptical rings are shown in Figure 2.17b; similarly, the results were then compared with the crack position predicted by theoretical analysis (shown in details in section 2.11). The outcome highlighted that most cracks occurred the region with the minimal area. In addition, the alkali affects the process of hydration and the formation of microstructure of cement paste as well as the cracking sensitivity of materials (He et al., 2004). Summarily, the studies undertaken by these researchers streamlined their attention on how materials and/or additives influence restrained shrinkage cracking of cement-based materials using the elliptical ring as a conduit to perform the operation. It is also to note here again, that these investigations did not involve the comparison between circular and elliptical rings

tests and hence, no out right evidence available for verifying whether the elliptical concrete ring will crack before circular concrete ring.

(a)

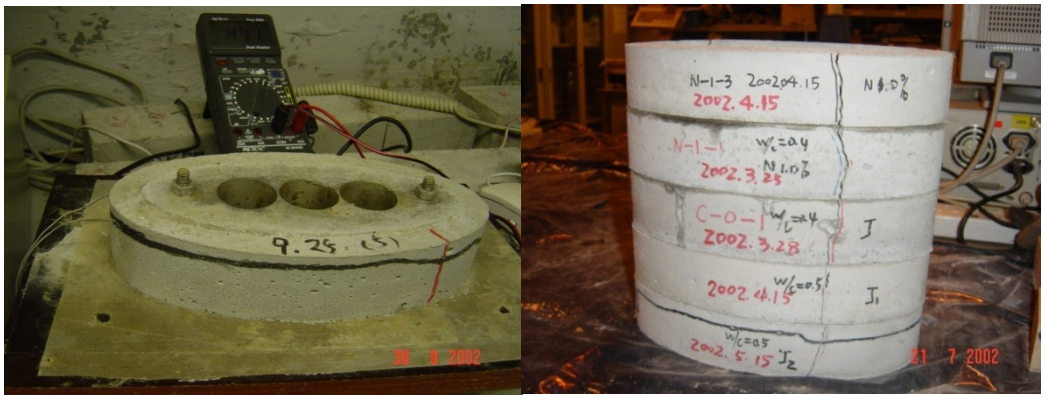

(b)

Figure 2.17—Experimental setup with elliptical ring test and results for (a) non-contact resistivity measurement (b) Location of early age cracking on the elliptical ring specimen (He et al., 2004).

2.8 Fracture Toughness

The performance of a material can be evaluated by its stress-strain response. For a linear elastic material, elastic response is terminated and stress suddenly drops to zero when it reaches the fracture strength of the material. Linear Elastic Fracture Mechanics (LEFM) was applied to cement-based materials by Kaplan in 1961 and Kesler and co-workers in 1972. The latter group of researchers concluded that LEFM was inadequate for concrete. The irrelevance of LEFM is a result of the relatively inelastic zone in concrete, which is

large in scale and fully cracks ahead of the crack tip. Therefore, several investigators have developed non-linear fracture mechanics models to describe fracture-dominated failure in concrete structures. These approaches include the fictitious crack model (FCM) (Hillerborg et al., 1976), the crack band model (Bazant and Oh, 1983), the two parameter fracture model (TPFM) (Jenq & Shah, 1985), the effective crack model (ECM) (Karihaloo and Nallathambi, 1988), the size effective model (SEM) (Bazant and Kazimi, 1990) and the double-K model by Xu and Reinhardt (1999). Considerable effort has been applied to develop robust numerical algorithms to describe tensile fracture in concrete and other quasi-brittle materials. The older approaches to the finite element modelling of fracture, the smeared crack and the discrete crack, have been successfully complemented in the past years by the application of the so-called strong discontinuity approach (SDA) (Simo et al., 1993). In contrast to the smeared crack model, in the SDA the fracture zone is represented as a discontinuous displacement surface.

Most cracks in concrete members occur due to thermal stress, shrinkage, drying shrinkage, and external causes. In actual construction, structures can collapse by cracks occurring at early ages before complete hardening of the concrete. Specifically, it influences durability and service life of concrete structures or structural elements within a structure. Therefore, the evaluation and control of cracks at early ages are essential. The Jenq & Shah two-parameter procedure, which is very easy to apply even with small structures, and the cohesive zone procedure; are procedures that can be used to predict the maximum load that a cracked concrete structure can sustain. When a cracked concrete element (structure) is loaded, a partially fractured zone develops ahead of the initial crack tip, and with a load control situation this zone increases in size until the load attains its maximum value when the structure fails in an unstable manner.

Many foregoing researches on early age concrete laid particular stress on the properties of material, but less on mechanical behaviour such as damage and fracture. In this research, based on the two-parameter mode test recommended by RILEM, a numerical analysis to the formation and propagation of cracks within fibre reinforced concrete under external load is implemented. The critical intensity factor K_{IC}^{S} and the critical crack tip opening displacement $CTOD_C$ of concrete are determined and compared with those of the plain concrete grade C30. (Jin et al, 2006).

2.8.1 Fracture Test

Concrete failure is usually synonymous with propagation of cracks in concrete. It is however of great essence to understand its mode of operation, i.e. how and when concrete fails; this is important for developing new cement-based materials which is subsequently crucial for designing concrete structures. Because of the cracks that occur in concrete as a result of self and drying shrinkage, external loads and thermal stresses, structures are prone to fail before hardening which will consequently affect its durability and service life **(**Jin et al., 2006). It is therefore good practice to focus more on its early ages. Concrete is conventionally described as quasi-brittle in nature, since it demonstrates stable pre-peak crack growth and strain softening post beak behaviour (Weiss 1999). The fracture mechanics approach has been used in the past and still being used to provide a method that quantifies brittleness, post-peak behaviour, strain localization and the effect of specimen size (Shah and Ouyang 1994; Bazant and Planas 1998). The non-linear behaviour of concrete as a brittle heterogeneous material has become increasingly more complicated especially during fracture analysis. It has become of great importance to be able to characterise the fracture resistance and energy dissipation of concrete and mortar. Although, the simplest fracture mechanics model for concrete is clearly that based on Linear Elastic Fracture Mechanics (LEFM), its validity to cementitious (concrete, rock) materials has been seriously challenged by the lack of experimental evidence, consequently suggesting a unique size dependent fracture toughness value (Saumoa, 2000). However, since an inelastic portion is ever present at the crack-tip when considering a real material, the stresses developed do not become singular; this portion is most often classified as the fracture process zone**.** The quasi-brittle nature of concrete means that its fracture process zone size is not small compared with the typical specimen or structural dimension**.** (Roesler et al., 2007). The fracture process is not concentrated at a point; in fact, it is distributed over a zone whose size is not negligible when compared to the dimensions of the body (Bazant et al., 1990). According to (Shah and Ouyang 1994), the presence of a sizeable fracture process zone may be attributed to the inherent material heretrogeneity in concrete. Furthermore, many toughness mechanisms that are responsible for the fracture process zone include crack shielding, crack deflection, aggregate bridging and crack surface roughness induced closure (Shah and Ouyang 1994). In retrospect, several experimental and theoretical approaches have been developed for the last 30 years to determine reliable parameters that characterise the behaviour of the cementitious system

and further accounts for the development of the fracture zone (Hillerborg A, 1976; Bazant Z. P., 1984; Jenq and Shah., 1985; Nallathambi, P 1986; Tang et al., 1996; Bazant and Li 1996). Comparisons of for different fracture models are elaborated in Table 2.2, highlighting the advantages and disadvantages of each model.

Table 2.2— Comparisons of four different fracture models

<table>
<tr>
<td>

Fictitious crack model (FCM) – Hillerborg et al (1976)

- Takes a softening stress – separation curve as a material property;
- For the determination of the softening stress – separation curve, at least three (3) fracture parameters are needed which are;
  - Fracture toughness ($\mathbf{G_F}$) – this defines the area under the curve.
  - Tensile strength (f_t)
  - Crack tip separation at zero stress (w_t)
- A softening stress – separation curve can be combined with a finite element code to predict fracture response of a concrete structure

Disadvantages/Difficulty with(FCM);

- How to experimentally measure the values of G_F, f_t and w_t for a material.
- A method was proposed by RELIM using the three point-bend beam test;
- However, the "Round Robin test", shows that the values of G_F obtained is beam size dependent
- No method for obtaining f_t and w_t have yet been proposed
- Inconsistency may be introduced by separately measuring values of f_t and w_t

</td>
<td>

Size effective Model (SEM) – Bazant & Kazimi (1990)

- Introduces two (2) material fracture parameters

G_f = the critical energy release rate

C_f = the critical effective crack extension

(For the infinite specimen)

- RELIM proposed a method to measure to values G_f & C_f by testing (several) 3-point beam specimens
- Beam are geometrically similar but must be at least three different sizes.

</td>
</tr>
<tr>
<td>

Two-Parameter fracture Model (TPFM) – Jenq & Shah (1985)

- This proposes;

K_{IC}^s = The critical stress intensity factor and;

$CTOD_c$= The critical crack-tip opening displacement

(both as material fracture parameters)

- According to RELIM, only one (1) size is needed using the 3-point beam test to measure values of K_{IC}^s & $CTOD_c$

<u>Difficulties/Challenges</u>

- Testing procedure commands an unloading when/or after the peak load testing;
- A closed loop system is usually required;
- The requirement of testing facilities has somehow restricted the application of TPFM.

</td>
<td>

Effective Crack Models (ECM) – Karihaloo & Nallathambi (1988)

- This method can be used to determine K_{IC}^s and have similar concept to RELIM recommendations and TPFM
- Three (3) - point bend beams are currently used by most of the proposed method of measuring materials fracture parameters.

</td>
</tr>
</table>

2.8.2 Two-Parameter Fracture Model (TPFM)

Cement-based materials exhibit pre-peak crack growth, therefore linear elastic fracture mechanics (LEFMs) cannot be directly applied to these materials. Over the last decades, several experimental and theoretical approaches have been developed to determine reliable parameters that can represent fracture properties of cementitious composites which are able to account for the development of the fracture process zone (Hillerborg et al., 1976; Bazant Z.P., 1984; Tang T et al., 1996). One, probably the most cited, fracture model which has been developed to account for the pre-critical crack growth for cement-based materials is the two-parameter fracture model (TPFM), proposed by Jenq and Shah (1985), which is based on the simple premise that a change in specimen compliance can be correlated to the length of the effective crack at the point when the critical (i.e. peak) load is reached. To introduce this model first the load *CMOD* (crack mouth opening displacement) of a notched specimen is considered.

A Linear elastic response up to a load corresponding approximately to P_{max} / 2; that is, the induced LEFM (linear elastic fracture model) K_I (Stress intensity factor) is less than K_{IC}/2. During this stage the *CTOD* (crack tip opening displacement) is zero as predicted by LEFM.

During the second stage, significant inelastic deformation takes place. This is caused by the formation of the process zone ahead of the crack tip (the existing crack being pre-notched or precast, and not the result of some prior crack nucleation/extension, for which a process zone first has to be developed). This process zone formation has also been referred as slow crack growth (Savastano H et al., 2009). As a result of this micro-cracking, the crack tip starts to open in a fashion similar to the blunting of sharp cracks in metals due to yielding. At the peak load, there are two conditions which are simultaneously satisfied:

At the peak load and for unstable geometries (i.e. increasing K_I with increasing crack length a), there are two conditions which are simultaneously satisfied:

$$K_I = K_{IC}^s \text{ and } CTOD = CTOD_c \quad (2.1)$$

Where the parameters on the right hand side are considered to be material properties and CTOD refers to the notch opening and not the crack opening.

The results of the fracture test using this model are specimen size-independent, hence the critical values, K_{IC}^s and $CTOD_c$ are size independent which is one of the major advantages

of using two parameter fracture model; another requirement of this mode is the analytical expression of the COD and K_I along the crack for the geometry considered.

2.8.2.1 Difficulties Using TFPM Based on Compliance Method

According to Tang and colleagues (1996), there is a concern of overestimating K_{IC} and $CTOD_C$ whilst carrying out experiment procedure because the crack can extend between the time of peak load and the time of unloading which will eventually result in recording larger measured change in compliance other than those associated with change exactly at the peak load.

Due to the large/*rapid decrease in strength of material* immediately after the peak load especially in highly brittle materials such as paste and high strength concrete, it has become a challenge to unload within 95% or exactly 95% of peak load. (Even though RELIM specifies that unloading should be done when peak load is decreased within 95% of the peak load). Some of these difficulties are summarised hence:

The response rate of dependency of the testing equipment results in variations in measurements taken between different laboratories. Close-loop method may not be available for most users.

The initial and unloading compliances (C_i ; C_u) are very sensitive to minor variations of slopes; therefore extra care should be taken when measuring these parameters.

The use of 3-point bend beam is not always convenient especially for field application.

The Modulus of elasticity is calculated from:

$$E = \frac{6Sa_o g(\alpha_o)}{C_i b^2 t} \tag{2.2}$$

$$g(\alpha_o) = 0.76 - 2.28\alpha_o + 3.87\alpha_o^2 - 2.04\alpha_o^3 + \frac{0.66}{(1-\alpha_o)2} \tag{2.3}$$

$$\alpha_o = \frac{a_o + HO}{b + HO} \tag{2.3.1}$$

$$E = \frac{6Sa_c g(\alpha_c)}{C_U b^2 t} \tag{2.3.2}$$

$$\alpha_c = \frac{a_c + HO}{b + HO} \tag{2.3.3}$$

Stress intensity factor can be calculated with the equation below:

$$K_{IC}^{S} = 3(P_c + 0.5W)\frac{S\sqrt{\pi a f(\alpha_o)}}{2b^2 t} \quad (2.4)$$

Critical crack tip opening displacement can be calculated with the equation below:

$$CTOD_c = \frac{6(P_c+0.5W)Sa_c g(a_c/b)}{Eb^2 t} \times \left[(1-\beta_o)^2 + \left(1.081 - 1.149\frac{a_c}{b}\right)(\beta_o - \beta_o^2)\right] \quad (2.5)$$

C_i= Initial compliance

C_u= unloading compliance

a_o= Initial crack length

a_c= Critical effective-elastic crack length

$g(\alpha_o)$= Geometrical function

t = thickness of specimen (beam)

K_{IC}^{S}= Critical stress intensity factor

$CTOD_c$ = Critical crack tip opening displacement

HO= Height of knife edge

In this research, the calculation of C_u, unloading flexibility was not achieved using the Instron machine in the labs, and in order to get the unloading compliance two approaches were examined. In light of this, Krason and Jirsa (1969) found a band of points on the stress-strain plane which controls the degradation of the concrete under continued load cycles. The band is reduced to a single curve which is then called the locus of common points. The common point limit shows the maximum stress at which a reloading curve may intersect the original unloading curve, this means that the assumption made about the unloading flexibility C_u is valid, the initial flexibility of the second cycle is taken as the unloading flexibility of the first cycle, the flexibilities of the concrete is the gradient of the curve produced by the Inston machine. This approach was assumed by the author, and the reason behind it is that the unloading was assumed to be nothing but the removal of the load cell from the beam; hence it will unload at the same rate to the loading of the second cycle. Because this assumption was

not strong enough, the second approach was also used, which was to calculate the unloading compliance (flexibility) using the following formula in Eq 2.6 (Zhao et al, 2005; Zhao et al, 2007).

$$C_u = CMOD_c / P_{max}. \quad (2.6)$$

Where P_{max} is the maximum load recorded during the test by Instron machine, and CMODc is its corresponding crack opening displacement.

In the linear elastic fracture model this formula was also used, the unloading flexibility was assumed to be a straight line and hence is calculated by dividing the maximum load be the corresponding *CMOD*, to get the gradient which is the value of C_u (See Figure 2.18).

As aforementioned, in order to obtain the *E*, a linear regression function was fit between 5% and 40% of the peak load from the initial slope of the Load vs. CMOD curve, as shown in Figure 2.18; this is also known as the initial loading compliance (C_i).

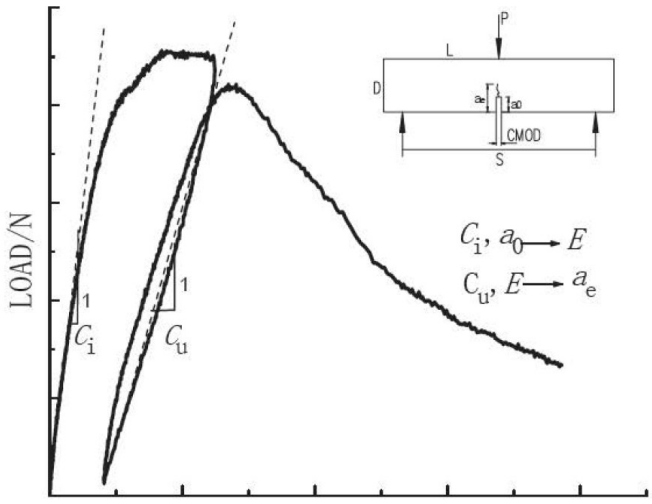

Figure 2.18—Typical curves for fracture toughness of concrete specimen using TPFM: Load versus CMOD curve

2.8.3 Concrete Beam Preparation

For all beam specimens, two knife edges shall be glued using a quick-setting epoxy to the smooth surface of the beam, centered across the notch. The shorter side of the knife edge should be placed against the concrete such that the long sharp edge is farthest from the concrete and spaced 10 mm (0.4 inches) apart as shown in Figure 2.19. The surface of the concrete must be dry in order for the epoxy to glue.

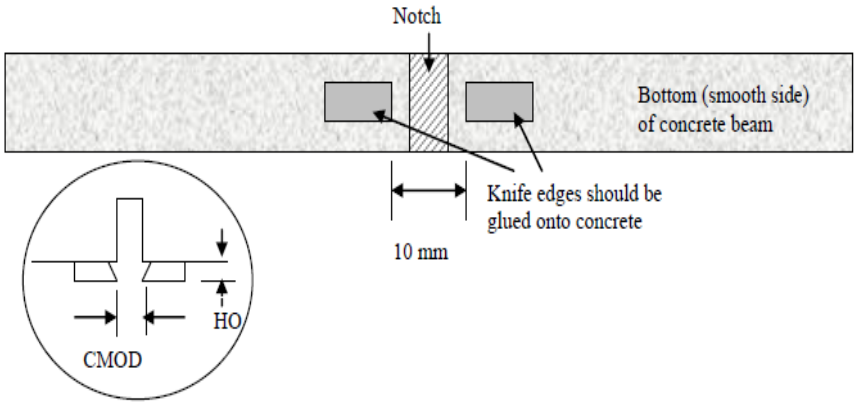

Figure 2.19—Details on attaching the knife edges to concrete beams which measure crack mouth opening displacement (*CMOD*).

If the epoxy used for the knife edges is not mixed well or does not adhere to the concrete surface, the beam may suddenly break during loading and the data will not be useful for analysis.

2.8.3.1 Size

The recommended size for testing concrete (plain or fiber-reinforced) is with a depth 150 mm. Larger beams can be made (such as 250 mm deep), but generally are too heavy. A concrete beam with dimensions shown in Figure 2.20 will weigh roughly 40 to 60 pounds. The weight of the concrete beam (preferably before testing while the beam is "dry") should be measured and is used in the analysis.

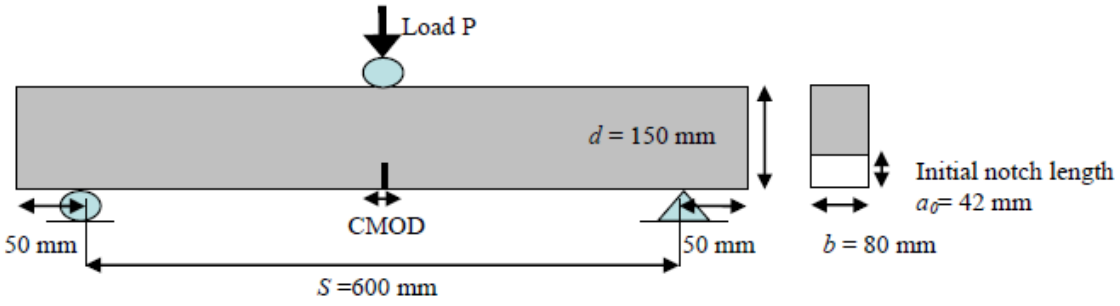

Figure 2.20—Beam schematics with suggested dimensions.

2.8.3.2 Saw-cutting

Each beam shall have a notch cut into the smooth (bottom of mould) edge of the beam. The notch depth will greatly influence the desired fracture properties, therefore be sure to make

the correct depth. Also be sure to record the actual depth of the notch to be used in the analysis. The concrete does not need to be dry for saw-cutting, but drying the surface in order to mark the location of the notch may be desired. The width of the notch shall be small compared to the depth of the notch.

2.9 Analytical Model for Circular Ring

The restrained ring test has recently become a popular method to assess the susceptibility of a mixture to restrain shrinkage cracking (Krause et al., 1995; AASHTO PP 34-99; Shah et al., 1992; Berk et al., 1997; Grzybowski 1989; Lim et al., 1999). Over the last decade, various researchers have considered several adoptions of the circular ring test. For instances, late in the last century, Carlson and Reading (1998) made use of the circular ring to compare qualitatively the shrinkage cracking potential of various cement composites. Conversely, Malhotra and Zoldners (1967) later proposed that performing the test procedure with a pressurised circular ring could be used as a potential method to assess the tensile strength of concrete. Years later, Swamy and Stravrides (1979) subsequently proposed a ring test where the strain could be measured for assessing the behaviour of fiber reinforced concrete. Similarly, Grzybowski and Shah (1989) used the ring test to investigate strain development in plain and fiber reinforced concrete using strain gauges on the concrete surface for the calibration of a modelling approach. Following, Kovler et al., (1993) combined the passive restraint from the classic ring test with the active approach proposed by Malhotra for the development of a test with an inner core ring that was made from a material with a higher thermal expansion coefficient. The test procedure developed by Kovler used the ring to apply passive restraint until a period when a tensile load was applied to the concrete ring by introducing a temperature rise in the specimen assembly. Furthermore, his approach enabled the testing time to be shortened as the temperature rise that was required to cause fracture was related to the potential additional stress capacity of the material. More recently, Weiss and Shah (2002) employed the ring geometry to demonstrate the benefit of fracture mechanics approach for predicting the geometry dependent failure of the restrained concrete ring. Following, Attiogbe et al. developed expressions based on the thin ring (See et al., 2003a; Attiogbe et al., 2003; See et al., 2003b). On the other hand, Weiss et al. (Weiss and Ferguson 2001; Hossain and Weiss 2003) proposed a solution for a thick-walled concrete circular ring under uniform radial drying. These efforts enabled the strain measured within the steel ring annulus to be used to determine the maximum tensile stress in the concrete ring using the expression below:

$$\sigma_{Actual-Max} = -\varepsilon_{Steel}\,(t).\,E_s \cdot \frac{R_{OS}^2+R_{OC}^2}{R_{OC}^2-R_{OS}^2} \cdot \frac{R_{OS}^2-R_{IS}^2}{2R_{OS}^2} \quad (2.7)$$

Where R_{OS} is the outer radius of steel ring, R_{IS} is the inner radius of steel ring, R_{OC} is the outer radius of the concrete ring, and E_S is the elastic modulus of the steel ring. It should be noted, however, that although steel was used in this expression, the restraining ring can be made of any material provided it remains linear and elastic during the test. It has been subsequently shown that this solution converges with the thin-ring solution for a sufficiently small specimen (Attiogbe et al., 2004). While Eq. 2.7 is appropriate for the case of uniform drying along the radial direction, according to (Bazant and Chern 1985; Weiss and Shah, 2001;Weiss and Shah, 2002; Kim and Weiss, 2003), moisture gradient develops due to circumferential drying, which can significantly influences the stress distribution as illustrated in Figure. 2.21.

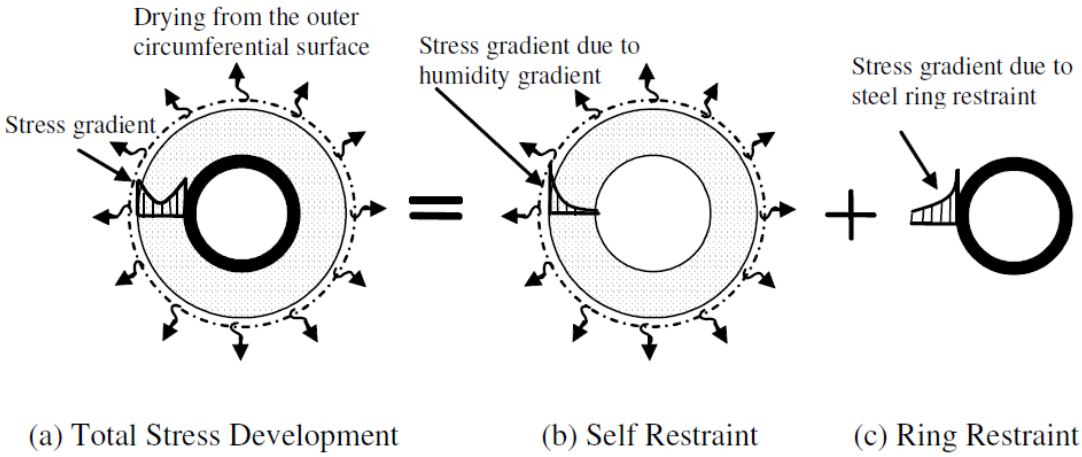

Figure 2.21—Conceptual illustration of the restrained components in concrete ring (Moon 2004)

With further research efforts employed, Hossian and Weiss (2004) discussed how the ring test can be used to provide quantitative information on early-age stress development and also used to assess the potential for early-age cracking. In this light, an analytical stress formulation was presented to compute the actual residual stress level in the concrete by using only the measured strain obtained from the steel ring. However, on the other hand, the theoretical elastic stress was computed using the free shrinkage, ring deformation and the elastic modulus of concrete. Besides, a comparison between the actual residual and the theoretical elastic stress was made and these stress levels provided information about the amount of stress

relaxation experienced in concrete. Along this line, the effects of autogenous shrinkage and drying shrinkage were determined

2.10 Analytical Model for the Elliptical Ring

A novel ellipse ring apparatus and its application for testing early-age cracking in restrained cement-based materials was conducted by He et al., (2004) for the sake of promoting crack initiation as shown in Figure 2.22 Compared with conventional ring test, the thickness of the elliptical ring sample is different along its circumference (see Fig. 2.23). In addition, cracking can be accelerated and the first crack location may be predicted by this method .Using this novel technique, the effects of different factors on early age shrinkage and cracking of cement-based materials were investigated.

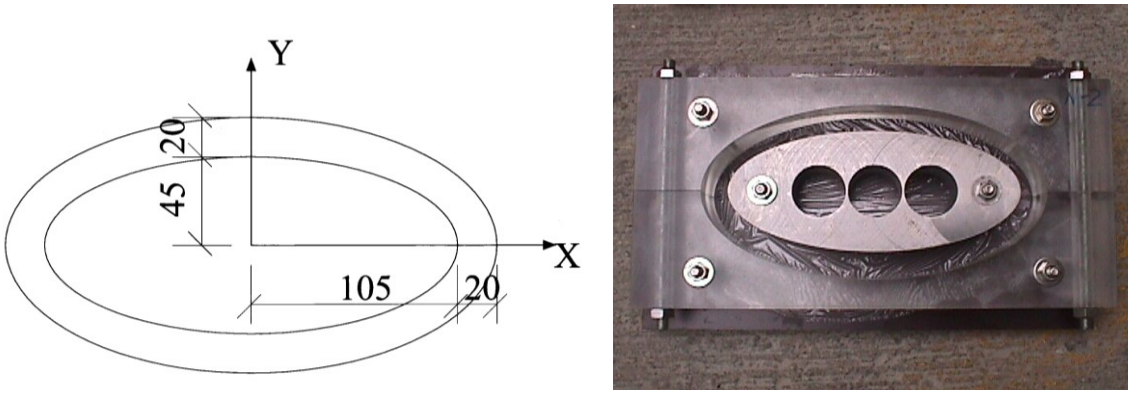

Figure 2.22— Geometry of the elliptical ring test

$$|\mathbf{AB}|^2 = [(a+t)\cos\theta_1 - a\cos\theta]^2 + [(b+t)\sin\theta_1 - b\sin\theta]^2 \qquad (2.8)$$

A preliminary analytical model for predicting the stress distribution of the elliptical ring example was proposed with the assumption that the central steel elliptical block provides uniform pressure to the ring sample, He et al 2004 (see Figure. 2.23). The pressure force applied on an element of the elliptical ring from A_1 (x_1, y_1) to A_2 (x_2, y_2) along X-direction is

$$\mathbf{F_X} = \int_{\phi_1}^{\phi_2} p\,dA\cos\phi = \int_{y_1}^{y_2} p\frac{dy}{\cos\phi}\cos\phi = \int_{y_1}^{y_2} p\,dy = p(y_2 - y_1) \qquad (2.9)$$

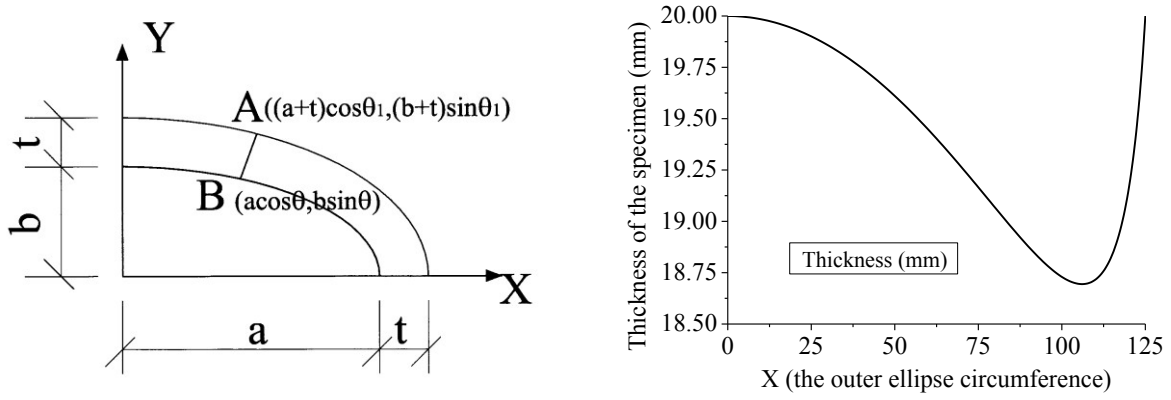

Figure 2.23—The thickness of the elliptical ring sample

The pressure force applied on the same part of the elliptical ring along Y-direction is

$$\mathbf{F}_y = \int_{\phi_1}^{\phi_2} p\,dA\sin\phi = \int_{x_1}^{x_2} p\frac{-dx}{\sin\phi}\sin\phi = \int_{x_1}^{x_2} -p\,dx = \int_{x_2}^{x_1} p\,dx = p(x_1 - x_2) \tag{2.10}$$

Stress σ_{r0} and $\sigma_{\theta 0}$ were defined as the radial stress and hoop stress, respectively, at the point x=a and y=0. It can be seen that the radial stress σ_{r0} is zero according to symmetry of X-axis while the hoop stress $\sigma_{\theta 0}$ was determined from Eq. (2.10) as:

$$\mathbf{F}_y = 2\sigma_{\theta 0}t = \int_{a}^{-a} p\,dx = p(a-(-a)) = 2pa \tag{2.11}$$

Then, $\boldsymbol{\sigma_{\theta 0}} = \dfrac{2pa}{2t} = \dfrac{pa}{t}$ (2.11.1)

It was assumed that the free body diagram of the ring was considered with the range from S (a, 0) to A (X_A, Y_A) in Cartesian coordinate system (shown in Fig. 2.24) and assuming that the normal line at point A (X_A, Y_A) has a slope angle of ϕ, the hoop stress $\sigma_{\theta A}$ and radial stress σ_{rA} acting on the cross-section can be obtained from the force equilibrium along X and Y directions, respectively, as:

$$-\sigma_{\theta A} t_A \sin\phi - \sigma_{rA} t_A \cos\phi + \int_0^{Y_A} p\,dy = 0 \tag{2.12}$$

$$\sigma_{\theta A} t_A \cos\phi - \sigma_{rA} t_A \sin\phi + \int_{X_A}^{a} p\,dx - pa = 0 \tag{2.13}$$

Solving the above equations,

$$\sigma_{\theta A} t_A = pX_A \cos\phi + pY_A \sin\phi \tag{2.13.1}$$

and $$\sigma_{rA} t_A = -pX_A \sin\phi + pY_A \cos\phi \tag{2.13.2}$$

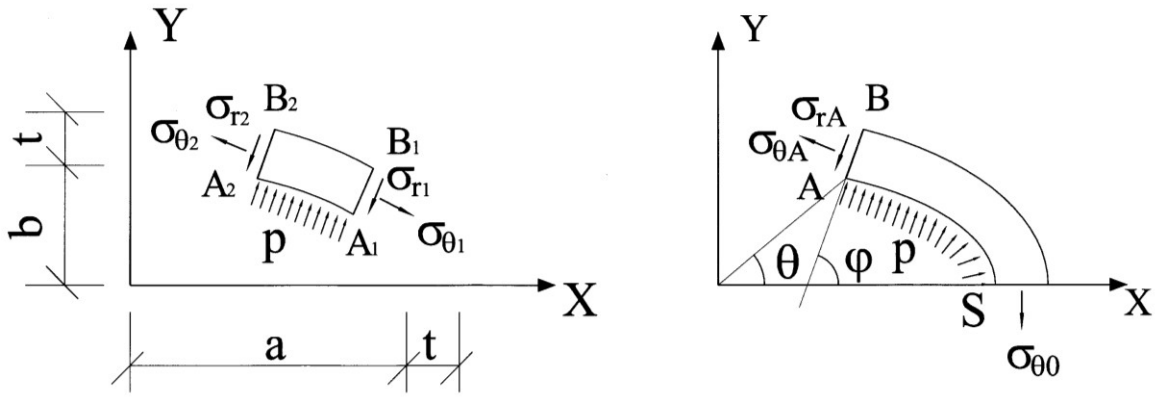

Figure 2.24—The free-body diagram of force on the elliptical ring segment

Substituting $\sin\phi = \dfrac{a^2 Y_A}{\sqrt{(a^2 Y_A)^2 + (b^2 X_A)^2}}$, $\cos\phi = \dfrac{b^2 X_A}{\sqrt{(a^2 Y_A)^2 + (b^2 X_A)^2}}$ into the above equations, the hoop and radial stress of the concrete ring are obtained from:

$$\sigma_{\theta A} t_A = \frac{p(a^2 Y_A^2 + b^2 X_A^2)}{\sqrt{(a^2 Y_A)^2 + (b^2 X_A)^2}} \tag{2.14}$$

$$\sigma_{rA} t_A = \frac{p(-a^2 + b^2) X_A Y_A}{\sqrt{(a^2 Y_A)^2 + (b^2 X_A)^2}} \tag{2.15}$$

After taking into account the thickness of the concrete ring, it was determined that the maximum hoop stresses occur at the principal axes. In the above derivation, uniform hoop stress and radial stress distribution was assumed on the cross-section of the concrete ring. However, it has been found from experiments that the first crack always occurred at the same location away from the region of the principal axes. Summarily, it was believed that the uniform internal pressure assumption is not correct. Rather, a displacement boundary condition at the inner surface of the elliptical ring example was believed to be probably better, i.e., the displacement of the ring along its radial direction is restrained and equal to zero.

He and colleagues (2004), subsequently introduced the displacement boundary assumption into the analysis, but while a constitutive model of concrete is needed, it largely increases the difficulties. At the moment, a linear tensile stress-strain relationship was believed to be reasonable, although the stress-strain relationship of concrete under compression still is a challenge. To overcome some of these challenges, it was suggested that the elliptical ring test should be modified with the ratio between 1st principal axis and 2nd principal axis of the inner ellipse equal to that of the outer ellipse. Subsequently it was then proposed to:

- Develop an analytical model for elliptical ring test
- Modify the elliptical ring test

In conclusion, the assumption of uniform pressure does not apply to the elliptical ring; so it is unlikely to use a close-form model for the elliptical rings and hence a numerical model is proposed in this research investigation.

2.11 Drying Direction in Ring Test

Since the ring test can be used or interpreted for a variety of applications, it has become of great need to measure the concrete material's response to specific stimulus under specific boundary conditions (i.e. specimen size, drying direction and degree of restraint). According to Moon (2006), no one specimen geometry or external stimulus can be used to simulate all the possible conditions encountered in the field or in service. In light of this, further research was concentrated on investigating how the drying direction of a concrete specimen can affect the potential of restrained concrete cracking. Moon and colleagues delved into classifying how different drying directions can generate stresses in sealed concrete specimens and

subsequently generate cracks. Figure 2.25 illustrates drying direction and the resulting stresses induced by the circular steel ring constraint.

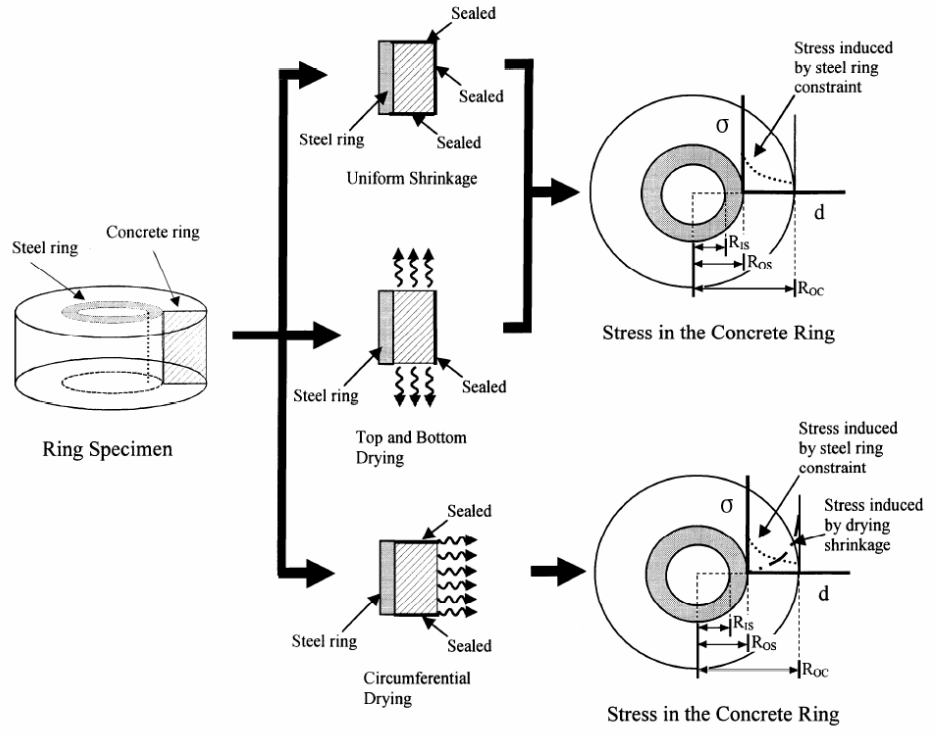

Figure 2.25—Drying direction in restrained circular ring (Moon 2006)

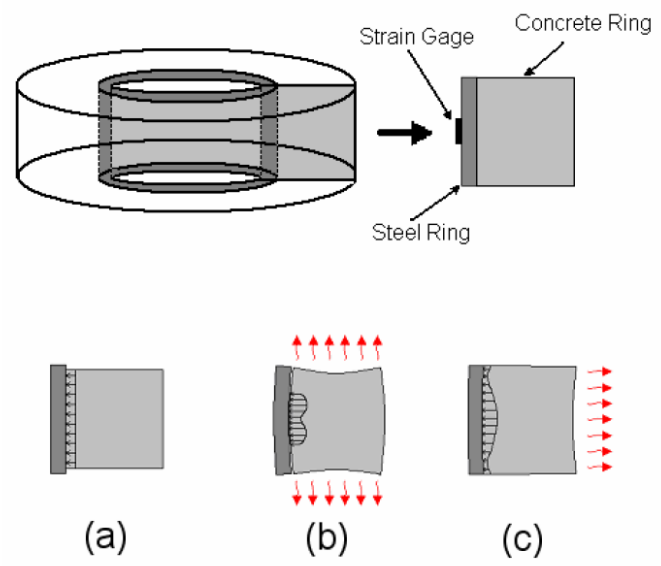

Figure 2.26—Influence of drying direction and shrinkage condition on deformation in concrete and steel (a) All surfaces exposed (b) Outer circumferential surface sealed (c) To and bottom surfaces sealed (Moon and Weiss 2006)

On the other hand, Figure 2.26 further demonstrates the stress contours (derived from simulation) that initiated as a combination of the steel ring effect and the drying direction employed on each concrete specimen. It was noticed again, that shrinkage assumes uniformity in an up and down direction, but since it is believed that the majority of the specimen moisture is lost at the outer circumferential surface, the stresses developed will be highest at this surface. This observation was supported by other researchers (Weiss and Shah, 2001; Moon et al., 2004; Moon and Weiss, 2006).In the same vein, complications are said to develop as a result of the varying stress distribution over a period of time. When specimens are sealed at the outer circumference however, a different behavioural pattern is observed, Figure 2.27 shows where stresses are concentrated in the restrained concrete specimen due to the restraining circular steel ring. Then again, according to Hossain and Weiss (2006), by allowing drying from the top and bottom surfaces only, moisture loss in the concrete ring is uniform and exhibits uniform shrinkage along the radial direction producing uniform shrinkage in the radial direction. Similarly, the stress calculations are believed to be simpler than those rings sealed at the top and bottom surfaces (i.e. drying from the outer circumference surface). In light of this, the latter causes drying gradient from the exposed surface and, therefore differential shrinkage in the radial direction. A conclusion was made hence, from test outcome of the two cases aforementioned (i.e. top and bottom drying; and circumferential drying). By the fact that uniform shrinkage is experienced along the radial direction for specimen drying from top and bottom surfaces (i.e. the circumference surface of specimen sealed), the residual stresses that develop are highest at the inner circumference of the circular ring specimen. The different drying regimes in their case were studied to determine which one most closely matched the shrinkage of the unrestrained ring specimens.

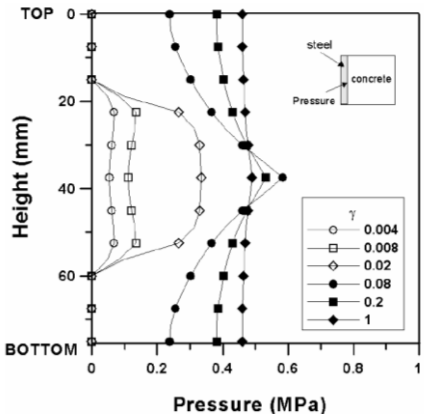

(a)

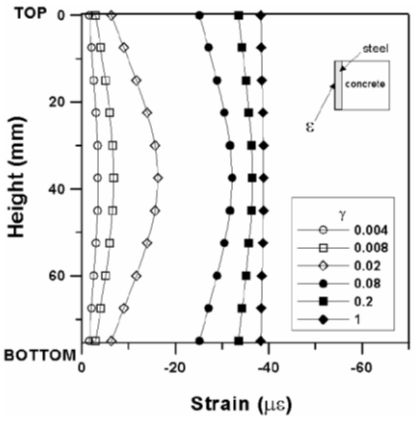

(b)

Figure 2.27—The effects of non-uniform deformation of the steel ring from simulation (a) Top and bottom drying and (b) Outer circumferential drying. (Moon 2006)

2.12 Steel Ring Size in Ring Test

The steel ring size is also believed to have a substantial influence on stress development, distribution, actual crack initiation and final propagation. From efforts employed to substantiate this hypothesis, previous investigations (Weiss et al., 2000) assumed that the stiffness of the steel ring to be too high, that the outer radius of the steel did not deform under loading in an effort to simplify calculations. Other efforts according to (Hossain and Weiss, 2004) discussed through experimental and theoretical formulation how stresses are developed in the concrete ring material due to the effects of the restraining steel ring. The rings used for investigation in their study were less rigid and consequently, the steel was expected to deform under such loading induced from the concrete. The experimental efforts included using steel rings of varying thicknesses for testing. Results were assessed and comparisons were made and it was deduced that thicker steel rings provided higher degree of restraint on the concrete ring specimen (as shown in Figure 2.28) which corresponded well to higher theoretical elastic stresses, greater stress relaxation, and hence earlier cracking. It was also observed that, the degree of restraint varied with time due to the variation in elastic modulus (Hossain 2003). When residual stresses were considered however, the actual maximum residual tensile stresses that were computed from postulated equations, showed gain that thicker steel rings demonstrated higher level of stress when compared to thinner rings as highlighted in Figure 2.29 with varying steel wall thicknesses. From deduction, the higher the degree of restraint the higher the resulting stresses. With further observation however, the difference in the

measured residual stress was very pronounced between 3.1 mm (1/8 inches) and 9.5 mm (3/8 inches) wall thickness. Nevertheless, it was believed from analysis, that the actual stress did not indicate a substantial difference between the stresses in the steel ring thicknesses (thin-9.5mm and thick-18 mm 3/4 inches). In addition, it was also observed that thicker steel rings are less sensitive (i.e. they have a lower magnitude of the strain is measures at the inner curvature surface of the steel ring) compared to thin steel rings.

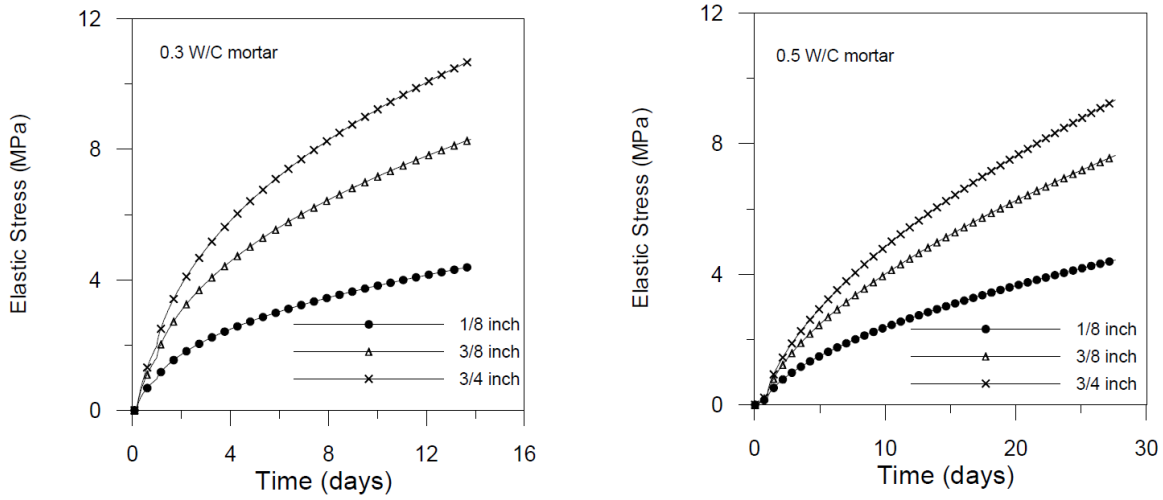

2.28—Estimated elastic stresses in concrete ring specimens (Hossain and Weiss 2004)

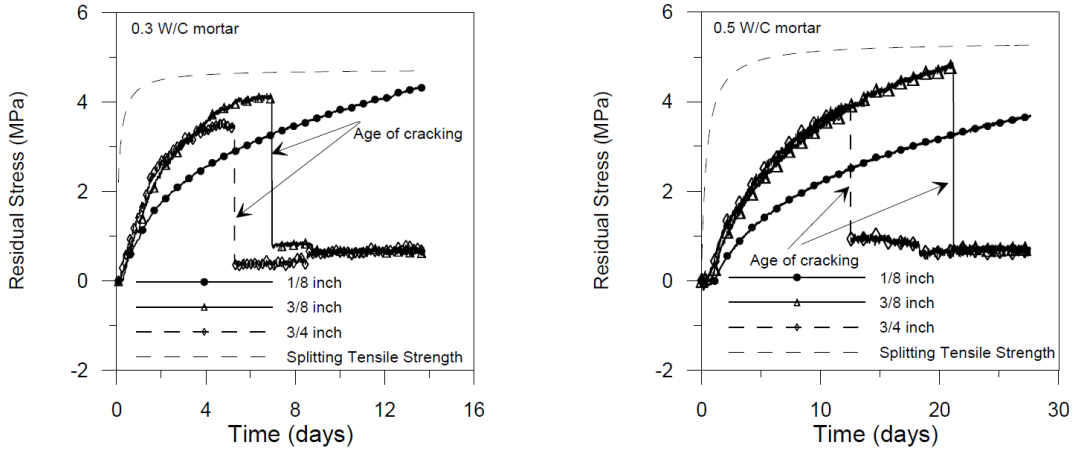

2.29—Residual stress development in concrete ring specimens (Hossain and Weiss 2004)

CHAPTER 3: MATERIALS AND TEST METHODS

The aim of this chapter is to present various material tests conducted in this research to obtain mechanical properties such as compressive strength, tensile strength and elastic modulus as well as volumetric properties such as free shrinkage of concrete at early ages. Procedures of restrained shrinkage tests using circular and elliptical rings are also documented. Further descriptions of experimental techniques and the interpretation of experimental results for the determination of material parameters are provided.

3.1 Introduction

Early-age concrete has a microstructure that is continuously evolving. Similarly, concrete failure in stress-based analytical/numerical models is usually considered to occur when the stress exceeds the strength. An accurate knowledge of the tensile strength development of concrete is just as crucial in determining the concrete cracking probability as knowing the stress that develops. The tensile strength of concrete is known to be affected by aggregate strength, smoothness and size, saturation level and cementitious materials (Riding 2007). The tensile strength has been found to develop faster than the compressive strength, but slower than the elastic modulus (Riding 2007). However, Raphael (1984) postulates that, in practice, the elastic modulus is often related to the compressive strength. In light of this, elastic modulus provides a link between restrained strains and stresses.

Although the elastic modulus is known to be dependent on the mixture proportions, unit weight, maturity, aggregate modulus, strength and moisture condition, it is believed to develop faster than the tensile and compressive strength, making it a vital property that influences concrete and hence, of great significance when conducting such tests. Conversely, shrinkage rates can change over time, allowing materials with high early shrinkage to have lower long-term shrinkage and vice versa. It is therefore imperative to investigate this early age shrinkage behaviour for better and easier understanding on its effect on the cracking behaviour of concrete when restrained.

3.2. Raw Materials for Concrete

This section will focus on the constituent materials used in the experimental program. These materials are used throughout the test program, due to the strong influence of constituent materials on mechanical parameters provided, so that the results can be comparable.

3.2.1 Aggregates

River sand with 2-mm maximum grain size, and gravel stone with 10-mm maximum particle size was used as coarse aggregates. Both fine and coarse aggregates were pre-treated in an oven with the temperature of 105^{o}C for 24 hours to eliminate any moisture assimilated prior to material preparation. They were then cooled down in air for 2 hours before they were used for concrete mix. The particle distribution is given in Figure 3.1.

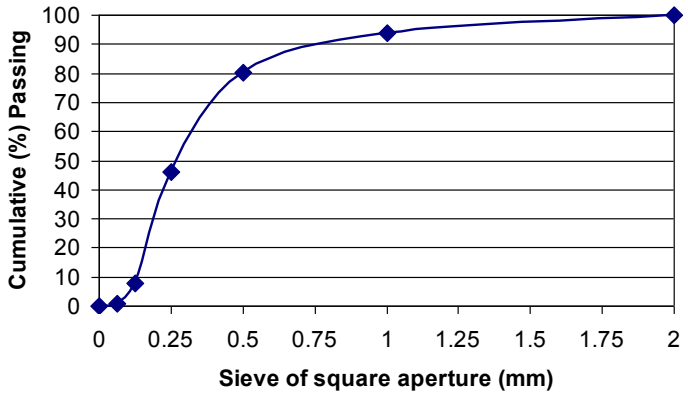

Figure 3.1—Cumulative (%) passing of sand particles

3.2.2 Cement

Commercially available CEM II Portland cement (from LAFARGE Cement UK) compatible with EN 197-1 was used as binder for preparing concrete. The specific gravity density of the CEM II Portland cement was 2.96 with Blaine fineness (specific surface area) of 423m^2/Kg measured conforming to EN 196-6. The chemical compositions by weight of the CEM II cement include CaO - 71.3%; SiO_2 - 15.78%; Al_2O_3 - 3.72%; SO_3 - 5.27%; Na_2O - 0.56%; MgO - 0.81%; K_2O - 0.94%; FeO – 1.99%, which was obtained through SEM-EDX analysis. The percentages of tricalcium silicate (C_3S), and tetracalcium aluminoferrite (C_4AF) were 70.35%, and 15.77%, respectively, by mass which were obtained through Bogue calculation based on XRD and SEM-EDX analysis results.

3.3 Mixing Procedure and Specimen Preparation

The details of the mixture proportion and mixing procedure and specimen preparation procedure are enumerated in this section. The therapy presented herein represents normal strength concrete. It should be noted though, that no admixture such as superplasticiser was added into concrete to avoid these admixtures affecting the shrinkage behaviour of concrete.

In addition, the emphasis of this research is to investigate the mechanism of the elliptical ring test for assessing the cracking potential of concrete and thus not focused on material's variation. Following, the details of the mixture proportions by weight are given in the table below:

Table 3.1—Mixture Proportions by Weight

Mixture Identification	Cement	Sand	Gravel	Water
w/c= 0.5	1	1.5	1.5	0.5

Concrete was produced using a drum-type mixer. At the beginning of concrete preparation, aggregates were mixed with one-third the total amount of water for about 3 minutes to moisture aggregates. Cement was then added with another one-third of the total mix water to the mixture and mixed for another 3 minutes. Finally the rest of the water was added and mixed for another 3 minutes. The fresh concrete mixture was left to rest in the mixer for a few minutes. Then the concrete mixture was poured into cylindrical, prismatic and ring moulds as shown in Figure 3.2, whose inner surfaces were coated with a thin layer of non-reactive release material (cream mould oil) to prevent the concrete from adhering to them.

Figure 3.2—Concrete moulds for cylinders and prisms

All the specimens (cylinders, prisms, circular and elliptical ring specimens) were filled with concrete in three layers in relevant moulds and compacted using a vibrating table for cylinders and prisms and a hand vibrator for the ring specimens respectively. The cylindrical specimens were 100mm in diameter and 200mm in length for measuring concrete compressive and splitting tensile strengths. The prismatic specimens for free shrinkage measurement were

$75\times75mm^2$ in cross-section and 285mm in length conforming to ISO 1920-8. In this study the depths of concrete and central restraining steel rings are all 75mm.

The outer diameter of the restraining steel circular ring, which is the same as the inner diameter of the circular concrete ring is 300 mm. For elliptical rings, the outer transverse diameter of the restraining steel ring along the major axis is 300 mm which is the same as the inner transverse diameter of the concrete ring, while the corresponding conjugate diameter along the minor axis varied from 120 to 250mm. The thicknesses of circular ring specimens used in this study are 37.5 and 75mm respectively which is the same as the nominal thickness of elliptical ring specimens according to (ASTM C1581/C1581M-09a) and (AASHTO PP34-99 (2004)), respectively. The restraining steel ring has a thickness 12.5mm. It should be noted here that 12.5mm is the thickness of the restraining steel ring recommended by both ASTM C1581/C1581M-09a and AASHTO PP34-99. Flat boards with smooth and water-resistance surface were used to carry the ring specimens and the ring moulds during concreting and first day curing.

Slump of fresh concrete mixtures was tested in accordance with EN 12390-3 right after concrete mixing was completed. The slump cone was inverted and filled to the top, the cone was filled in three layers and rodded 25times for each layer until the concrete mix reached the top level. Following this, the excess concrete at the top of the slump cone was adjusted with a leveller to ensure a flat surface. The cone was then raised in the upward direction and then the concrete was allowed to flow downwards under its own weight. The resulting slump experienced by the concrete is determined by measuring the slump against the length of the cone and finding the difference. This procedure was repeated a couple of times more and the average measurement was taken and subsequently recorded. It should be noted that the slump test was conducted for plain concrete to account for workability of the concrete mix used for the experimental procedure. The freshly cast concrete cylindrical, prismatic and ring specimens in moulds were immediately covered with a plastic sheet to prevent moisture loss with water sprayed on its top surface to keep a moisture atmosphere whilst placed in laboratory environment.

3.4 Compressive and Splitting Tensile Tests

Mechanical properties, i.e., compressive, splitting tensile strengths (see Figure 3.3), of plain concrete were measured on cylinders with the dimensions of 100mm in diameter cross-section and 200 mm in height at five different ages (1, 3, 7, 14 and 28 days) conforming to EN

12390-3:2009 for compressive strength and EN 12390-6:2009 for splitting tensile strength, respectively, to determine the age-dependent material properties. Compressive strength f_c was evaluated under a constant loading rate of 3kN/s while splitting tensile strength f_t was tested under a constant loading rate of 1.2kN/s. Six (6) cylindrical specimens were tested at each age, three for compressive strength and three for splitting tensile strength, to ensure repeatability. Cylindrical specimens for compressive strength measurement were capped conforming to EN 12390-3:2009 using sulphur compound before testing. It is important to note here again that, elastic modulus (E) of the concrete was obtained from the fracture test, having obtained the measurement from a formula postulated from TPFM method (Jenq and Shah, 1985) which is already outlined and described in Chapter (2) of the project review and further described in sub-section 3.6.4. The elastic modulus equation was developed and used to obtain the time dependent material property in this case.

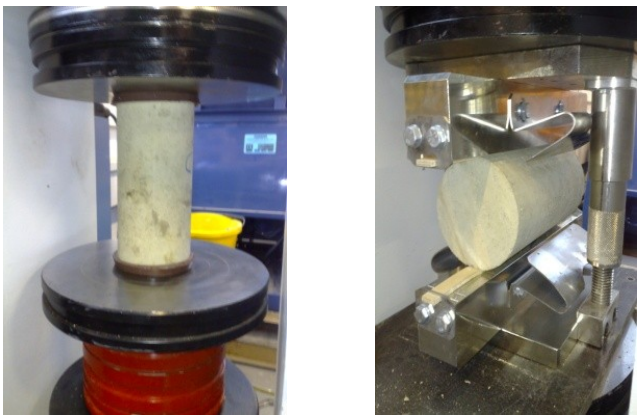

(a) (b)

Figure 3.3—Mechanical tests conducted (a) Compressive Strength test (b) Splitting tensile Strength test

3.5 Factors Influencing Shrinkage

According to Bangash, (1989), shrinkage is considered to a time dependent deformation in concrete which occurs due to the movement of the gel water from within the gel pores. Furthermore, the evaporation process of the drying out of the concrete is sufficient to cause such shrinkage strain. In most cases however, shrinkage due to drying and creep due to stress occur in the same concrete (structure). On the other hand however, the type of cement definitely has an influence on the shrinkage of concrete. The shrinkage process reduces the volume of the unloaded concrete at constant temperature and also induces stress acting over extended time periods (Bangash, 1989). Consequently, these stresses generated are otherwise

reduced by creep and that is the reason the shrinkage phenomenon is taken into account with the problem of creep. Volumetric changes in concrete as a result of exposure to the environment are dependent on relative humidity, temperature, size of the concrete member as well as the characteristics of its constituent materials. Weiss, (1999) simplified driving forces responsible for shrinkage into thermal and moisture related shrinkage. On the one hand, thermal shrinkage occurs when concrete structures undergo temperature reduction (Hossain A. B, 2003), and according to Springenschmidt et al., 1985, it is the response of massive concrete structures to heat generated during hydration. On the other hand likewise, moisture related shrinkage is the response of concrete to internal and external moisture conditions. These two driving forces (i.e. thermal and moisture related) responsible for shrinkage are further investigated in Chapters 5 and 6, on how they influence cracking behaviour in concrete when numerical analysis is applied for simulating the development of stress that eventually leads to cracking in concrete due to shrinkage. In light of this, the temperature evolution is discussed in the next sub-section.

3.5.1 Temperature Evolution

The influence of the evolution of temperature on the material properties of concrete is vital in classifying shrinkage. It is however important to discuss the influence of various conditions on the thermal coefficient of expansion of concrete. The thermal coefficient of expansion varies with moisture content, i.e., it decreases with age but increases with temperature. Indeed, the moisture content and thermal coefficient which is related to the temperature rise or drop due to the hydration reaction in concrete are interrelated. However in the ANSYS FE application package, the shrinkage of concrete is not a recognised tool for simulation. Therefore, since the FEA program in this case, does not support the drying shrinkage loading directly, shrinkage is introduced using a temperature load variable substitution. According to Moon and Weiss, 2006), the length change of a concrete element caused by change in temperature is equivalent to a change in length recorded by the length comparator. Hence, the thermal expansion coefficient will be input for the concrete (since by approximation, the change in length measurement from the free shrinkage test due to thermal expansion is related to the temperature change by a “linear expansion coefficient”) to obtain the same effect as drying shrinkage.

3.5.2 Free Shrinkage Test

Free shrinkage tests were performed on 285mm-long prisms with a 75mm-square cross section in accordance with ISO 1920-8. The prismatic specimens were allowed to dry on all exposed surfaces. Longitudinal length change of the prismatic specimens was monitored using a dial-gage meter mounted in a free shrinkage measurement frame. The dial-gage was attached on the top of the concrete prismatic specimens (see Figure. 3.4).

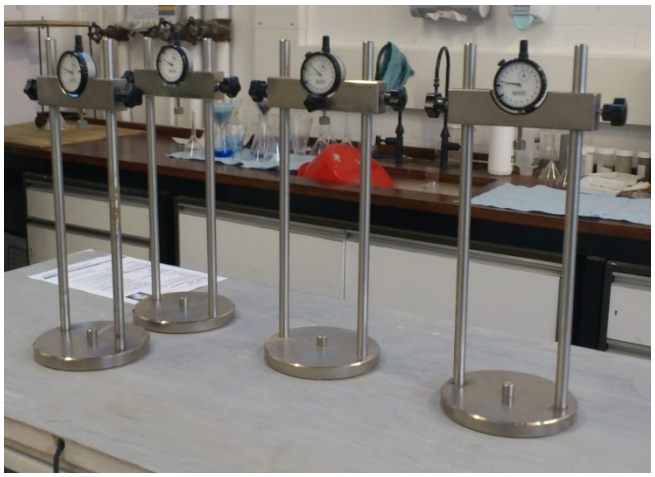

Figure 3.4—Free shrinkage equipment setup with dial gauge meter

The length change was determined using the demoulded reading of the prismatic specimen at 1 day as the reference state. The readings of dial-gage were recorded twice a day and the average was taken as the representative value of that day. Then it was converted into shrinkage strain with respect to the original length of the prismatic specimen, 285mm in this case. Three prismatic specimens were measured for free shrinkage for each concrete mixture to ensure repeatability.

3.6 Fracture Toughness

In this study, fracture toughness of concrete was determined in accordance with RELIM recommendation on fracture of concrete based on the two parameter fracture model (TPFM). (RELIM 1991a) was proposed by Jenq and Shah (1985). Accordingly, elastic modulus (E), critical intensity factor (K_{IC}), and critical crack tip opening displacement ($CTOD_c$) of concrete can be obtained through interpreting results of three-point bending test of notch beam using the TPFM.

3.6.1 Test Equipment

The three point test was conducted using the Instron machine and the supports were provided by the steel rollers. Experimental procedure was conducted using the INSTRON 5584 K4212 hydraulic machine together with a 2810-200 series bend fixture with maximum static load of 250kN as shown in Figure 3.5. The upper roller diameter is 100mm and lower roller diameters are 50mm each. The upper roller is the load acting from the top at the centre of the beam and is readily available with the 2810-200 series bend fixtures. Three-point bending test was conducted with upper pivoting steel while bottom reactions were provided by both pivoting base roller reaction.

Figure 3.5—Fracture test setup with Instron hydraulic machine and a bend fixture

3.6.2 Specimen Setup and Test Procedure

The beams were casted in a steel mould with 100×100×500mm^3 dimensions, with a central notch depth of 33mm, 1/3 of the depth of the beam; the beam was subjected to a stable three-point-bending load. To ensure stability, the test was carried out under crack mouth opening displacement (CMOD) control mode. Subsequently, the values of (CMOD), the load and the deflection at mid span were measured. The initial crack length (a_0) was introduced by using a notch (1/3) of the beam depth (D) respectively. The beam moulds were modified to accommodate different notch lengths and shapes which are inserted mid-point of the beam length (500mm); the notch piece made from structural steel (height - 33.3mm) is introduced into the beam before casting commences so that it fits into the sides of the newly modified

side pieces of the beam. The freshly mixed concrete is then poured and compacted in the beam mould with notch piece inset. To ensure an evenly distributed load area upon application of load by the upper roller the top surface of the demoulded concrete beam was smoothened out. This action was necessary in an event when the top surface of the beam did not appear level. However, if it has a flat smooth loading area, the above action will not be necessary. For this reason and in order to avoid subsequent scenarios in the future with successive testing, the notch position was modified so that the notch piece of size (100 × 33× 6 mm^3) was inserted perpendicular to the inner base surface of the cuboidal steel beam mould. After freshly mixed concrete is placed into the beam mould, and allowed to cure for at least 24 hours, the beam surface (in direct contact with the beam mould) opposite the side where the notch piece is fixed now becomes the surface where the demoulded beam will contact the upper roller of the bend fixture already set up as shown in Figure 3.5. The initial specimen dimensions were measured and recorded including the cross section height, specimen width, notch depth, and specimen weight. The COD gauge was then attached across the notch (i.e. initial crack opening) to monitor crack mouth opening during test operation and was subsequently connected to the transducers on the side of the closed loop hydraulic machine to provide readings as output signal. After zeroing all gauges, the specimen was pre-loaded with approximately 5% of the anticipated load. The test was performed using crack mouth opening displacement (CMOD) as feedback signals throughout the test process. All beams were loaded at a constant rate of 0.0075mm/min. The CMOD increased steadily until the peak load was achieved, at the point when the peak load is achieved, the load began to drop. After reaching the peak the load began to drop and at about 95% of the peak load the specimen was unloaded in CMOD control to a value of approximately 5% of the peak value. The specimen was reloaded again and the same process was again carried out; the load-CMOD graph is plotted from data acquired during the test.

3.6.3 Fracture Properties

Generally, it is widely accepted that two parameters are necessary to characterise the quasi-brittle fracture nature of concrete due to pre-critical crack growth and large process zone (Shah 1997). This study utilised the TPFM which is based on the work of Jenq and Shah (1985) and subsequently recommended by the RELIM committee on fracture of concrete (RELIM 1991a). Similarly, the beam used was tested to determine three material properties namely (*E,* K_{IC} and $CTOD_C$) of which the priority was to acquire the values of *E* for a

stipulated time period. The elastic modulus was calculated after relating the load compliance with the geometrical factors as expressed in equation 2.3.2 from Chapter 2.

3.7 Restrained Shrinkage Testing Method

The test setup typically comprises of a steel ring with four strain gauges, each at the vertex of the ellipse, attached at mid-height of the inner surface of the central restraining steel ring. The strain gauge setup comprised of a data acquisition system in a quarter-bridge configuration, so that a desktop computer running suitable data analysis software compatible with strain instrumentation is able to automatically record the readings of each strain gauge independently as shown in Figure 3.6.

In this study though, an 8-channel strain conditioner input module was found adequately to provide the required resolution of the system and therefore used herein. Concrete was then cast around the steel ring, resulting into a ring specimen being formed, after which was immediately covered with a plastic sheet to prevent moisture loss with water sprayed on its top surface to keep a moisture environment for concrete. Next, the concrete ring specimens were cured in the laboratory environment for one day before their outer moulds were stripped off. They were then immediately sealed with two layers of aluminium tape on the desirable surfaces, either the top and bottom surfaces or the outer circumferential surface to prevent undesirable moisture loss from these surfaces.

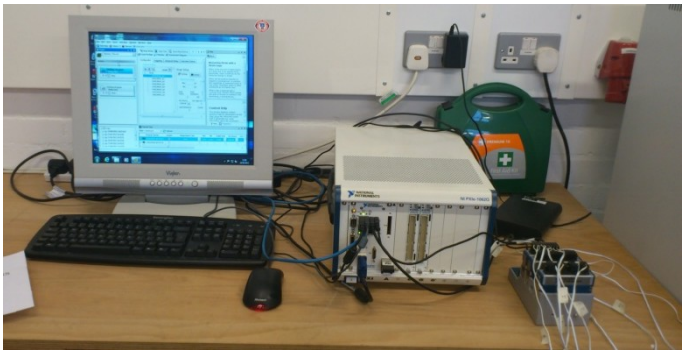

Figure 3.6—Restrained shrinkage test setup

The concrete ring specimen, together with the instrumented central restraining steel ring, was then moved into an environmental chamber with temperature of 23°C and 50% relative humidity for continuing uninterrupted curing with strain of the restraining steel ring monitored throughout the test period for regularity as shown in Figure. 3.7.

Figure 3.7—Temperature and Humidity chamber

3.7.1 Ring Geometry

Initial cracking age and position of concrete are largely dependent on the degree of restraint provided by the central steel ring in restrained shrinkage test. In circular ring test, a higher degree of restraint can be achieved by increasing the steel ring wall thickness, which consequently results in higher stress developed in concrete. In elliptical ring test, although a thicker steel ring can provide a higher degree of restraint to concrete ring surrounding it, the main restraining contribution comes from the elliptical shape of the steel core with the major and minor semi-axes denoted as *a* and *b*, respectively (this is further illustrated in Chapter 4). It is believed that an elliptical shape can generate higher stress concentration than a circular one does. The geometry effect of restraining steel ring on initial cracking age of concrete has not been reported so far in literature. Therefore, it is significant to quantify the effects of geometry of the restraining steel ring on the degree of restraint to concrete ring surrounding it in restrained ring test for assessing cracking tendency of concrete. Steel ring modifications were made in the course of experimental efforts to generate greater effects from the elliptical steel ring on cracking tendency.

3.7.2 Steel Ring Size

The steel ring size is also believed to have a substantial influence on stress development, distribution, actual crack initiation and final propagation. Other efforts (Hossain and Weiss, 2004) have indicated that a thick steel ring will provide greater restraint on the concrete ring

specimen, and hence lead to earlier cracking, but it has also been observed that thicker steel rings are less sensitive (i.e. they have a lower magnitude of the strain measured at the inner curvature surface of the steel ring) compared to thin steel rings. Figure 3.8, illustrates the variation in size thickness in the circular and elliptical steel rings used in this investigation. This study is based on the steel ring with 12.5mm wall thickness for all series of concrete rings tested.

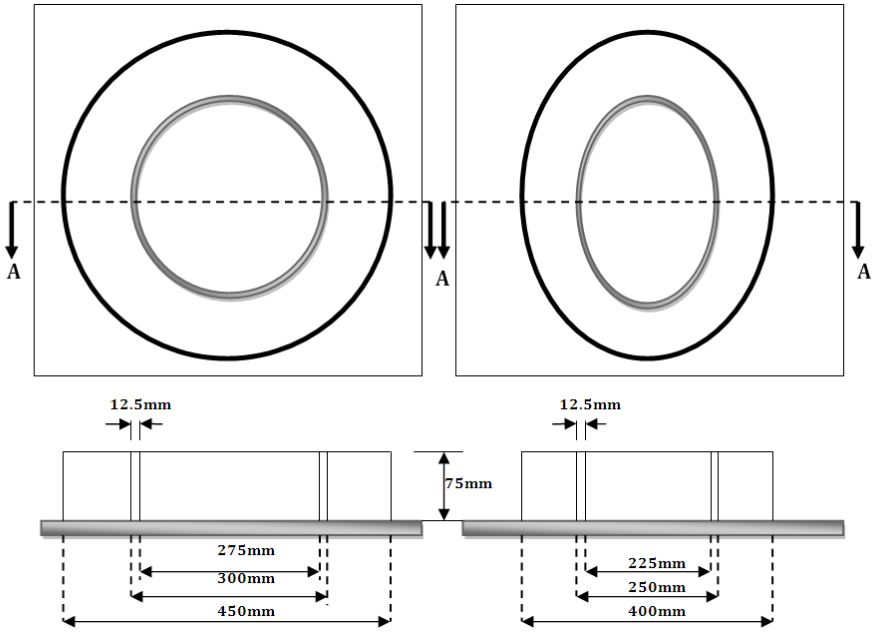

Figure 3.8— Steel ring sizes for circular and elliptical ring using thin steel ring and concrete ring cast around

CHAPTER 4: THIN RING TEST SPECIMENS UNDER RESTRAINT

The aim of this chapter is to present the use of thin elliptical rings to assess cracking potential of concrete, the effect of ring geometry on the cracking behaviour of concrete under restrained shrinkage. Experimental efforts employed using the elliptical ring specimens to provide information for a simple geometry to enable an improved understanding of shrinkage cracking and better evaluation of cracking tendency of concrete by comparing with the circular ring specimens.

4.1 Introduction

The circular ring test method has been used by various researchers for investigating cracking potential of concrete or other cement-based materials under restrained conditions (Bentur and Kovler, 2003). So far, these researches have fundamentally concentrated on three fields namely the effects of concrete mixture compositions, (Li et al., 1999; Passuello et al., 2009; Turcry et al., 2006; Mokarem et al. 2005; Tongaroonsri and Tangtermsiriku, 2009; See et al., 2003) moisture gradients and drying conditions (Moon and Weiss, 2006; Branch et al., 2002; Hossain and Weiss., 2004; Weiss et al., 2000; Weiss and Shah, 2002; Moon et al., 2006; Hossain and Weiss, 2006) as well as ring size and geometry (Moon and Weiss, 2006; Moon et al., 2006; Hossain and Weiss, 2006).

In practice however, the circular ring test is also widely used to determine the effects of material variations on induced tensile stresses in restrained concrete and cracking potential of concrete mixture. These variations may include, aggregate source, aggregate gradation, cement type, cement content, water content, fibre reinforcement, supplementary cementing materials or chemical admixtures. Nevertheless, the test methods recommended by ASTM and AASHTO, both using circular ring specimens, have been noted to have a low degree of restraint, resulting in a fairly long time before the first crack initiates (Bentur and Kovler, 2003; Moon et al., 2006). It is also regarded to have a low cracking sensitivity and not efficient for large amounts of material evaluation (See et al., 2003). In addition, because the degree of restraint is largely dependent on stiffness and geometry of the central restraining steel ring, concrete in a circular ring test may not develop a visible crack if the steel ring is not thick enough, (Hossain and Weiss, 2006) i.e., the restraining stiffness of the steel core is not big enough. Meanwhile, due to geometry effect, there is an equal opportunity of the crack

occurring along the circumference of circular concrete ring, so that it is not possible to predict the exact position of the crack.

Therefore, in a bid to overcome the problems from traditional circular ring tests and to improve the ability of generating a visible crack within a shorter period, a novel elliptical geometry was adopted by He et al., (2004), when investigating the effect of alkali on early-age cracking properties of cement-based materials. They believed that for the sake of promoting crack initiation and determining cracking sensitivity in a shorter period, the elliptical geometry is more effective in evaluating early-age cracking properties for mortar or concrete (He et al., 2004). It was also expected that, unlike the circular ring specimens, the first cracking is concentrated at certain positions depending on the elliptical ring geometry and will largely reduce instruments and resources needed for detecting crack initiation and propagation in the ring test. Nonetheless, their effort did not include comparing cracking tendencies in the circular rings in relation to the newly developed elliptical rings, rather it was believed, without solid scientific evidence, that cracking initiation can be accelerated by the elliptically shaped rings due to stress concentration.

It should be noted however, that the circumferential stress in the elliptical ring specimen is different along its circumference because the degree of restraint provided by the central elliptical restraining steel ring is different along its circumference which is the main difference from the case with a circular ring specimen in which the circumferential stress is uniform along its circumference. Meanwhile, the degree of restraint is believed to be sensitive to the geometry of the central restraining steel ring, especially the major and minor semi-axes of its outer elliptical circumference having the most significant effect on initial cracking age and position of concrete elliptical rings under restrained shrinkage. Because of this, characterising cracking sensitivity of concrete can be achieved within a shorter period so that the new elliptical ring test could become a certified method for replacing the traditional circular ring test for faster assessment of cracking potential of concrete and other cement-based materials.

However, there is no research published so far on comparing circular and elliptical ring test for assessing the relative likelihood of cracking of concrete. This chapter will investigate how the elliptical ring specimen can provide information for a simple geometry to enable an improved understanding of shrinkage cracking and better evaluation of cracking tendency of concrete. From this assessment, a novel, faster and reliable test method is proposed for

assessing cracking potential of concrete which may be attributed to the elliptical geometry adopted. The elliptical ring geometry will help generate new ways of analysing cracking sensitivity of concrete and potentially cracks will concentrate at a certain position, which largely reduces resources required for detecting crack initiation and propagation in rings.

4.2 Experimental Procedure

4.2.1 Ring Geometry

Retrospectively, initial cracking position and age of concrete in ring specimens under restrained shrinkage were associated with the degree of restraint provided by the central restraining steel ring. Although higher degree of restraint can be achieved by increasing the wall thickness of the central restraining steel ring which consequently results in higher stress developed in concrete. The elliptical ring test exhibits a different behaviour. In this case however, the main restraining contribution comes from the geometrical effect of the central steel ring (circular and elliptical as shown in Figure 4.1) with the major and minor principal semi-axes of its external circumference labelled '*a*' and '*b*' respectively, which coincide with the major and minor principal semi-axes of the inner circumference of the concrete ring specimen.

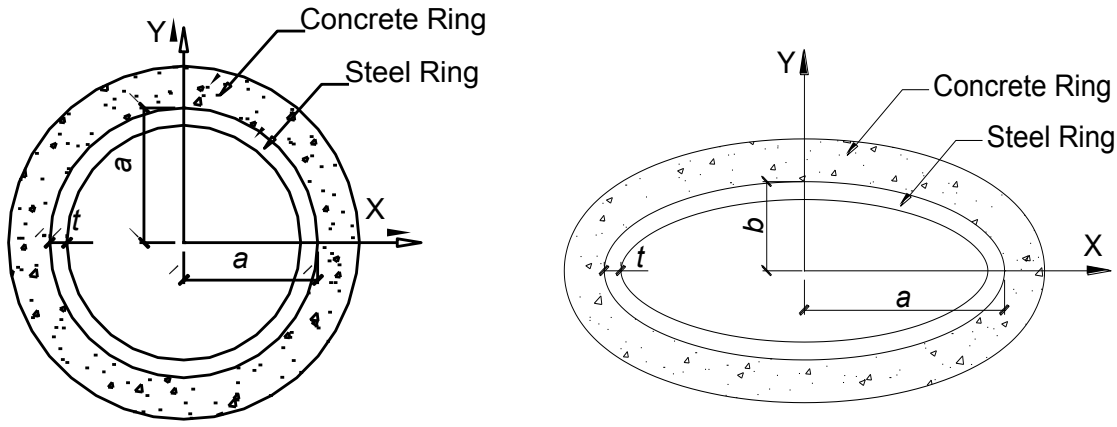

(a) Circular ring (b) Elliptical ring

Figure 4.1—Notations of geometries of ring specimens

In case of an elliptical shape, the degree of restraint along the circumference provided by the central steel core is not uniform due to its geometrical effect. By illustration, the steel ring acts as a restraint to concrete ring surrounding it when concrete shrinks. As a result of this

action, compressive stress is induced in the steel ring, and tensile stress in the concrete ring. Once the developed tensile stress in the concrete ring exceeds the tensile strength of concrete, cracking will be induced.

It should be re-iterated here that this particular study is focused on investigating the mechanism of the elliptical ring test irrespective of materials. It is therefore necessary to quantify how the geometry or shape of the central steel ring changes the degree of restraint to concrete surrounding it, and consequently the age of cracking of concrete in ring test. This is achieved by testing a series of thin circular and elliptical rings, with different geometries, subjected to the same curing environment, under restrained shrinkage. As aforementioned, a standard test method for assessing concrete shrinkage cracking was developed by AASHTO utilising a 12.5mm thick restraining steel ring with outer diameter 305mm surrounded by a concrete ring of thickness 75mm subjected to drying in the circumferential direction with the top and bottom surfaces sealed.

However, according to See and Co, (2003), the circular steel ring used in this test method provides a low degree of restraint thereby prolonging the time for first crack. Therefore, in order to accelerate the occurrence of the first crack so as to shorten the duration of the ring test, a new ring geometry was adopted by ASTM i.e., ASTM C1581/C1581M-09a, by reducing the concrete ring wall thickness from 75 to 37.5mm, which does accelerate cracking in ring specimen to some extent. In this study, a series of circular concrete rings with the inner diameter of $2a$=300mm were tested under restrained shrinkage until cracking occurred in concrete. For elliptical rings, the outer transverse diameter of the restraining steel ring along the major axis remained constant at $2a$=300 mm but the corresponding conjugate diameter $2b$, along the minor axis varied from 120 to 250 mm (refer to Figure 4.2). Table 4.1 summarises the ring specimens tested. This test employed a series of thin rings, with a concrete wall thickness of 37.5 mm, same as that recommended by ASTM C1581/C1581M-09a.

All rings were dried from the outer circumferential cylindrical surface with top and bottom surfaces sealed as shown in Figure 4.3, for the sealed thin specimens the same exposure condition as that recommended by AASHTO PP34-99 and ASTM C1581/C15881M-09a. With such exposed condition, shrinkage of concrete is uniform throughout the height of the ring specimen but not through its radial direction. All the circular and elliptical rings irrespective of their thicknesses had a height of 75mm, while the wall thickness of the central restraining steel ring was 12.5 mm.

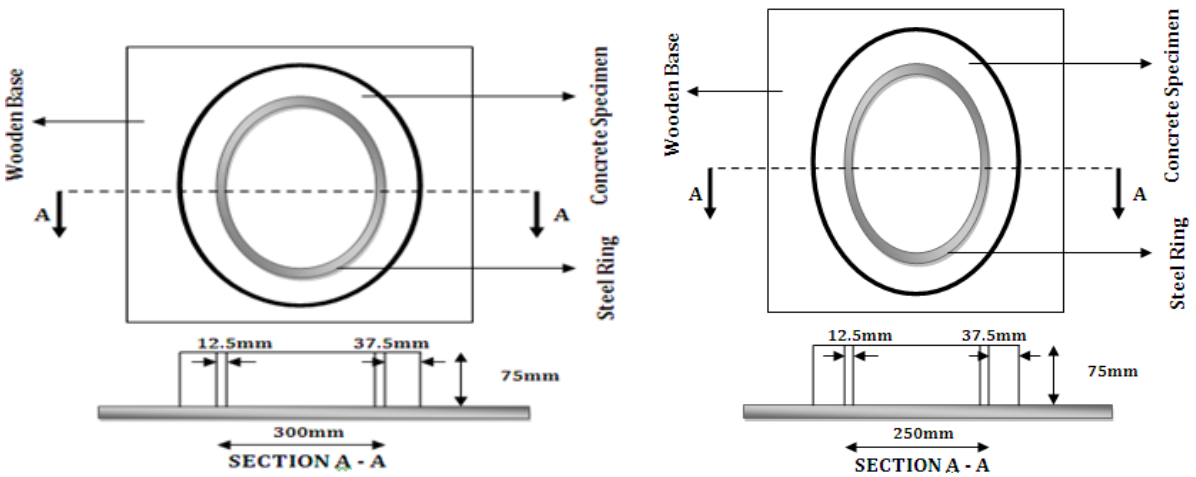

(a) (b)

Figure 4.2—Dimensions of thin ring specimens: a) Circular ring with a=150 mm2; b) Elliptical ring with a×b=150×125mm2

Table 4.1—Thin ring specimens tested

Ring Type	Steel ring core: $a \times b$(mm×mm)	a/b	Steel ring thickness(mm)	Concrete ring thickness(mm)
Circular ring	150×150	1	12.5	37.5
Elliptical ring	150×125	1.2	12.5	37.5
Elliptical ring	150×100	1.5	12.5	37.5
Elliptical ring	150×75	2	12.5	37.5
Elliptical ring	150×60	2.5	12.5	37.5

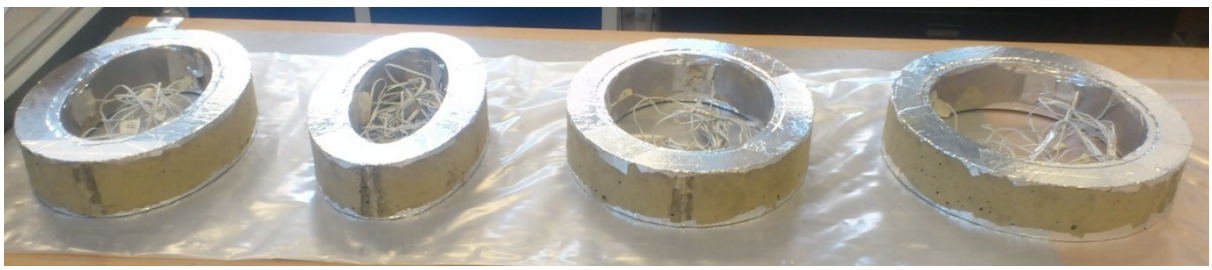

Figure 4.3—Elliptical ring specimens with top and bottom surfaces sealed

It should be noted however that the restrained ring test is not intended to measure a fundamental material property of concrete. Rather the ring test assesses the material's

response (i.e. potential of cracking) to specific stimulus (e.g., drying) under specific conditions (e.g., specimen size, drying direction, and degree of restraint). However, it can be used for relative comparison purpose for assessing cracking potential of concrete and other cement-based materials and the effects of individual ingredients on cracking potential of concrete. It can also be used for aiding in the selection of concrete mixtures that are less likely to crack. Furthermore, no one ring geometry or external stimulus can be used to simulate all possible restrained conditions that may be encountered by concrete in the field. It is therefore of great importance that procedures, like those published by AASHTO and ASTM for circular ring tests, are developed to enable the elliptical ring test to be interpreted for a variety of applications (Moon et al., 2006).

4.3 Restrained Ring Test

The test setup typically comprises of a steel ring attached to a wooden base as shown in Figure. 4.4, with four strain gauges, attached at mid-height of the inner cylindrical surface of the central restraining steel ring which has already been elaborated in Chapter 3. The strain gauges were then connected to the data acquisition system which then records and decimates the data measured (see Figure 4.5 and Figure 4.6).

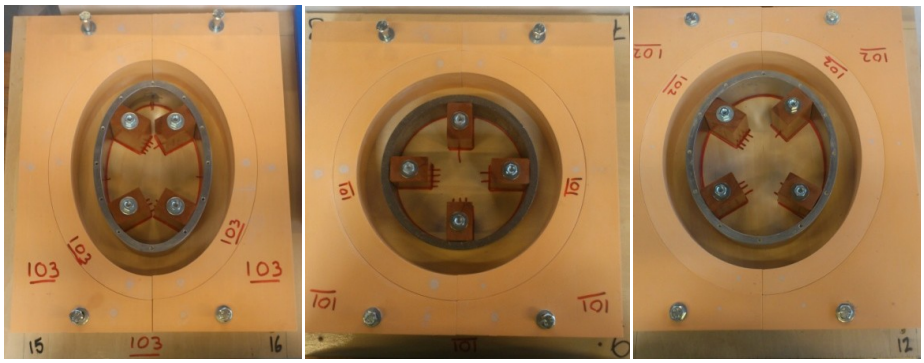

Figure 4.4—A series of steel ring setup coupled to base for testing

Figure 4.5—Ring specimens in mould after concrete placement

As concrete dries, the concrete ring tends to shrink with the steel ring restraining its shrinkage. Consequently, tensile stress is developed in the concrete ring along the circumferential direction which may lead to cracking in the concrete if the tensile stress exceeds the tensile strength of concrete.

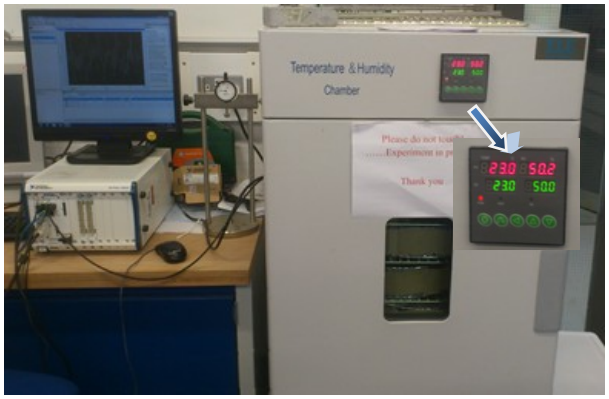

Figure 4.6—Ring specimens connected to the data logger and under testing in environmental chamber

4.4 Strain Measurement and Representation

The measured strain from the restraining steel ring upon crack initiation in concrete is presented in Figure 4.7. It can be seen that the measurement indicates a gradual increase with age followed by a sudden and significant drop in strain. As concrete dries, its shrinkage increases with age.

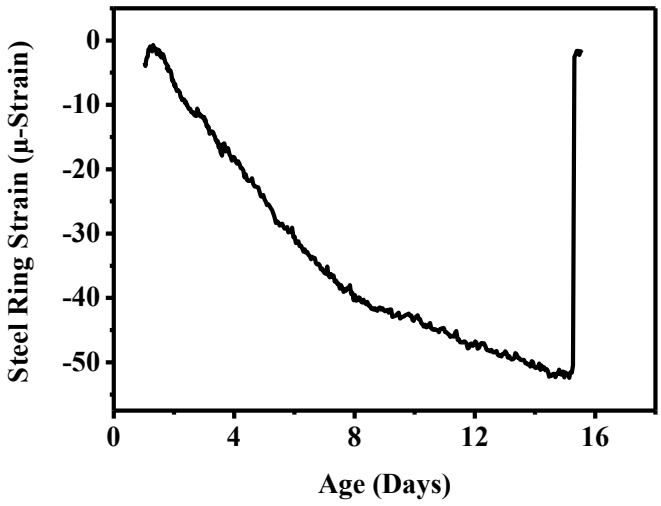

(a) Circular ring a = 150mm

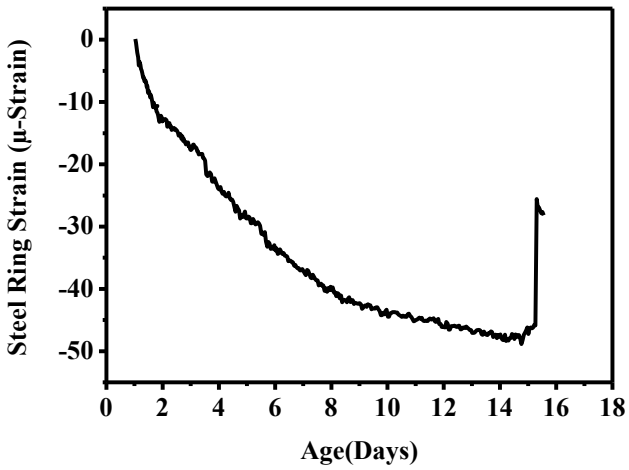

(b) Elliptical ring with $a \times b$=150×125mm^2

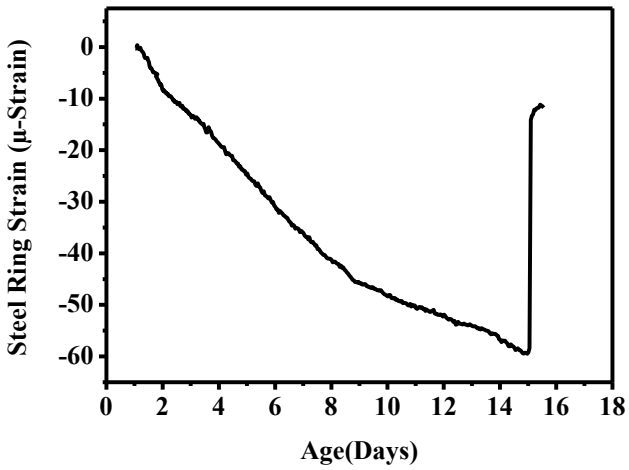

(c) Elliptical ring with $a \times b$=150×120mm^2

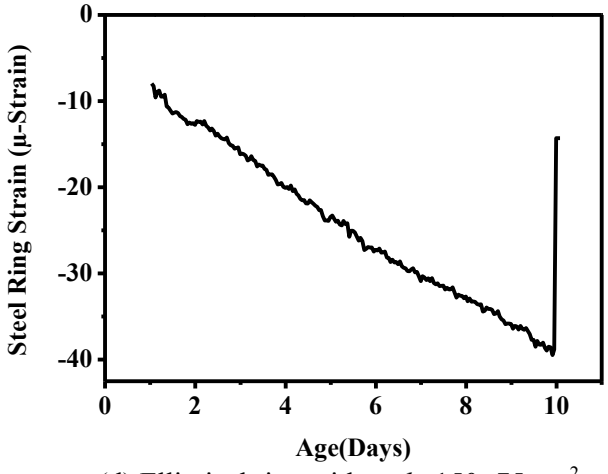

(d) Elliptical ring with $a \times b$=150×75mm^2

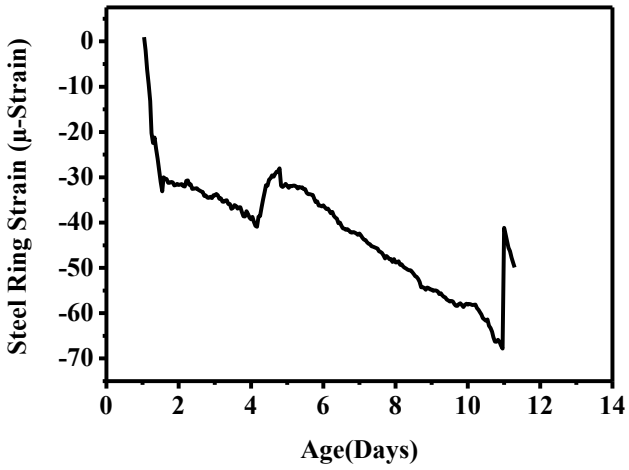

(e) Elliptical ring with $a \times b$=150×60mm^2

Figure 4.7—Strain development with age recorded in restrained ring test

The increasing concrete shrinkage is restrained by the central restraining steel core, thus an increasing pressure is imposed on the central steel core by the surrounding concrete ring. Consequently, compressive stress is developed in the steel ring which becomes greater and greater and is reflected by the increasing strain with age picked by the strain gauges. Simultaneously, tensile stress is developed in the concrete ring which also increases with age. Once the tensile stress exceeds the tensile strength of concrete, crack initiates and the pressure imposed on the central steel ring is released resulting in the stress thus strain suddenly drops in the central restraining steel ring.

Effectively, the sudden drop in steel strain in one, two, three or all four strain gauges signalled that crack initiated which is the same technique as that recommended by ASTM C 1581-04 and AASHTO PP34-99 for crack detection in their standard circular ring test. Nevertheless, stress developed prior to the occurrence of visible crack can be attributed to the level of restraint, suggesting that there is a likelihood of steel ring restraining effect on crack initiation. Cracking can be detected immediately after it initiates because of the high sensitivity of strain gauges. But it takes time for the crack to propagate throughout the concrete ring wall, so it is believed that the sudden strain drop picked by strain gauges indicates crack initiation, as strain gauges are very sensitive, rather than the crack eventually propagating through the ring wall, which is supported by the final crack pattern of rings observed from experiment in this study and will be discussed in details later. As

aforementioned, concrete ring specimens were also visually examined at regular basis alongside strain monitoring for cracking. But it should be noted that visual observation only gives the age when the crack penetrates through the wall of the concrete ring reaching the exposed outer circumferential surface and not the day cracking was initiated.

4.5 Effects of Ring Geometry on Cracking in Thin Ring Specimens

It can be found from experimental results (see Table 4.2) that thin ring specimens with shorter minor axes usually cracked earlier than those with longer minor axes. For instance, the elliptical rings with $a \times b$=150×75mm^2 cracked on average at age of 10 days, compared to those with $a \times b$=150×125mm^2 and $a \times b$=150×100mm^2 which both cracked at the age of 14.5 days respectively. It can also be seen that the cracking age of the circular ring with a=150 mm and the elliptical rings with the geometry factor a/b, (the ratio between the major and minor semi-axes less than 2), in this case those elliptical rings with $a \times b$=150×125mm^2 and $a \times b$=150 ×100mm^2, were very close, i.e. all at 14.5days.

Table 4.2—Recorded cracking age for thin concrete ring specimens

Ring Geometry: a×b (mm×mm)	Exposed Surface	Crack Age (days)	Average (days)
150×150	Outer Circumferential Surface	15 14	14.5
150×125	Outer Circumferential Surface	15 14	14.5
150×100	Outer Circumferential Surface	15 14	14.5
150×75	Outer Circumferential Surface	10 10	10.0
150×60	Outer Circumferential Surface	11 15	13.0

The results further suggests that the ratio between the major and the minor semi-axes (i.e. geometry factor) of the elliptical ring is a contributing factor affecting the maximum circumferential tensile stress, thus cracking age of concrete rings when subjected to restrained shrinkage. According to experimental results presented in Table 4.2, thin elliptical rings with appropriate geometry, in this case the geometry factor a/b>2, can cause crack initiating earlier than the circular ones. They are therefore capable of accelerating ring test to assess the relative likelihood of cracking of concrete mixtures. Consequently, as a result of the

favourable geometrical effect, higher stress concentration occurred at a certain position in elliptical rings which are usually close to the vertex along its major principal axis as expected and shown in Figure 4.7 in which the three thin elliptical rings with b=60, 75 and 100mm (from left to right) all cracked in the region of the major principal axis. Therefore it can be concluded that ring geometry has a significant effect on cracking age and crack position of concrete in restrained elliptical rings. It should be noted here again that these concrete rings were sealed on the top and bottom surfaces in the course of testing and a part of the aluminium tape was stripped off from ring surfaces after testing to examine the crack patterns on the rings as shown in Figure 4.8.

(a) (b) (c)

Figure 4.8—Similar positions of cracking in thin elliptical rings (a) with a×b=150×60mm^2; (b) with a×b=150×75mm^2; and (c) with a×b=150×100mm^2

The elliptical rings tested according to geometry size exhibited similar crack patterns at about the same position as shown in Figure 4.9; suggesting that with repeatability in testing rings there was a common trend which further emphasises the reliability of results. Elliptical rings with b=60, 75 and 100mm all cracked in the region of the major principal axis and are marked accordingly. Hence the sensitivity of the elliptical ring is thus highlighted in comparison with the circular ring which is believed to be less sensitive. Conversely, the circular ring with 2a=300 mm showed one crack propagating through the concrete wall thickness in the time frame of testing, but another crack propagated after the test was stop making two through cracks (i.e. one before the test was stopped and the other after) as shown in Figure 4.10, in light of the fact that it is a circular geometry and stresses are believed to be uniformly distributed along the circumferential surface, cracks can initiate and subsequently propagate at any position in the concrete ring which is clearly illustrated.

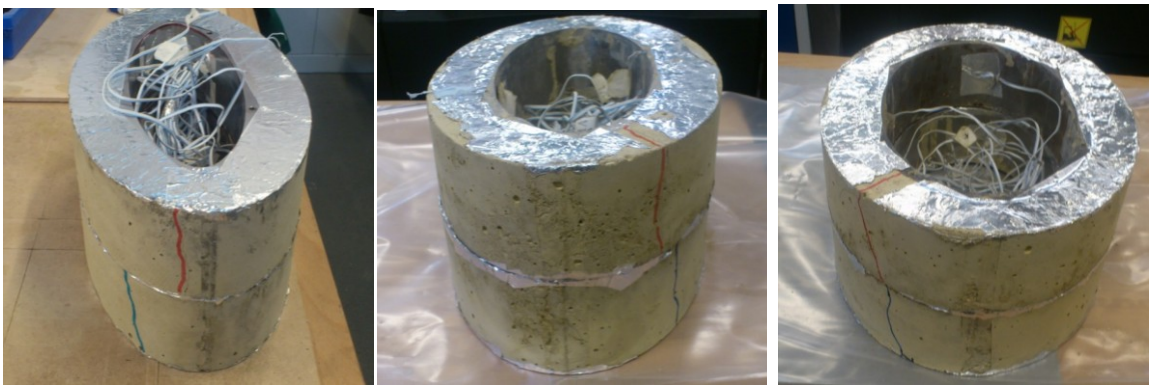

(a) (b) (c)

Figure 4.9—Same sized thin concrete elliptical rings illustrating crack positions (a) with $a \times b$=150× 60mm^2; (b) with $a \times b$=150×75mm^2; and (c) with $a \times b$=150×100mm^2

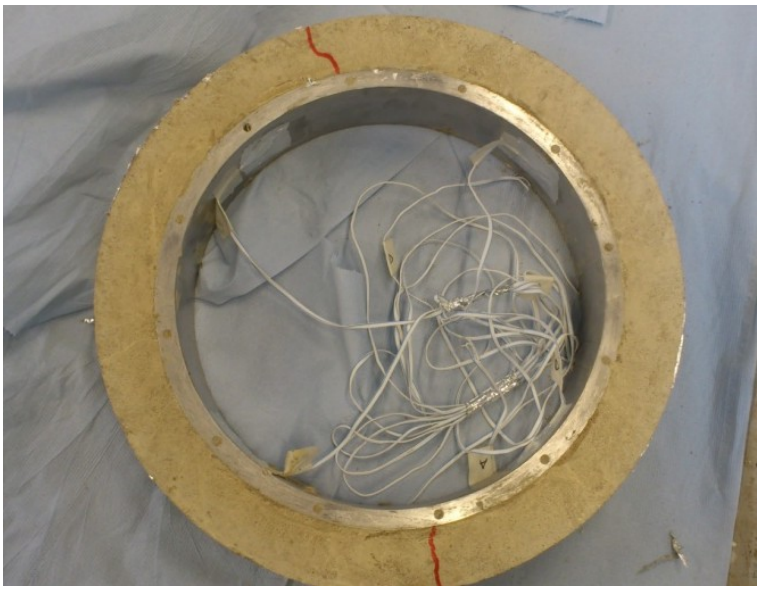

Figure 4.10—Crack position in circular rings with 2a=300mm

With further observation, other cracks were observed to have propagated through the wall on some of the elliptical ring specimens after the test was terminated see Figure 4.11; the same as the circular ones. These cracks were located at the same region as the first cracks that initiated along the major principal axis. The section labelled (A) are the first cracks that propagated through the wall thickness of the elliptical ring before the test was stopped and (B) represents the second crack that propagated after the first (i.e. A) following the test execution; this procedure was always carried out by visual observation.

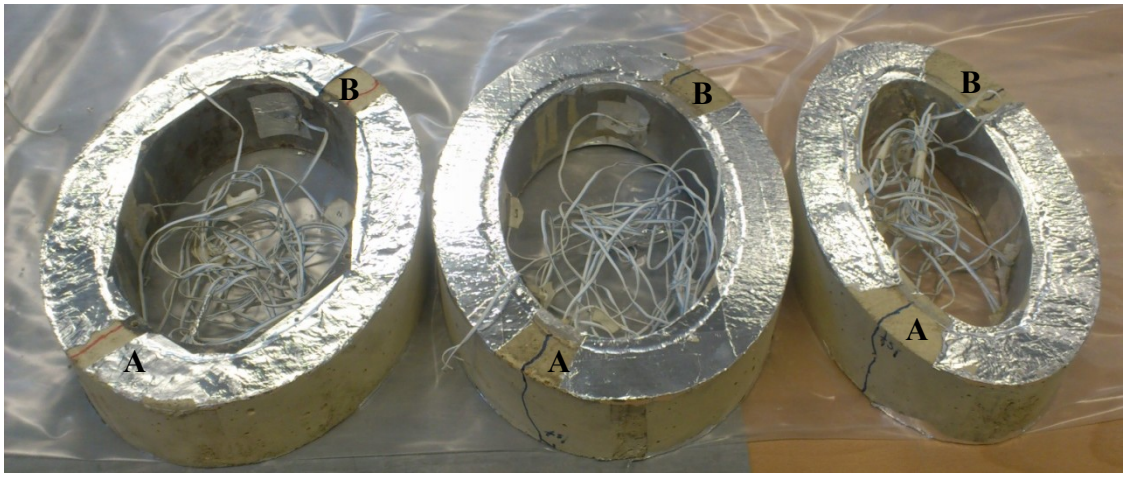

Figure 4.11—Crack position-from left to right: - $a \times b$ =150×100mm^2 (*2); $a \times b$ =150×75mm^2: concrete thickness=37.5mm

4.6 Crack Propagation in Thin Elliptical Rings

Cracks were carefully examined across the inner circumference, alongside the top and bottom surfaces of the thin elliptical ring specimens, after test was completed and the aluminium tape and the central steel rings were stripped off the concrete ring. As shown in Figure 4.12a & b, there were notable cracks in the thin elliptical ring with $a \times b$=150×125mm^2 on its inner circumferential surface along the major principal axis. I and II highlights the cracks that initiated without propagating while III illustrates more vividly crack that propagated through the concrete wall as shown in Figure 4.12b.

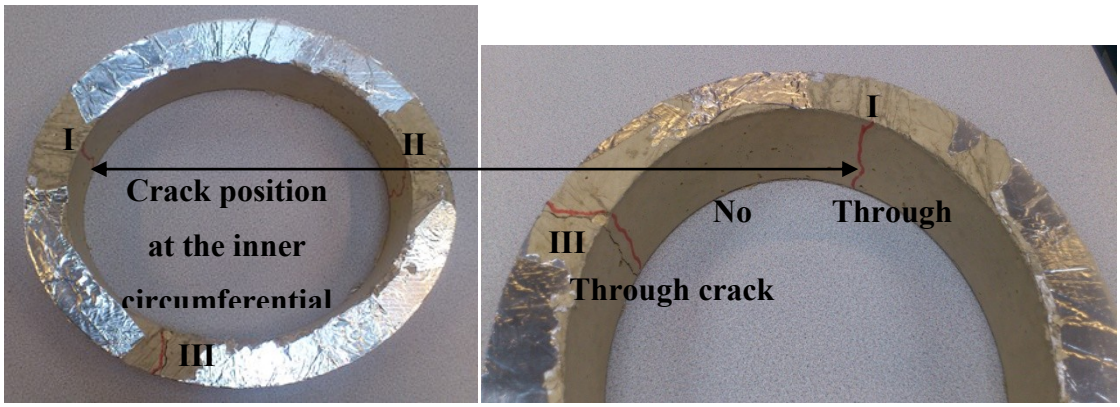

(a) (b)

Figure 4.12—Final crack positions in thin elliptical ring with $a \times b$=150×125mm^2

Cracks were also examined on the thin elliptical ring specimens with $a \times b$=150×100mm^2; $a \times b$=150×75mm^2 and $a \times b$=150×60mm^2 (Figure 4.8) which occurred very close to the vertex

in the region where maximum circumferential tensile stress is expected. However, with further observation, these cracks seen at the inner surface along the major principal axis (i.e. I and II) did not manage to propagate through the concrete ring wall to reach the outer circumferential surface neither did it appear across the top surface of the concrete ring specimen as is usually the case when crack propagates. It is also possible that the crack actually does not propagate fully through the concrete ring wall. In the course of the test, cracking could not be observed from the outer circumferential surface of the ring as they did not propagate through to the outer surface. In the Figure 4.13 other sized elliptical rings with $a \times b$=150×60mm^2; $a \times b$=150×100mm^2 and $a \times b$=150×25mm^2 are presented with cracks initiating from the inner circumferential surface (i.e. at I) which did not manage to propagate through the thin concrete wall thickness.

(a) (b) (c)

Figure 4.13—Crack positions in different sized thin elliptical ring with $a \times b$=150×60 mm^2 $a \times b$=150×100mm^2 and $a \times b$=150×125mm^2

It was found from this study that cracks were usually noticed by visual observation one day after being detected by strain gauges for thin ring specimens. This further ascertained that the abrupt drop in measured strain detected by strain gauges indicated that crack initiated rather than it propagating throughout the ring wall because crack can only be visually observed after propagation takes place through the wall of the ring specimen and subsequently takes time for it to propagate throughout the ring wall after it initiates. In the case of the thin rings, due to geometry effect, stress concentration may take place at a specified position which is usually close to the vertex along the major axis at the inner circumferential surface of the elliptical

concrete ring. Therefore cracks are more likely to initiate at these regions. Subsequently, other cracks may initiate and propagate at areas along the minor axis further away from the vertex as a result of stress redistribution.

4.7 Summary

In this chapter, thin elliptical ring specimens were adopted for assessing cracking potential of concrete under restrained condition together with thin circular rings. Cracking age, cracking features and final cracking patterns of a series of thin elliptical and circular rings were examined for discovering the mechanism of using elliptical thin ring specimens for assessing cracking potential of concrete and other cement-based materials. The approach presented in this chapter can be extended in determining the effects of concrete variations and the degree of restraint on cracking tendency of concrete. Based on these results analysed, the following conclusions were drawn:

1. Thin elliptical rings with a wall thickness of 37.5mm as recommended by ASTM C1581/C1581M-09a, can increase the likelihood of crack initiation in concrete specimens at expected positions and are seen to crack at an earlier age with a decrease in minor principal axis.

2. The abrupt drop observed from steel strain recorded during restrained ring test indicated crack initiation and was usually one day for thin ring specimens before visible cracking was observed.

3. In restrained thin elliptical rings, crack initiated at the vertices on the major axis of the inner elliptical circumference and propagated from the inner circumference to the outer one.

4. Thin elliptical rings were observed to have cracks on the inside surface of the concrete ring along the major principal axis as would have been expected but without propagating through the concrete ring wall. As such, it is possible that some cracks initiate but do not necessarily propagate fully through the concrete ring wall.

CHAPTER 5: NUMERICAL MODEL FOR THIN RING SPECIMENS

In the previous chapter, an elliptical ring test method was proposed to assess the cracking potential of concrete based on experimental efforts. In this chapter, a numerical model is presented for predicting stress evolution and cracking age in concrete ring specimen subject to restrained shrinkage to underpin the mechanism of the proposed elliptical ring test. Assuming shrinkage in concrete results from a fictitious temperature drop applied on it, crack initiates when the maximum circumferential tensile stress developed in a concrete ring exceeds the corresponding concrete tensile strength. To implement the proposed numerical method, free shrinkage test was carried out to obtain the age-dependent relationship between free shrinkage and Surface area-to-volume ratio (A/V), which was further converted into the age-dependent relationship between fictitious temperature drop and A/V ratio of a concrete element. The proposed method was then applied to simulate stress development and crack initiation based on maximum tensile stress cracking criterion in a range of circular and elliptical concrete ring specimens subject to restrained shrinkage. The age of first cracking by the numerical model exhibits a favourable comparison with the experimental observations, which verifies the proposed numerical model. The validated numerical model was then employed to predict cracking age of thin ring specimens with various geometries, which were not necessarily tested in this project, to investigate the effect of ring geometry and restraining stiffness on cracking pattern and cracking age of the concrete ring specimens under restrained shrinkage to further explore the mechanism of the proposed elliptical ring test.

5.1 Introduction

Early-age cracking can often be observed in concrete when low fracture resistance is experienced, particularly in flat concrete elements and structures, such as industrial floors, concrete pavements and overlays, with large exposed drying surface area-to-volume (A/V) ratio. When volume change of concrete from autogenous, drying and/or thermal shrinkage is prevented, residual stress will be developed and crack may occur once the tensile stress exceeds the tensile strength of concrete. ASTM C 341 (2012) adopts 400 mm long and 100 mm square concrete prisms with all surfaces exposed for drying to assess free shrinkage of concrete through monitoring the change of their longitudinal length. Generally, drying shrinkage of a concrete element is largely dependent on its A/V ratio. So, in order to directly

use the measured free shrinkage conforming to ASTM C 341 (2012) through prismatic specimen in analysing other concrete elements or structures, in principle, those concrete elements and structures should have the same A/V ratio as that of the prism recommended; it should be noted that it is not always able to achieve this in practice. Furthermore, although free shrinkage measurements are useful in comparing different mix proportions, they do not provide sufficient information to determine how concrete will crack in service (Shah et al., 1998a).

Therefore, in order to predict the initial cracking position, He et al. (2004) assumed that the elliptical concrete ring specimen is subjected to a uniform internal pressure, which is the same assumption as that taken in the study of shrinkage cracking in a circular ring specimen by many other researchers (Kovler et al., 1993; Shah et al., 1998b; Hossain and Weiss, 2004). However, due to geometrical effect, the deformation of the elliptical steel ring is not uniform along its radial direction due to concrete shrinkage, so that it is believed that the uniform internal pressure assumed will not apply to elliptical ring specimens in the restrained shrinkage test. To further evaluate stress development in elliptical rings, a numerical model was developed to simulate the behavior of elliptical concrete ring specimens under restrained shrinkage. A series of circular and elliptical ring specimens were tested and subjected to restrained shrinkage to validate the numerical model in predicting initial cracking age. The validated numerical model was then used to investigate the effects of geometry of an elliptical ring on the circumferential stress in concrete under restrained shrinkage. Moreover, by comparison with circular ring specimens, it has been found that crack can occur at earlier ages in elliptical ring specimens if appropriate elliptical ring geometries are adopted and crack location can be predicted reasonably well.

5.1.1 Drying Direction in Concrete Rings

Firstly, the influence of drying direction will be assessed. Concrete ring specimens are exposed to drying from the outer circumferential surface but with the top and bottom surfaces sealed. This agrees with the drying condition suggested by the standard procedures ASTM C 1581-04 and AASHTO PP34-99. In ring specimens that dried from the outer circumferential surface, shrinkage is uniform throughout the height of a specimen, but not through the radial direction. Albeit, since the specimen loses the majority of water in the circumference (i.e. the drying surface), the stresses are highest at this drying face (Weiss and Shah, 2001; Moon et al., 2004; Moon and Weiss, 2006), which eventually leads to a complicated stress distribution

that changes over time. Conversely, the drying condition considered for numerical analysis will include three cases which will be further elaborated in sub section 5.4.1. However, according to Hossain and Weiss, (2006), specimens exposed to drying from the top and bottom surfaces are believed to be preferred when compared to circumferential drying, since it allows the concrete to be sufficiently thick to enable large aggregate and fibre reinforced concrete to be tested. On the other hand, top and bottom surface drying results in uniform shrinkage along the radial direction but not in the height direction. Consequently, the residual stresses that develop in these cases are the highest at the inner surface of the concrete ring. Details have already been discussed in chapters 2 and 3.

5.2 Experimental Procedure

The following section provides an overview on the measured age-dependent mechanical and physical properties of concrete used for making the concrete ring specimens tested in this project. These mechanical and physical properties are to be used in numerical simulation of the concrete ring specimens to be conducted in this chapter.

5.2.1 Mechanical Properties

The mechanical properties of concrete, such as compressive strength (f_c), and tensile strength (f_t), were tested at different ages using cylindrical samples of 100mm diameter and 200mm length. While Elastic modulus (E) was tested at different ages using notched beam specimens, 100mm×100mm×500mm.

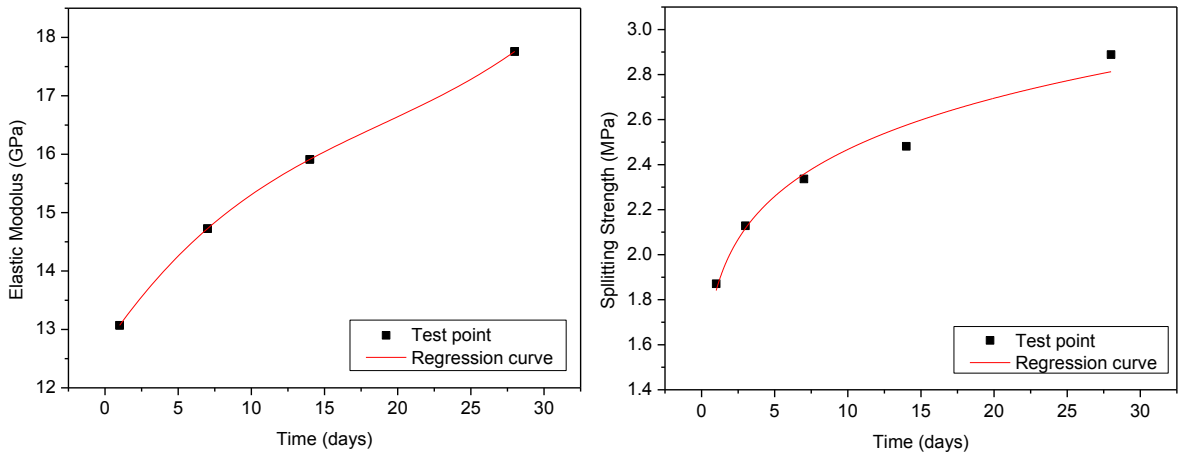

(a) (b)

Figure 5.1—Age-dependent regression (a) Elastic modulus of concrete and (b) Splitting tensile strength of concrete

The mix proportions for the concrete mixture investigated in this study were: 1:1.5:1.5:0.5 (cement: sand: coarse aggregate: water) by weight which represents a therapy of normal strength concrete. After obtaining results from testing, regression analyses were then conducted on these data to obtain continuous equations to ideally represent the age-dependent mechanical properties such as elastic modulus and tensile strength (i.e. E and f_t) and thus presented in Figure 5.1. Each data in this case is the average of the same property of three specimens tested at the same age and regression analyses were based on the available data rather than the average value shown in Figure 5.1.

Following, Eq.5.1 is found to be able to predict the age-dependent elastic modulus E (in GPa) of concrete at early ages.

$$E(t) = 0.0002t^3 - 0.0134t^2 + 0.3693t + 12.715 \quad (t \leq 28) \quad \ldots\ldots\ldots\ldots\ldots\ldots \quad (5.1)$$

While splitting tensile strength, f_t, (in MPa) can be predicted using Eq. 5.2.

$$f_t(t) = 1.82t^{0.13} \quad (t \leq 28) \quad \ldots\ldots\ldots\ldots\ldots\ldots \quad (5.2)$$

Where, t is the age of concrete (in days) in both equations (5.1) and (5.2). It should be noted at this point that the values E and f_t for concrete at other ages were not directly measured through experimental efforts but from Eq. 5.1 and 5.2.

5.2.2 Free Shrinkage

Free shrinkage tests were performed on 285 mm-long prisms with a 75 mm-square cross section in accordance with ISO 1920-8. This study considered that concrete shrinkage depends on the value of A/V (Neville (1996), hence four different exposure conditions were investigated, i.e. all surfaces sealed, all surfaces exposed, two sided surfaces sealed and three sided surfaces sealed respectively as shown in Figure 5.2, with the corresponding A/V ratio being 0, 0.00605, 0.0267, and 0.0133 mm^{-1}, respectively. A doubled-layer of aluminum foil tape was used to seal the desired surfaces not intended for drying. Longitudinal length change of the prismatic specimens was monitored using a dial-gage meter mounted in a free shrinkage measurement frame. The dial-gauge meter with the resolution of 0.001mm was attached on the top of the concrete prismatic specimen and eventually mounted on the free shrinkage test ring and transferred into the controlled environmental cabinet set to temperature of 23°C and 50% relative humidity, refer to Figure 5.3. The length change was determined using the reading of the de-moulded prismatic specimen at 1 day age as the reference point. The readings of dial-gage were recorded twice a day and the average was

taken as the representative value of that day for 28 days. Then it was converted into shrinkage strain with respect to the original length of the prismatic specimen, 285 mm in this case. This procedure is carried out experimentally in order to obtain the fictitious temperature field which was adopted to represent the effect of shrinkage concrete in this study; further details are enumerated in the section 5.3.

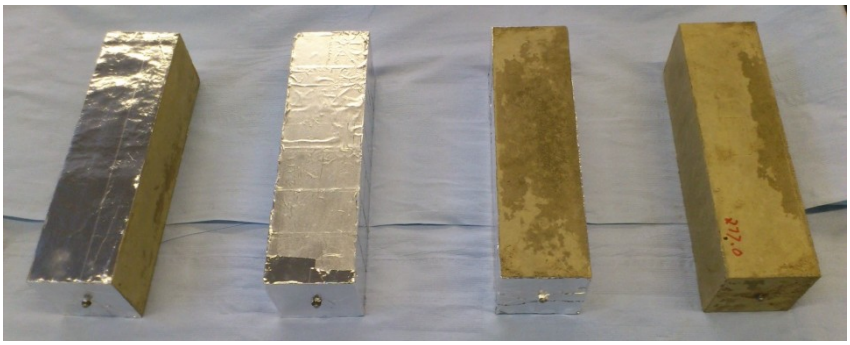

Figure 5.2—Prismatic specimens prepared for testing

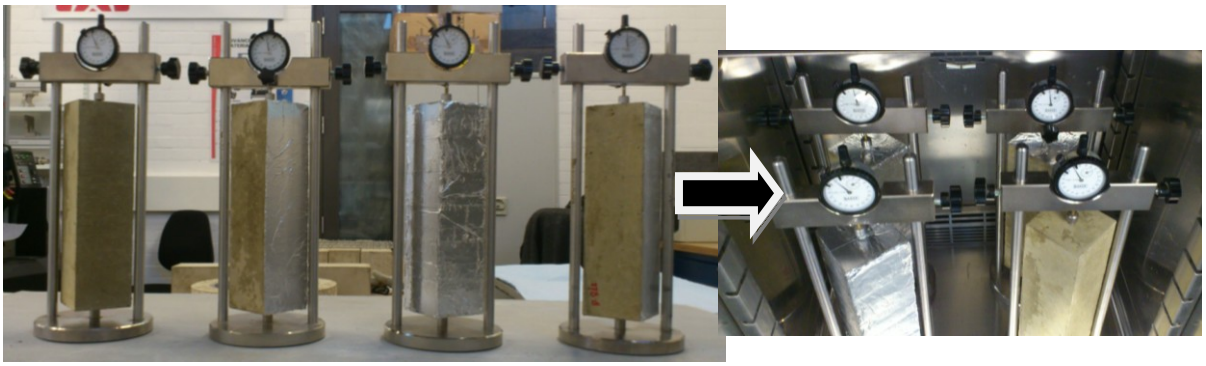

Figure 5.3—Concrete prismatic specimens mounted and placed for free shrinkage test

5.3 Numerical Model and Validation

In this study, a circular concrete ring with an inner radius a=150 mm, subject to restrained shrinkage, was analyzed and the maximum circumferential tensile stress at various ages up to cracking in the concrete ring was calculated by the numerical model. Correspondingly, the analysis was also carried out for elliptical rings with the inner major radius a equal to 150mm but the inner minor radius b varied from 50 to 150 mm see Table 3.1. All the circular and elliptical rings had a height of 75 mm, while the wall thickness of the restraining steel ring and concrete ring was kept constant as 12.5 and 37.5 mm, respectively. It should be noted that these values are nominal for elliptical rings.

Table 5.1—Geometry of central restraining steel ring

Ring Type	Major axis a (mm)	Minor axis b (mm)	a/b
Circular ring	150	150	1
Elliptical ring	150	125	1.2
Elliptical ring	150	100	1.5
Elliptical ring	150	75	2
Elliptical ring	150	60	2.5
Elliptical ring	150	50	3

5.3.1 Numerical Modeling

Early age cracking sensitivity has become a universal phenomenon associated with mechanisms which are related to microstructural changes, chemical reactions, taking place during the first few days after mixing the binder (cement) and water. Volumetric change of concrete is usually ascribed to two broad categories of effects: thermal shrinkage and drying shrinkage (Hossain (2003); Weiss (1999)). Thermal shrinkage in concrete is as a result of hydration and/or the changes of environmental temperature. Drying shrinkage results from internal and external moisture movement in concrete. There is an obvious difference between thermal and drying shrinkage with the latter depending much more on A/V ratio. When a concrete element is exposed in a drying environment without any restraint, its length will change, a phenomenon often referred to as free shrinkage which does not cause any internal stress.

As aforementioned, shrinkage is an intrinsic property of concrete which is not usually possessed by many other engineering materials. In many finite element (FE) codes, there is no direct entry for shrinkage being included as a material property for concrete. Therefore, in this study, free shrinkage of a concrete element is assumed to be caused by a fictitious temperature field applied on it which causes the same value of length change to the concrete element as free shrinkage does. Furthermore, by introducing coefficient of linear expansion of concrete, which is considered as a constant of $10\times10^{-6}/℃$, the relationship between free shrinkage and fictitious temperature field can be established for a concrete element at various ages. So, for a concrete prism specimen subject to drying, the relationship of fictitious temperature drop vs.

concrete age can be established by measuring the change of the longitudinal length of a concrete prism with respect to concrete age in the free shrinkage test.

Moreover, shrinkage of a concrete element caused by drying is mainly dependent on its A/V ratio (Almudaiheem and Hansen, (1987); Neville, (1996); Hossain, (2003)). Therefore, there is another assumption adopted in the numerical model proposed in this study, which is the value of free shrinkage being the same for specimens with the same A/V ratio even with different geometries, i.e., they will be subject to the same fictitious temperature field acting on the specimens with the same A/V ratio but maybe different geometries. By applying this assumption to a concrete ring specimen in restrained shrinkage test, the ring specimen is considered to be put in the same fictitious temperature field as the prism specimen with the same A/V ratio.

In conclusion, for a ring specimen with the same A/V ratio as that of a concrete prism, its fictitious temperature drop-age relationship can be established based on the free shrinkage-age relationship obtained from free shrinkage test results of prismatic concrete specimens. The fictitious temperature field acting on the ring specimen makes concrete shrink. Once the shrinkage is restrained by the inner steel ring, stress will develop in the concrete ring surrounding it. When the circumferential tensile stress caused by the fictitious temperature field exceeds the tensile strength of concrete at a specific age, crack will initiate in the concrete ring specimen. In summary, the following approaches were included in developing the numerical model for predicting the cracking age in restrained ring specimen subject to drying.

1. Test mechanical properties, such as uniaxial compressive strength f_c, splitting tensile strength f_t and elastic modulus E, of concrete cured at 23℃ and 50% RH, the exposure environment where the ring test was conducted as suggested by AASHTO PP34-99.
2. Measure free shrinkage of concrete prisms with the dimensions of 285 mm in length and 75 mm square in cross section, conforming to ISO 1920-8, under the exposure environment of 23℃ and 50% RH. In order to simulate different exposure conditions with different A/V ratios, four different cases were investigated in this study in free shrinkage test, which are all surfaces sealed, all surfaces exposed, two side surfaces sealed and three side surfaces sealed with the corresponding A/V ratio being 0, 0.0605, 0.0267, and 0.0133 mm^{-1}, respectively.

3. Calculate the fictitious temperature field, i.e. temperature drop, at different ages for the four exposure cases based on the free shrinkage test results of concrete prisms with the same A/V ratios under the same drying environment in this case 23℃ and RH 50%.
4. For a given concrete ring specimen, calculate its A/V ratio and derive the relationship between fictitious temperature drop and concrete age by linear interpolation from the relationships of A/V ratio-age obtained from free shrinkage test using prismatic specimens in step (3).
5. Conduct a combined thermal and structural analysis to obtain the maximum circumferential tensile stress in a concrete ring at a given age by applying the corresponding fictitious temperature field obtained in step (4) on it.
6. Compare the maximal circumferential tensile stress in concrete ring obtained through numerical analyses with the tensile strength of concrete. If the former becomes greater than the latter, the ring will crack. Otherwise, forward to next age, and repeat steps (4) to (6) until the ring cracks.

Figure 5.4 shows the measured free shrinkage strain of concrete at various ages under different exposure conditions with four A/V ratios for a 28 day period, and the converted fictitious temperature drop as a linear thermal expansion coefficient of concrete (10×10^{-6}/ºC) was introduced in this case. Based on the converted fictitious temperature in Figure 5.4b, the relationship between fictitious temperature drop and A/V ratio was then obtained for concrete element irrespective of its shape i.e. concrete rings, with different values of A/V at different ages, and the resulting relationship is established in Figure 5.5.

Although this correlation presents the curves at 3 days interval, fictitious temperature drop was actually calculated for each day using above method which was subsequently used to update input data for finite element analyses conducted in this investigation.

5.3.2 Validation

In this numerical approach, finite element analyses were carried out using ANSYS code to simulate stress development with age in a concrete ring specimen under restrained shrinkage till crack initiates. The whole process of simulation can be divided into two steps, which are thermal and structural analyses. In thermal analysis, the 3-D 20-node solid element (SOLID 90) was used for simulating concrete, which has compatible temperature shape and are well suited to model curved boundaries. Through the thermal analysis, the temperature distribution in concrete can be achieved. In the following structural analysis, the elements for simulating

concrete were replaced by the equivalent structural element, i.e. SOLID 186, which is 3-D 20 nodes solid element and supports plasticity, creep and large strain capabilities. In case of the mesh size, the circumference was divided into 80 sections. In addition, the thicknesses of concrete and of steel were divided into 8 sections and 2 sections respectively, as well as the height divided into 8 sections. The number of elements and nodes are outlined as follows: Concrete ring 10240, steel ring 1280, contract 1820 and nodes 51840. These descriptions are the same for each model.

In order to eliminate the effect of friction between concrete and steel, the outer circumferential surface of the steel ring, which contacts the inner circumferential surface of the concrete ring, was coated with a release agent as suggested by AASHTO PP34-99 and ASTM C1581/C1581M-09a when preparing ring tests. Accordingly, contact element with zero friction between the contact pair was utilised in the numerical model to simulate the effect of this measure in conducting concrete ring tests conforming to AASHTO PP34-99 and ASTM C1581/C1581M-09a.

The materials parameter used in the simulations were as follows: the Elastic modulus and Poisson's ratio of steel are 210 GPa and 0.3, respectively; the Elastic modulus of concrete is determined using Equation (1) and Poisson's ratio is 0.2.

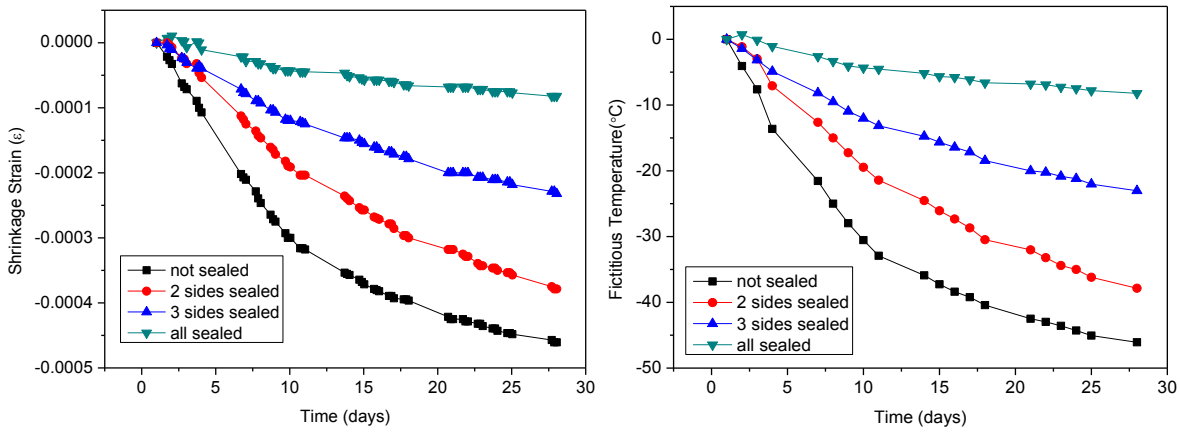

(a) (b)

Figure 5.4—(a) Time-dependent free shrinkage strain and (b) Converted time-dependent fictitious temperature drop for concrete prismatic specimens

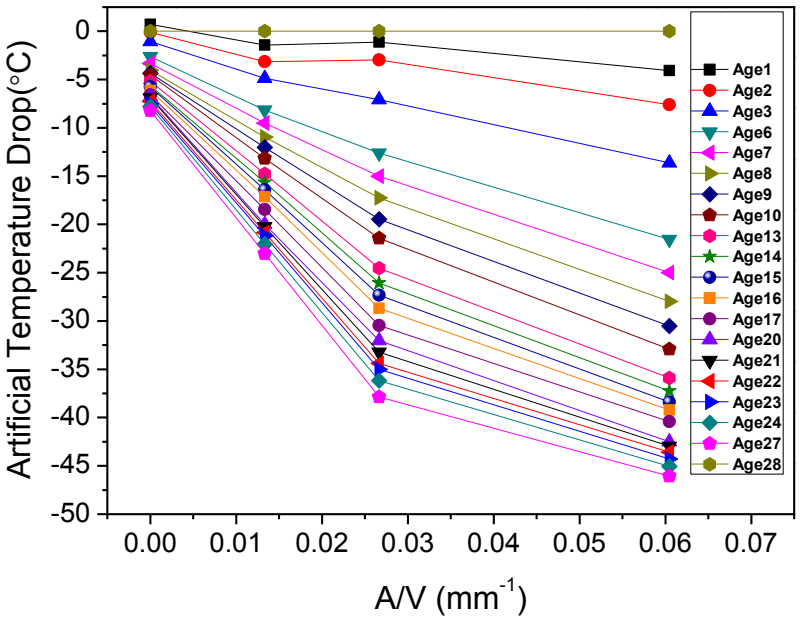

(a)

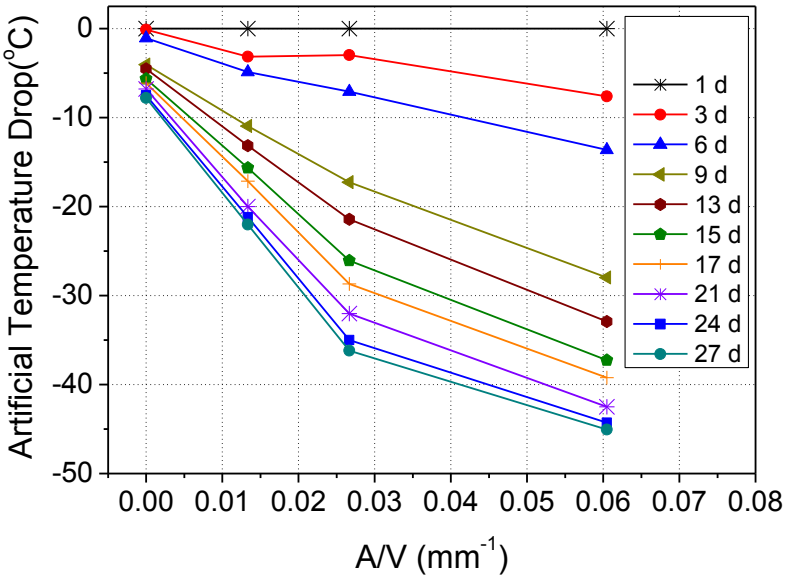

(b)

Figure 5.5—A/V ratio-dependent fictitious temperature drop for exposed concrete elements at (a) 1-Day interval and (b) 3-Day interval

5.4 Cracking in Thin Concrete Ring Specimens

Early age cracking sensitivity is a well-known phenomenon, which is ultimately associated with mechanisms that are related to the microstructural changes and chemical reaction that takes place in the first few days after the cement comes in contact with water (Bentur and

Kovler, 2003) in a concrete element. Besides, early age cracking is observed when the residual tensile stress developed surpasses the tensile strength of the concrete element. The work presented herein describes concrete ring specimens under restrained shrinkage analysed using a numerical model for predicting cracking age of concrete. The FE modeling of the ring test was performed using the pre-processor of ANSYS, the geometry setup for both circular and elliptical ring specimens have been illustrated in Chapter 4 of this document.

For both circular and elliptical ring specimens, three different exposure conditions were considered in the simulation process, i.e. Case 1: top and bottom surfaces sealed with outer circumferential surfaces exposed to drying; Case 2: the outer circumferential surface sealed but top and bottom surfaces exposed to drying; and Case 3: no surface sealed-all exposed for drying. The inner circumferential surface of the concrete ring specimen is in continuous contact to the outer circumferential surface of the steel ring annulus so that it is not exposed for drying, in other words, it is considered as a sealed surface in the simulation process and subsequent analyses. Figure 5.5 shows the age-dependent fictitious temperature drop for concrete elements with various A/V ratios; they were derived from by using the step methodology described in Section 5.3.

Hence, the relevant time-dependent temperature drop of the ring specimens can therefore be obtained by inserting the A/V ratio of a concrete ring specimen into the relationship between the fictitious temperature drop and the A/V presented, representing the outcome of this procedure which further showed the fictitious temperature drop for the circular ring and the elliptical rings with a×b= 150×75mm^2 as shown in Figures 5.6 and 5.7 respectively under different exposure conditions. In like manner, regression analyses were conducted to obtain a continuous equation that represented the age-dependent fictitious temperature drop applied to the ring specimen with the same effects as shrinkage does and the corresponding results are also presented in Figures 5.6 and 5.7. Early-age stress relaxation also known as the progressive reduction in stress with time occurs as a result of creep of concrete. Therefore it is necessary to consider the effect of creep when analysing the stress that develops in the concrete ring. With further consideration, characterising creep of concrete is complicated as it depends on the stress level, specimen age, loading age, degree of hydration, temperature and drying condition.

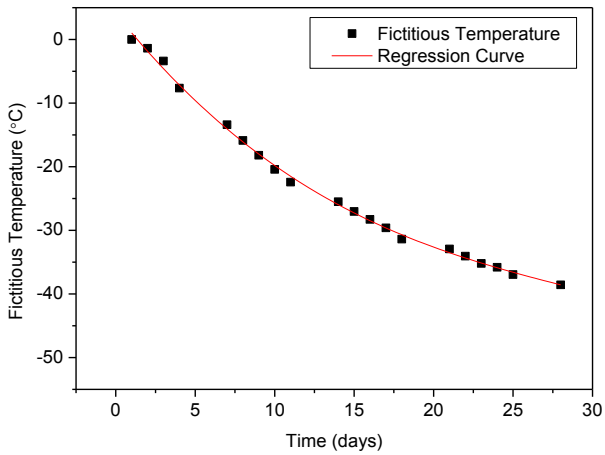

(a) case 1

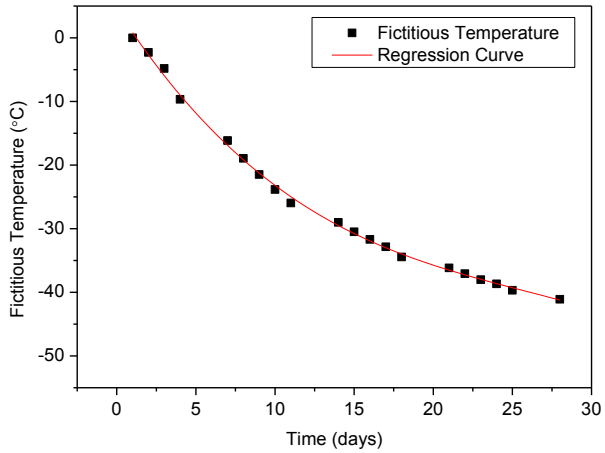

(b) case 2

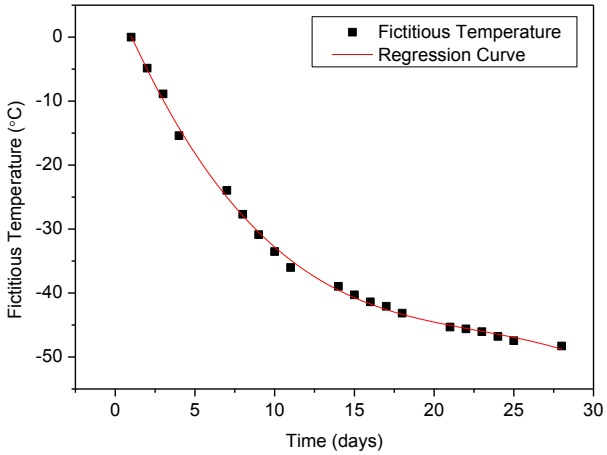

(c) Case 3

Figure 5.6—Fictitious temperature drop for the circular ring specimen under various exposure conditions

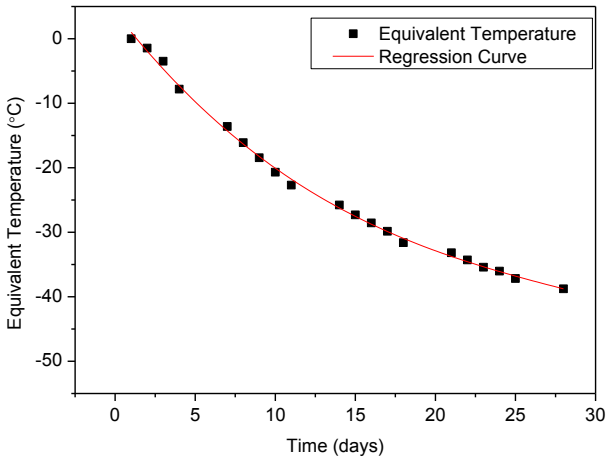

(a) Case 1

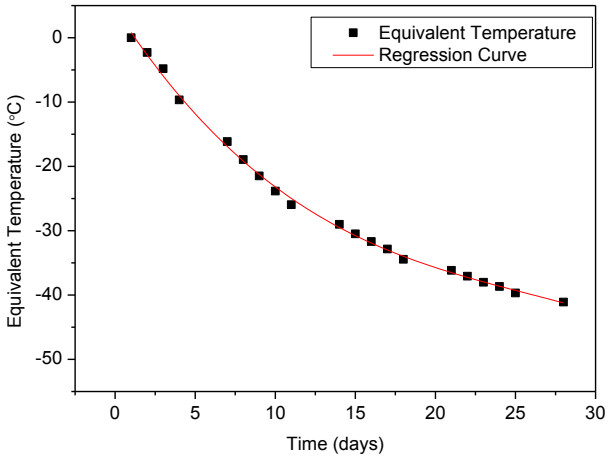

(b) Case 2

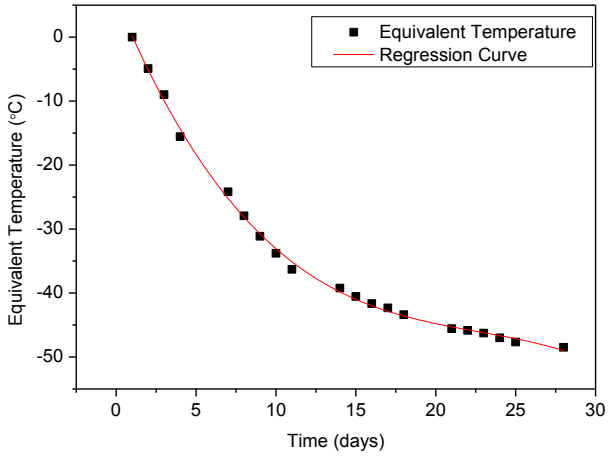

(c) Case 3

Figure 5.7—Fictitious temperature drop for the elliptical ring specimen (a×b=150×75mm^2) under various exposure conditions

For the benefit of this study, the age dependent effective elastic modulus of concrete was reduced to 60% of the actual measured/calculated value from Eq. (5.1) to account for the creep effects. Moon et al., 2006b employed the same procedure in reducing elastic modulus to take into account creep effect when analysing cracking in circular concrete rings under restrained shrinkage. Taking these parameters into finite element analyses, the circumferential tensile stress developed in concrete rings with respect to age under restrained shrinkage was obtained for a series of circular and elliptical ring specimens.

When the maximum circumferential tensile stress becomes greater than the splitting tensile strength of concrete at the same age, crack will initiate in the ring specimen. Based on the proposed method, the numerical results of the circular and elliptical rings are illustrated in Figure 5.8. The proposed method predicts that, for the circular ring specimens with a=150 mm, crack initiates at the age of approximately 18 days under the exposure condition of Case 1, and of approximately 19 and 11 days under the exposure condition of Cases 2 and 3, respectively; for the elliptical ring specimens with a=150 mm and b=75 mm, crack initiates at the age of approximately 11 days under the drying condition of Case 1, and of approximately 12 and 7 days under the drying condition of Case 2 and 3, respectively.

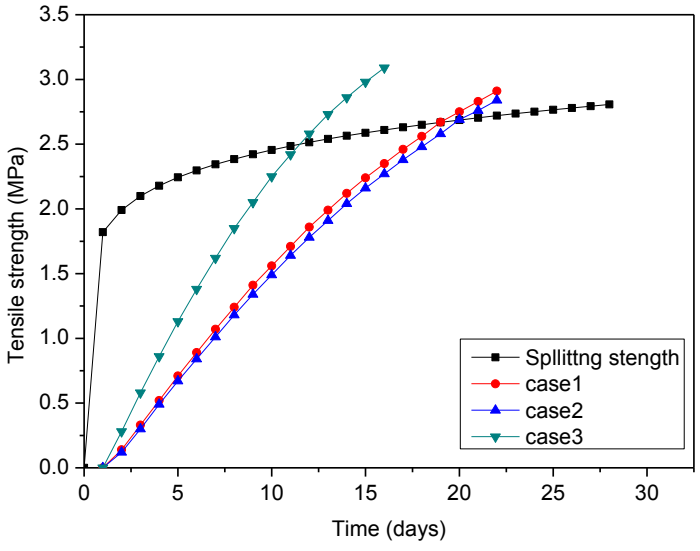

(a) circular ring (a=150mm)

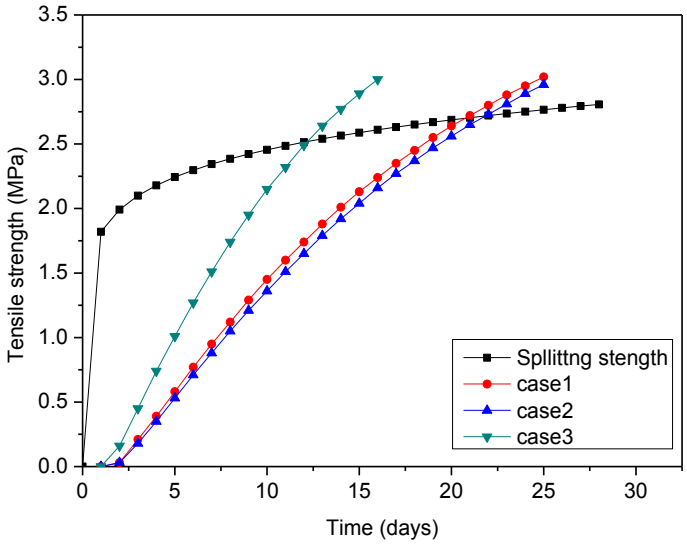

(b) elliptical ring (a=150mm, b=125mm)

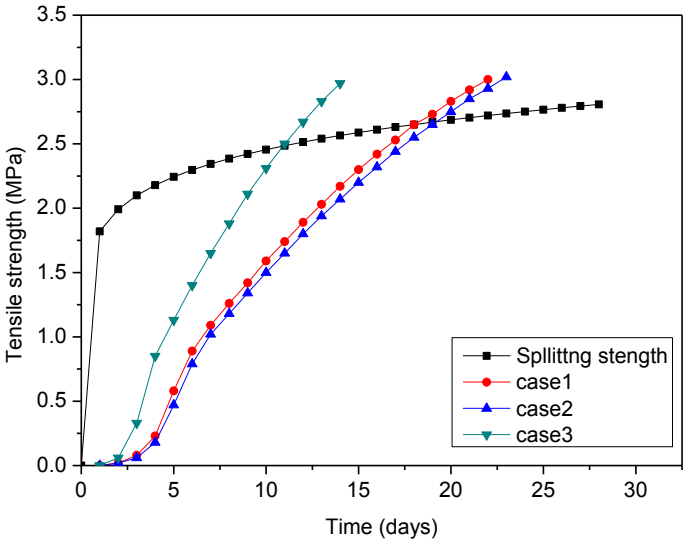

(c) elliptical ring (a=150mm, b=100mm)

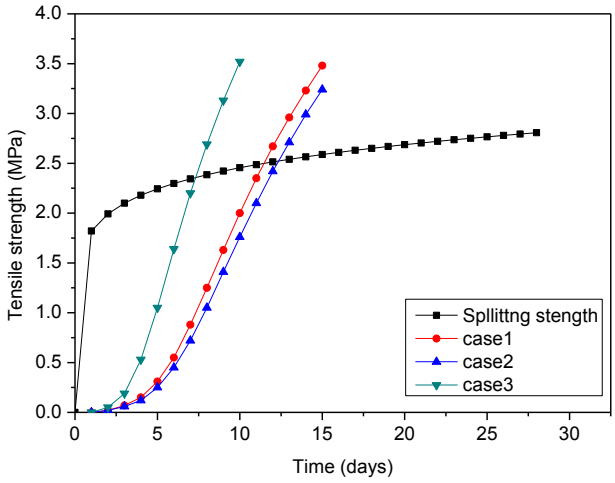

(d) elliptical ring (a=150mm, b=75mm)

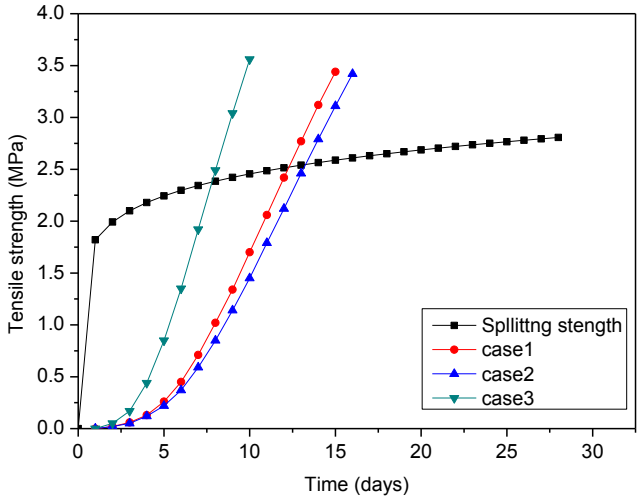

(e) elliptical ring (a=150mm, b=60mm)

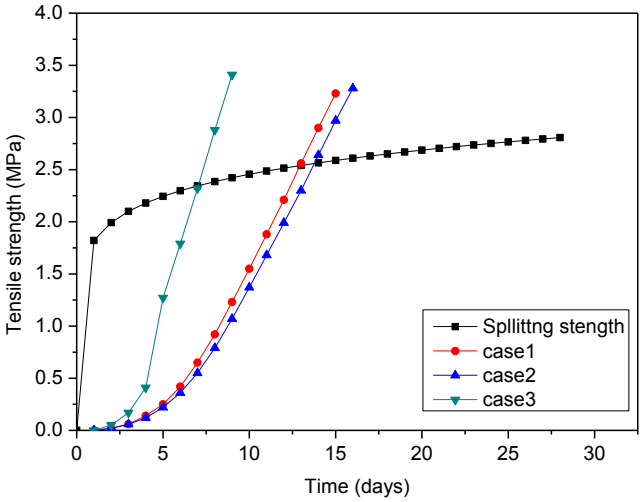

(f) elliptical ring (a=150mm, b=50mm)

Figure 5.8—Maximum circumferential tensile stress in various ring specimens from numerical analyses

5.5 Influence of Drying in Thin Concrete Ring Specimens

The effect of drying direction was again very influential in the cracking behaviour of thin rings. Table 5.2 highlights the A/V ratios of the thin circular and elliptical concrete rings as comparisons are made for those with both top and bottom surfaces sealed and those with outer circumferential surface sealed. The purpose for this comparison is to assess if the drying direction has a significant effect on crack initiation in concrete ring specimens. The results obtained experimentally agree well with numerical analysis as the results have already been presented.

Table 5.2—A/V ratios of circular and elliptical thin ring specimens

a×*b* (mm×mm)	Top and bottom surfaces sealed (mm^{-1})	Outer circumferential surface sealed (mm^{-1})
150×150	0.0296	0.0267
150×125	0.0299	0.0267
150×100	0.0301	0.0267
150×75	0.0304	0.0267
150×60	0.0306	0.0267
150×50	0.0307	0.0267

Table 5.3—Initial cracking ages (days) from numerical analyses for various thin ring specimens

Case	Circular ring	Elliptical ring (a=150mm)				
	a=150 mm	*b*=125mm	*b*=100mm	*b*=75mm	*b*=60mm	*b*=50mm
1	18	20	17	11	12	12
2	19	21	19	12	13	13
3	11	12	10	7	7	7

Since that is the case, the comparisons made here are solely based on the numerical analysis carried out using the FEA code in ANSYS. Three exposure conditions were simulated and the results were discussed. Table 5.3 provides a complete summary of the specimens used to study each drying direction in this research from numerical analysis. The illustration thereby highlights that specimens allowed drying from the top and bottom surfaces always cracked 1 or 2 days after specimens allowed drying from the outer circumferential surface varying with different specimen geometry. It should be noted here also that, the restrained ring specimens drying from the top and bottom surfaces had equivalent A/V (i.e. 37.5mm top surface and 37.5 mm bottom surface thickness) when compared to the specimens drying from the outer circumferential surface (i.e. 75mm in depth). As a result of this close similarity, concrete specimens will tend to crack at about the same age as is the case from numerical results. On the contrary, specimens where all surfaces were exposed to drying (apart from the area where

the steel ring is in continuous contact with the inner surface of the specimen) cracked much earlier, which is also attributed to the A/V of the specimen when exposed in specific directions. In essence, the A/V of the concrete specimens in Case 3 from Table 5.3 were highest hence the earliest crack age, while those of the Case 2 were lowest as highlighted in Tables 5.2 and 5.3.

5.5.1 Validating Numerical Model

In order to verify the proposed numerical model, ten (10) ring specimens (same with those measured in Chapter 4) with different geometries were prepared, with the inner major radius *a* equal to 150mm but the inner minor radius *b* varied from 150, 125, 100, 75 to 60mm, and tested subject to restrained shrinkage under the drying environment of 23ºC and 50% RH till crack initiated. The wall thickness of the restraining steel ring and concrete ring was at 12.5 and 37.5mm, respectively. The experimental procedure has been described in details in the previous chapter as abovementioned.

In this study, and for comparisons to be made between experimental and numerical efforts, the ring tests were performed in a similar way to the ASTM C1581/ C 1581M-09 protocol, i.e., the top and bottom surfaces of ring specimens were sealed using two layers of aluminum tape and drying was only allowed through the outer circumferential cylindrical surface. According to the experimental results obtained and discussed in Chapter 4, the age of first cracking was determined at the sudden drop in the measured strain, which is the same technique used for crack detection in restrained ring test recommended by both AASHTO PP34-99 and ASTM C1581/C1581M-09. It should be noted here with clarity however that, the thin concrete rings used for validating the results from numerical analysis in this chapter are from results of test specimens discussed in Chapter 4.

5.6 Cracking Age (Experimental versus Numerical)

It should be noted that not all elliptical rings can accelerate cracking of concrete as it might be expected. Experimental results in Figure 5.9 indicate that elliptical rings with b=125 and 100 mm cracked on average at the same age of 14.5 days as the circular one, details are also presented in Table 4.2 and section 4.5 respectively. On the other hand, elliptical ring specimens with b= 75 and 60mm cracked on average at 10 and 13 days respectively; while numerical results reveal that the elliptical ring with b=75mm cracked earliest, followed by the

elliptical ring with b=60mm, the difference between the experimental and numerical results appears marginal when considering the complexity in predicting cracking of concrete.

However, from a practical point of view when the geometrical factor a/b is too big, the steel ring at the major principal axis becomes too sharp, making it inconvenient to attach strain gauges which was employed to detect strain in the central steel ring hence to determine cracking of the concrete ring surrounding it, bearing in mind that the elliptical ring geometry may provide a higher degree of restraint to enable concrete crack earlier. Hence, an appropriate elliptical ring geometry with geometric factor a/b=2~3 can be recommended in order to accelerate the restrained ring test so that concrete will crack in a shorter time frame because of its increased cracking sensitivity in comparison with the conventional circular ring geometry.

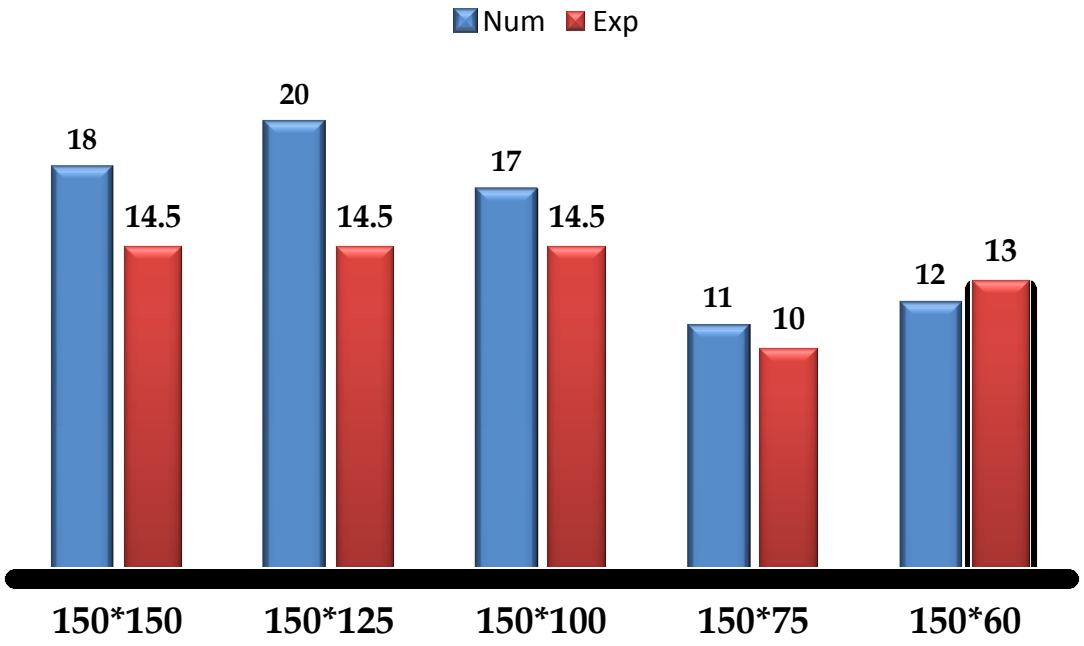

*Num=Numerical results; *Exp=Experimental test results

Figure 5.9—Initial cracking ages (days) from numerical analyses and experimental tests for various thin ring specimens

5.7 Cracking Position

For a ring test, it is advantageous if the position of cracking can be predicted in advance so that the resources required for detecting cracking occurrence and propagation can be minimized during the test. It should be noted however that the discussion in this section is based just on Case 1 exposure condition, i.e., top and bottom surfaces sealed with outer

cylindrical surface exposed for drying same as that recommended by ASTM C1581 / C1581M- 09. On the other hand, it is not possible to predict the position of initial cracking in circular ring specimens because of an equal chance of crack initiating and propagating around their circumferences due to axisymmetric geometry. Figure 5.10a shows the maximum circumferential stress along the circular concrete ring when crack initiates at 18 days, obtained through numerical analysis and experimental test specimens alongside showing crack propagation through concrete wall thickness. However, due to geometrical effect, stress concentration may take place elsewhere in the elliptical ring specimen, which is usually close to the two vertices on the major axis of the inner elliptical circumference. Figure 5.10(b-f) presents the contour of circumferential stress in elliptical concrete rings, with the semi-minor axis *b* equal to 125, 100, 75, 60 and 50mm respectively, at the moment when crack initiates. The corresponding test specimens from experimental results further illustrates regions of crack propagation along the major principal axis as shown in Figure 5. 10 (c-f).

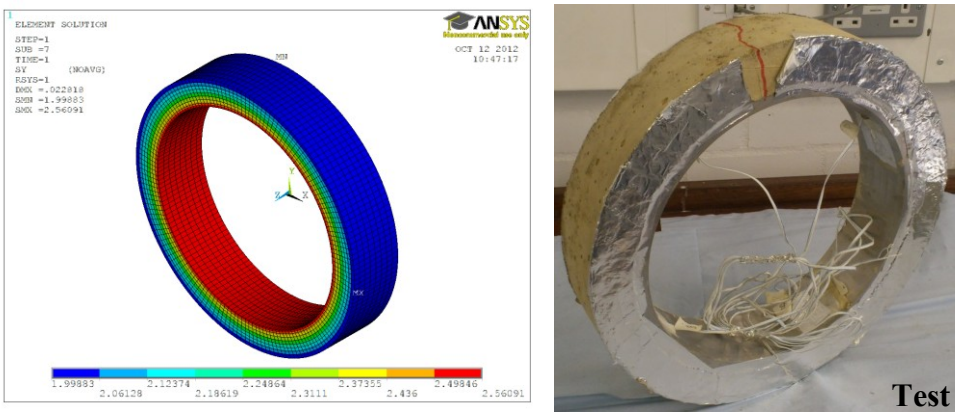

(a) Circular ring with 2*a*=300 (18 days)

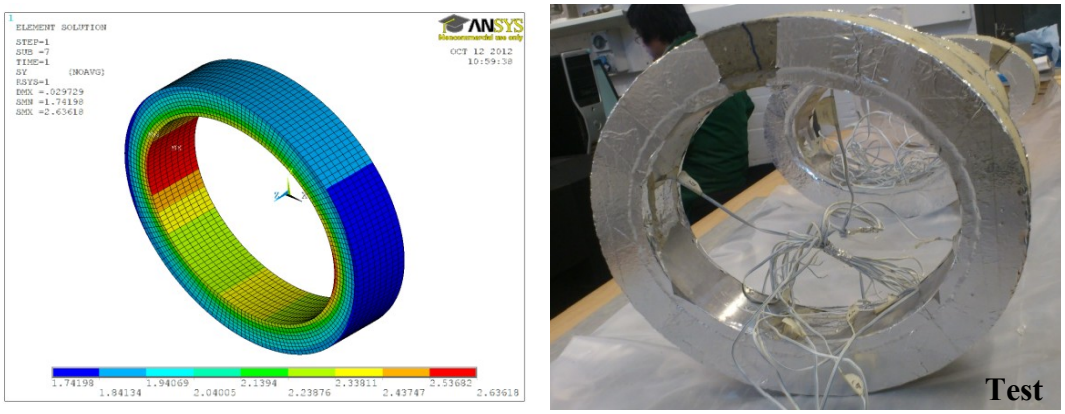

(b) Elliptical ring with *b*=125mm (20 days)

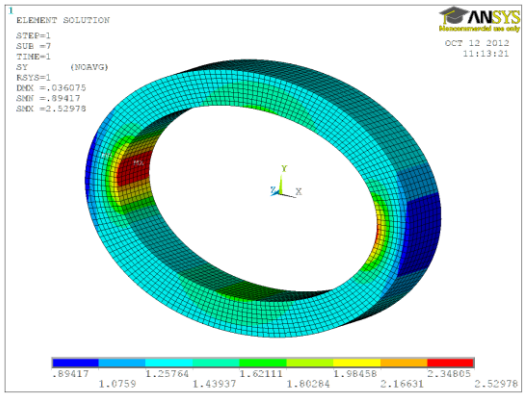

(c) Elliptical ring with *b*=100mm (17 days)

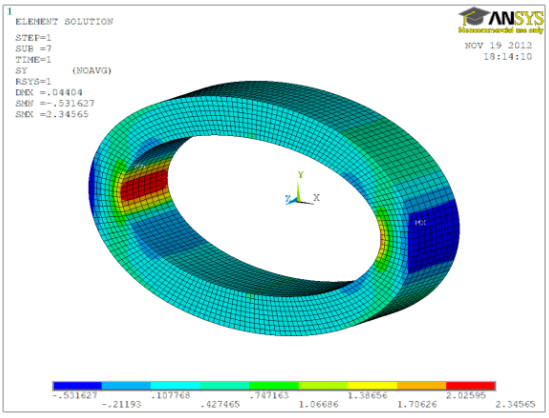

(d) Elliptical ring with *b*=75mm (11 days)

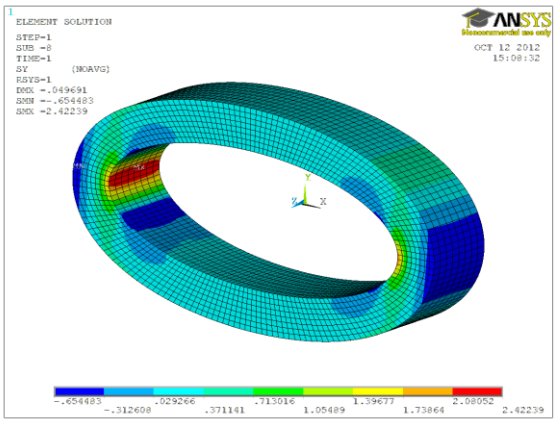

(e) Elliptical ring with *b*=60mm (12 days)

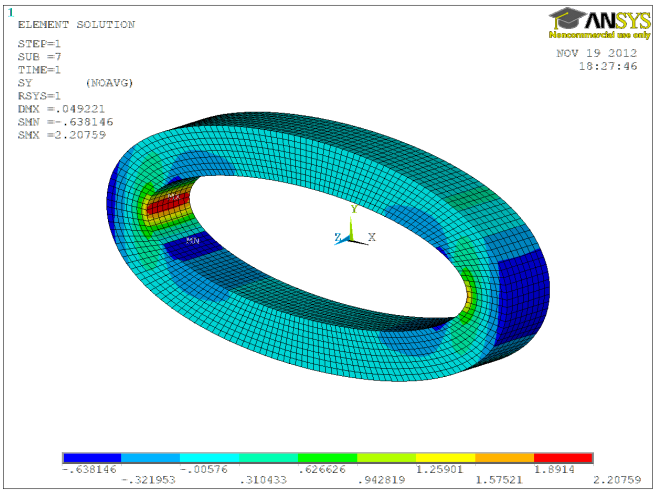

(f) Elliptical ring with *b*=50mm (12 days)

Figure 5.10—Circumferential stress contour in concrete rings when crack initiated together with crack position in test ring specimens

It is apparent that the maximum stress concentration is more significant in elliptical ring which is illustrated in the contour as shown compared to the circular ring. In this case, crack initiates close to the vertices on the major axis of an elliptical concrete ring. However, due to the inhomogeneousness of concrete, crack position on elliptical rings demonstrated three different behavioural patterns as observed from experimental results: (i) Only one visible crack occurred between the major and minor axes (see Fig. 5.10b) in the elliptical concrete ring with *b*=125mm. Furthermore, from numerical analyses according to the stress contour shown in Fig. 5.10b for the same concrete ring, it can be seen that the variation in tensile stress along the circumferential direction is not great and stress concentration is not significant either. Similar to the circular ring specimen, the crack position may be mainly dependant on defects or inhomogeneousness of concrete, which results in the randomness of crack position along the ring circumference. (ii) There are several cracks which occurred along the major axis and other positions, see Figure 5.11a.

The three cracks are marked as crack A, B and C, respectively. Crack A and B are close to the vertices on the major axis, but Crack C is between the major and minor axes. Moreover, there is an interesting phenomena which is of worth to note here, that Crack A and B did not propagate throughout the wall of the elliptical concrete ring from the inner circumference where they initiated to the outer circumference and as a result, they could not be visually observed from the outer circumferential surface of the ring during experimental procedure.

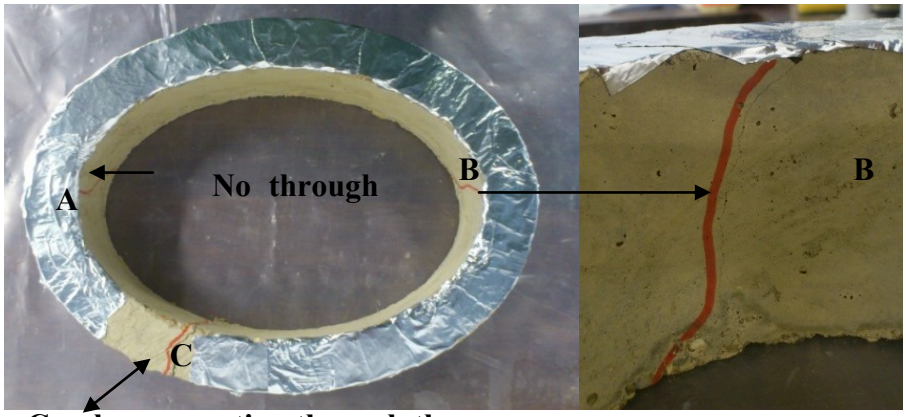

(a)

(b)

Figure 5.11—Crack positions in the (a) thin elliptical ring with a×b=150×100mm^2 and (b) in thin elliptical ring with a×b=150×75mm^2

Conversely, as the top and bottom surfaces of the ring were also sealed, they could not be visually observed from these two surfaces either. They were found only after the test was stopped and the sealed aluminium foil and inner steel ring were stripped off from the concrete ring specimen. This happened in the elliptical ring specimen with *b*=100mm. The degree of stress concentration provided by this elliptical ring to concrete is less than that provided by other ones with *b*=60 or 75mm which is consistent with the findings from experiment. It is well known that crack propagation in concrete usually experiences the stable and unstable stages after initiation. In the stable propagation stage, crack can propagate only under the increasing driving force or energy. The driving energy for crack to propagate in a concrete ring is actually provided by shrinkage of concrete; as concrete gets mature, its shrinkage

increases (Weiss and Shah 2002). Therefore it can be reasonably concluded that the driving force increases for crack propagation as concrete matures. Based on the stress contour obtained from numerical simulation shown in Figure 5.10c, the stress gradient in the area close to the major axis is greater in comparison to anywhere else in the elliptical ring, and the circumferential stress evolves from tension at the inner circumference to compression at the outer circumferential surface. Consequently, in this case, Crack A and B may have initiated earlier at the vertices along the major axis, which were detected by stain gauges. Although after that, circumferential tensile stress elsewhere increased and a new crack, in this case Crack C generated and propagated throughout the wall of the concrete ring reaching the outer circumferential surface and then become visible. Due to stress, thus strain energy, in the zones close to Crack A and B was partially released after their initiation, the position of Crack C should be far away from them, i.e., from the major axes. Moreover, the circumferential stress gradient near Crack C is smaller than those near Crack A and B, resulting in Crack C eventually penetrating through the wall of the concrete ring earlier than Crack A or B. Therefore, in this case, Crack C was visually observed on the outer circumferential surface of the concrete ring. (iii) Only one crack was observed close to one vertex on the major axis (see Figure 5.10b) which is in the zone where the maximum circumferential tensile stress occurs. This happened in the elliptical ring specimens with b=60 or 75 mm which provide the highest degree of stress concentration to concrete surrounding it. Circumferential stress contour of the elliptical ring with b=75mm from numerical analyses is presented in Figure 5.10(d). It can be seen that stress concentration in this elliptical ring is most significant compared with the previous three elliptical rings.

Although there are three different representation of crack positions in restrained concrete rings as discovered in this study, it can be concluded based on experimental and numerical results that crack position depends on the degree of stress concentration in concrete ring subject to restrained shrinkage, which is ascribed to the geometrical factor a/b of an elliptical ring. When a/b is between 2 and 3, the crack position observed from experiment agreed very well with that predicted by the numerical model proposed in this research which further validates the reliability of the numerical model in analysing cracking behaviour of concrete rings subject to restrained shrinkage to underpin the mechanism of the proposed elliptical ring test for assessing cracking potential of concrete and other cement-based materials.

5.8 Summary

A numerical model was developed for predicting stress evolution and cracking age in concrete ring specimen subject to restrained shrinkage to underpin the mechanism of the proposed elliptical ring test. The proposed method was then applied to simulate stress development and crack initiation based on maximal tensile stress cracking criterion. Subsequently, the validated numerical model was employed to predict cracking age of thin ring specimens with various geometries. Hence based on experimental and numerical studies, the following conclusions can be drawn:

(1) Cracking ages from numerical analyses agreed well with experimental results for a series of circular and elliptical thin ring specimens indicating that the proposed numerical model is reliable.

(2) Both experimental and numerical results suggested that the geometrical factor a/b of an elliptical thin ring is the main factor affecting stress developed in a concrete ring when subject to restrained shrinkage. Compared with traditional circular rings, elliptical thin rings with a/b between 2 and 3 can provide higher degree of restraint which leads to shorter cracking period in restrained shrinkage ring test.

(3) There are three cracking scenarios in the elliptical concrete thin ring specimens under restrained shrinkage, depending on the geometrical factor a/b, an interesting finding which was discovered for the first time in this study. By comparing experimental and numerical results, it can also be concluded that initial crack position in thin elliptical concrete rings subject to restrained shrinkage can be predicted reasonably well by the proposed numerical model.

CHAPTER 6: NUMERICAL MODEL FOR THICK RING SPECIMENS

A series of thick circular and elliptical concrete rings were tested and subjected to restrained shrinkage till crack initiated and subsequently propagated throughout the exposed concrete ring surface to investigate the effect of ring geometry and concrete wall thickness on stress development in concrete rings. A numerical model, by introducing artificial temperature fields to represent the mechanical effect of shrinkage of concrete, was developed for predicting stress development and cracking initiation in concrete rings subject to restrained shrinkage. Different temperature fields were derived to take into account the effect of concrete wall thickness on moisture gradient, thus shrinkage strain, across a ring wall. Cracking age, position and stress development were predicted for a wide range of circular and elliptical concrete rings under restrained shrinkage. Numerical results were compared with experimental ones for both thin and thick rings and it was found that they agreed reasonably well.

6.1 Introduction

For better evaluation of the potential of cracking of a concrete mixture, it is significant to investigate the mechanism of the ring test itself and understand how this new elliptical ring test, can provide quantitative information about stress development in concrete under restrained condition. Several investigations have been employed over the past two (2) decades as regards cracking of concrete in restrained circular ring specimens. In a circular ring specimen for example, due to uniform distribution of circumferential stress in concrete, the restraining effect from the central steel ring on surrounding concrete ring can be conveniently replaced by a pressurising force applied to the interface between the steel and concrete rings when applying numerical analyses according to researches carried out so far (Hossain and Weiss (2004), Moon et al. 2006, Kovler et al 1993, Shah and Weiss 2006, Shah et al 1998). In comparison, as a result of efforts to overcome limitations posed by the circular ring, He et al. (2004), proposed the use of elliptical geometry and assumed that an elliptical concrete ring is subject to a uniform internal pressure provided by the central steel core, which is the same assumption taken in analysing shrinkage cracking in circular ring specimens by several researchers (Hossain and Weiss (2004), Moon et al. 2006, Kovler et al 1993, Shah and Weiss 2006, Shah et al 1998); although, till date, very limited research has been carried out on elliptical concrete rings under restrained shrinkage. Indeed, due to geometrical effect, the radial deformation of the central restraining elliptical steel ring is not uniform along its

circumference when concrete shrinks. Therefore it is believed that the assumed uniform internal pressure becomes inappropriate for elliptical ring specimens in restrained shrinkage test. Meanwhile, the degree of restraint is largely dependent on the geometry of the central elliptical restraining steel ring, especially its major and minor semi-axes which is believed to have significant effect on initial cracking age and cracking position of concrete rings surrounding it. On the other hand, the concrete ring wall thickness is believed to have a significant effect on the amount of stress developed in the concrete specimen as a result of the restraining condition presented by the steel ring core. It is therefore of great essence to investigate how the concrete mixtures will behave when the thin and thick rings are compared. Again, it is important to note here that the concrete wall thickness were selected according to ASTM C1581/C1581M-09a recommendation for thin rings (i.e. 37.5mm) and AASHTO PP 34-99 for thick rings (75mm). A comparison test between circular thin and thick rings have been discussed in literature (Hossain and Weiss 2004, 2006), concluding that, thicker rings exhibited greater resistance when compared to thin rings; and also developed slightly higher interface pressure. Although it was also noticed that there was no dramatic difference between the maximum stresses that developed in concrete ring with different wall thicknesses, Hossain and Weiss (2006). This chapter describes in detail a second series of ring specimens (i.e. thick ring specimen) which were tested to investigate the influence of specimen thickness on the overall cracking behaviour, as the first series (i.e. thin ring specimens) was already discussed in chapter 5. And although the approximation of uniform stress distribution across concrete ring wall worked well for thin geometries, the influence of moisture gradients becomes more pronounced as the thickness of the concrete specimen increases.

Moreover, due to the increase in concrete wall thickness, a complex stress field appears across the wall thickness of a concrete ring specimen when drying from the outer circumferential cylindrical surface. It is believed that the assumption, i.e. shrinkage strain, and thus the resulting stress, is uniform across the ring wall adopted for analysing thin rings is not appropriate for analysing thick rings. Therefore, in order to characterise stress development with the consideration of the effect of ring geometry and drying direction, analytical models were developed to assess residual stress in restrained ring specimens (Moon and Weiss 2006, Moon et al 2006, Hossain and Weiss 2006, Weiss 1999, Hossain 2004). But it should be noted that those analytical models were developed for circular ring specimens only and they may not be appropriate for elliptical ones. Hence to determine whether cracking occurs in the ring

specimens, the stress level that the specimen could resist was determined over time by developing a numerical approach in this chapter in order to simulate the shrinkage behaviour of concrete in restrained ring specimens drying from their outer circumferential cylindrical surface which agrees with the exposure condition in the ring tests recommended by AASHTO and ASTM respectively.

An artificial temperature field is applied on a concrete ring specimen in numerical analyses to simulate the mechanical effect of concrete shrinkage on the ring under restrained condition. The artificial temperature field is derived based on free shrinkage test of concrete prisms by considering that the free shrinkage strain of the prisms is caused by the artificial temperature field applied on them which results in the same value of contraction as shrinkage does (the procedure has been enumerated and discussed in Chapters 3 and 5). When the exposed drying surface area-to-volume ratio (A/V) of an elliptical ring specimen is equal to that of a concrete prism in free shrinkage test, the elliptical ring specimen can be regarded as being under the same temperature field as the concrete prism. Therefore, by measuring the longitudinal length change of a concrete prism and assuming that this length change is caused by a temperature field applied on it, the artificial temperature field which is able to simulate the mechanical effect of shrinkage of concrete rings under restrained condition can be obtained. The artificial temperature field will generate thermal load on the restrained concrete rings with internal stress in concrete obtained through a combined thermal and structural analyses. Based on this argument, a numerical model was developed in Chapter 5 for thin circular and elliptical rings and further developed in this chapter to analyse stress development and to predict cracking age and position in a series of thick circular and elliptical concrete ring specimens subjected to restrained shrinkage. Initial cracking ages of those rings are obtained from experimental efforts and then compared with the results from numerical analyses to verify the proposed numerical approach. Finally, the effect of ring geometry on cracking age and position on concrete rings under restrained shrinkage is also discussed. It is expected that the experimental and numerical investigations presented here will lead to a better understanding on how the elliptical ring geometry affects stress development, crack initiation and propagation in restrained concrete rings so that the proposed elliptical ring test, as an improved method, complements the circular ring tests recommended by ASTM and AASHTO for faster and reliable assessment of the likelihood of cracking of concrete and other cement-based materials and also to reduce the cost of instrumentation in due course. This chapter by using the thick ring series aims to illustrate the response of concrete thickness on cracking

when concrete wall is increased from 37.5 to 75mm. It will also attempt to provide explanations for the observed results obtained via investigation.

6.2 Experimental Assessment

In this study, a series of circular and elliptical concrete ring specimens, with the concrete wall thicknesses of 75 mm quoted as thick, were subject to circumferential drying under restrained shrinkage to investigate the initial cracking age and position in concrete rings. The geometries of circular and elliptical rings tested are shown in Figure 6.1. The mix proportion of the concrete for making those specimens was 1:1.5:1.5:0.5 (cement: sand: coarse aggregate: water) by weight with the maximal coarse aggregate size of 10 mm, all being the same as those used in making thin rings in Chapter 4.

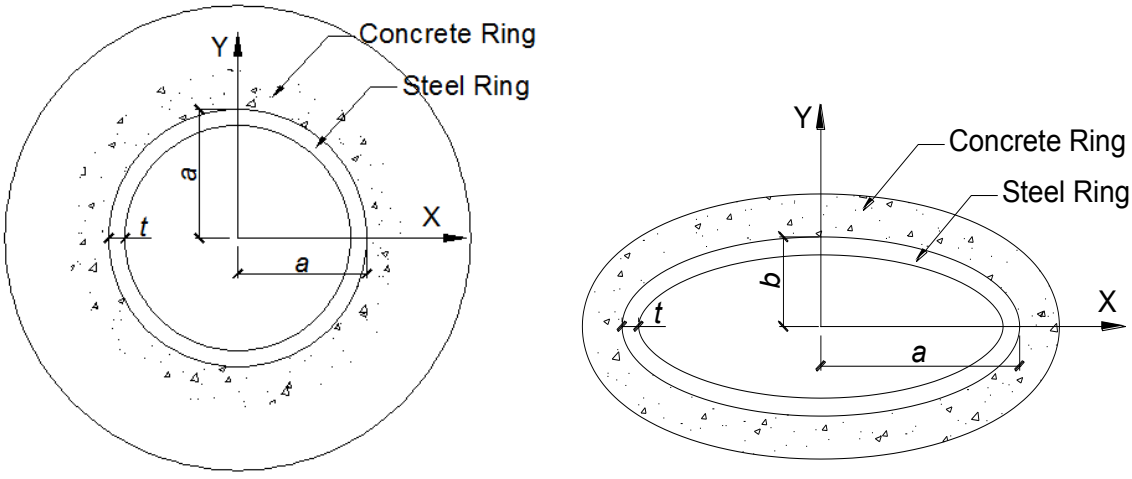

a) Thick Circular ring (b) Thin Elliptical ring

Figure 6.1—Notations of geometries of ring specimens

The thick rings with a concrete wall thickness of 75mm, same as that recommended by AASHTO PP34-99 were tested. All rings tested for the thick specimen series were dried from the outer circumferential cylindrical surface with top and bottom surfaces sealed as shown in Figure 6.2, the same exposure condition as that recommended by AASHTO PP34-99 and ASTM C1581/C15881M-09a. With such exposure condition, shrinkage of concrete is uniform throughout the height of the ring specimen but not through its radial direction. All the circular and elliptical rings had a height of 75mm, while the wall thickness of the central restraining steel ring remained at 12.5mm as that used for thin concrete ring specimens.

Table 6.1—Thick ring specimens tested

Ring Type	Steel ring core: a × b(mm × mm)	a/b	Steel ring thickness(mm)	Concrete ring thickness(mm)
Circular ring	125×125	1.2	12.5	75
Elliptical ring	150×125	1.2	12.5	75
Elliptical ring	150×100	1.5	12.5	75
Elliptical ring	150×75	2	12.5	75
Elliptical ring	150×60	2.5	12.5	75

6.3 Thick Ring Test

Thick ring specimens with a 75 mm-thick wall, which was recommended by AASHTO PP34-99, were also tested under restrained shrinkage. Five different ring geometries and two rings for each of the geometry tested, making it a total of 10 rings; all these were prepared with their geometries listed in Table 6.1, and dried under the environment of 23°C and 50% RH within a closed environmental chamber whilst under restraint till at least one crack initiated and propagated through the concrete ring wall. In the same way as the thin ring specimens were tested, top and bottom surfaces of the thick ones were sealed with the outer circumferential surface exposed for drying.

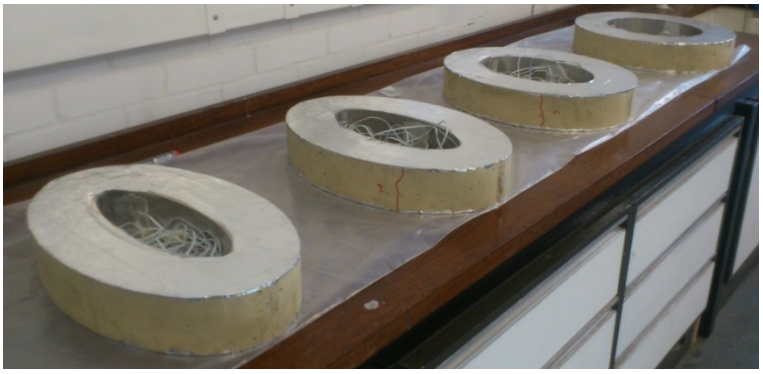

Figure 6.2—Thick elliptical ring specimens with top and bottom surfaces sealed

The experimental procedure adopted for the thick rings was the same as that for thin rings described in chapters 4 and 5. Again, it should be noted that no circular thick ring with

a=150mm was tested due to the size restriction of the environment chamber. A circular thick ring specimen with *a*=125mm was tested instead.

6.4 Numerical Modelling

Since experimental results suggested that different restraint effects are provided by circular and elliptical steel rings to surrounding concrete, it is significant to investigate stress development in restrained thick concrete rings when subjected to drying from their outer circumferential surface. Therefore, a numerical approach was developed to explore the mechanism of the circular and elliptical ring tests. In this numerical approach, finite element analyses were carried out using ANSYS code to simulate stress development with age in a thick concrete ring specimen, circular or elliptical, under restrained shrinkage till crack initiates. It should be noted however that ANSYS code does not directly support shrinkage loading. Neither is there direct entry for shrinkage being included as a material property of concrete as most engineering materials do not possess shrinkage like concrete. Therefore, as an alternative method, shrinkage effect in concrete was represented by an artificial temperature field applied on concrete ring specimens in numerical analyses.

6.4.1 Artificial Temperature Fields

Volumetric change of concrete can usually be classified into two broad categories: thermal shrinkage and drying shrinkage (Weiss (1999); Hossain (2004)). Thermal shrinkage of concrete is as a result of hydration of cement and/or changes in environmental temperature while drying shrinkage is the response of concrete to moisture movement. There is an obvious difference between thermal and drying shrinkage with the latter depending more on the A/V ratio of a concrete element when compared to the former. When a concrete element is put into a drying environment without any restraint, its size/volume will change anyway, a phenomenon often referred as free shrinkage which does not cause any internal stress in concrete. Firstly, free shrinkage of concrete was measured using prisms with different surface area-to-volume ratio (A/V) ratios, to simulate different exposure conditions, by monitoring their longitudinal length change. On the other hand, free shrinkage of a concrete prism can be regarded as being caused by an artificial temperature field applied on it which results in the same length change as free shrinkage does. Through this, the relationship between free shrinkage and artificial temperature field can be established for concrete at various ages by employing numerical analyses.

In line with this, concrete prisms with the dimensions of 285mm in length and 75mm square in cross section, conforming to ISO 1920-8, were subject to drying without any restraint in the same environment as for curing concrete ring specimens. Their longitudinal length change was monitored by a dial gauge, which was then converted into shrinkage strain. Considering that concrete shrinkage depends on A/V ratio of a concrete element, four different exposure conditions each with an individual A/V ratio, were investigated, i.e. all surfaces sealed (with A/V=0), all surface exposed for drying (with A/V=0.0605), two side surfaces exposed for drying (with A/V=0.0267) and one side surface exposed for drying (with A/V=0.0133), respectively, in experiment (see Figure 6.3). It should be noted here however, that the numerical model described in this chapter/section is just for thick rings.

Figure 6.3—Concrete prisms for free shrinkage test placed in the environmental chamber

A double-layer aluminium tape was used to seal the surfaces which were not intended for drying. Figure 6.4 shows the measured average free shrinkage strain of concrete at various ages up to 28 days under the four exposure conditions.

There is another assumption adopted in the numerical analyses, i.e. free shrinkage is the same for concrete elements with the same A/V ratio but maybe different geometries/shapes. Therefore, there will be an identical artificial temperature field applied on concrete specimens with the same A/V ratio but maybe different geometries/shapes which results in the same volume change to concrete as shrinkage does. Applying this assumption in numerical analyses to a concrete ring specimen in restrained shrinkage test, the ring specimen is considered to be

put in the same artificial temperature field as the concrete prism with the same A/V ratio. In summary, the artificial temperature drop-age relationship for a concrete ring specimen can be established based on the free shrinkage-age relationship of concrete prisms obtained from free shrinkage test.

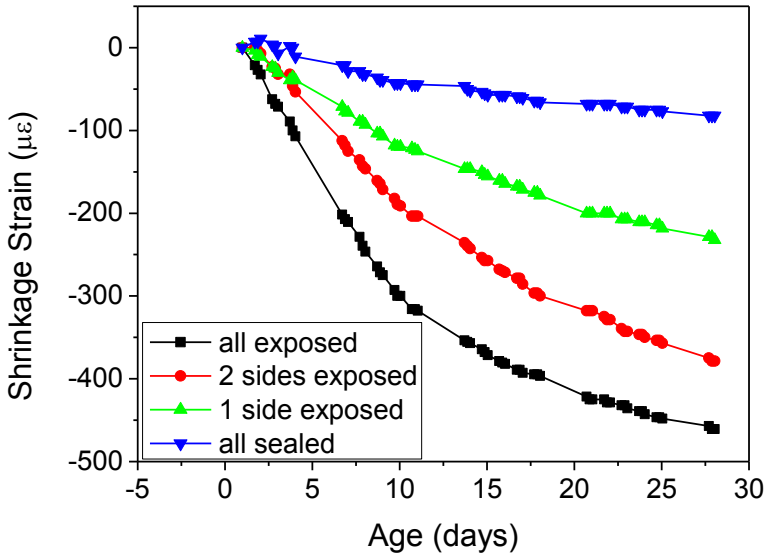

Figure 6.4—Shrinkage strain of concrete obtained from free shrinkage test

6.4.2 Thick Rings

With the increase of the thickness of a concrete element, the influence of moisture gradient across the thickness becomes more and more significant and cannot be neglected (Weiss, 1999). It is therefore believed that the assumption of a uniform shrinkage, consequently temperature distribution, across the thickness of the ring wall adopted for analysing thin rings is not appropriate for a thick concrete ring (Moon and Weiss, 2006). Therefore, in this chapter, an artificial temperature field with gradient, consisting of different temperature drops at sealed and exposed surfaces, was applied across the thick ring wall taking into account the moisture gradient across the thick concrete ring wall. For a thick ring with top and bottom surfaces sealed but outer circumferential surface exposed for drying, two temperature drops were derived in order to accurately simulate the shrinkage effect, one of which is the temperature drop acting on the sealed concrete surfaces and the other is the one acting on the exposed concrete surfaces. With these two temperature drops, a non-uniform artificial temperature field was able to be derived and consequently applied across concrete ring wall in numerical analyses.

The abovementioned two temperature drops, one for sealed surfaces and the other for exposed surfaces, can be obtained by introducing free shrinkage test results of concrete prisms. Similar to the assumption on shrinkage in analysing thin rings, the length change of a concrete prism can be regarded as caused by a temperature field with gradient, consisting of different temperature drops at sealed and exposed surfaces. In the case of the prism with all surfaces sealed, i.e. A/V=0, there is only one temperature drop, i.e., uniform temperature field, to be derived acting on all surfaces. Thus, the artificial temperature drop can be calculated by deriving the relationship between the measured shrinkage strain and the coefficient of linear expansion of concrete, i.e. 10×10^{-6}/°C. In the case of the prisms with one or more surfaces exposed and one or more surfaces sealed, two different temperature drops act on the exposed and sealed surfaces of the prisms respectively. Taking the prism with one side surface exposed (with A/V=0.0133) for drying as an example. Since the artificial temperature drop acting on sealed surfaces of a concrete element corresponds to the scenario of a concrete prism with all surface sealed in free shrinkage test conducted in this study, it can therefore be derived from a free shrinkage test of the prism with all surfaces sealed. Furthermore, through FEM analysis of the concrete prism in free shrinkage test, the temperature drop acting on the exposed surface, corresponding to A/V=0.0133 in this case, can be derived by considering that the length change of the prisms under the two temperature drops, i.e., those corresponding to A/V=0 and 0.0133, respectively, is equivalent to the experimental one under the same exposure condition. In the case of the prism with all surfaces exposed (A/V=0.0605), similar to the prism with all surfaces sealed, only one temperature drop resulting in the length change of the prism is to be derived. So, the derived relationship between artificial temperature drop and A/V, considering the temperature gradient, can be derived and the results are presented in Figure 6.6 for concrete elements at various ages where the results are presented at 3-days interval though the exercise was conducted for each day using the above method. The temperature contours in the prisms with all surfaces sealed and one side surfaces exposed at the age of 9 days are shown in Figure. 6.5. Likewise, the temperature drops acting on the sealed and exposed surfaces are designated as T1 and T2, respectively. In the numerical analysis of a ring specimen subject to restrained shrinkage, to start with, the A/V ratio of the ring specimen is calculated and the relationship between fictitious temperature drop and concrete age is derived through linear interpolation from the relationship of A/V ratio-age presented in Figure 6.6.

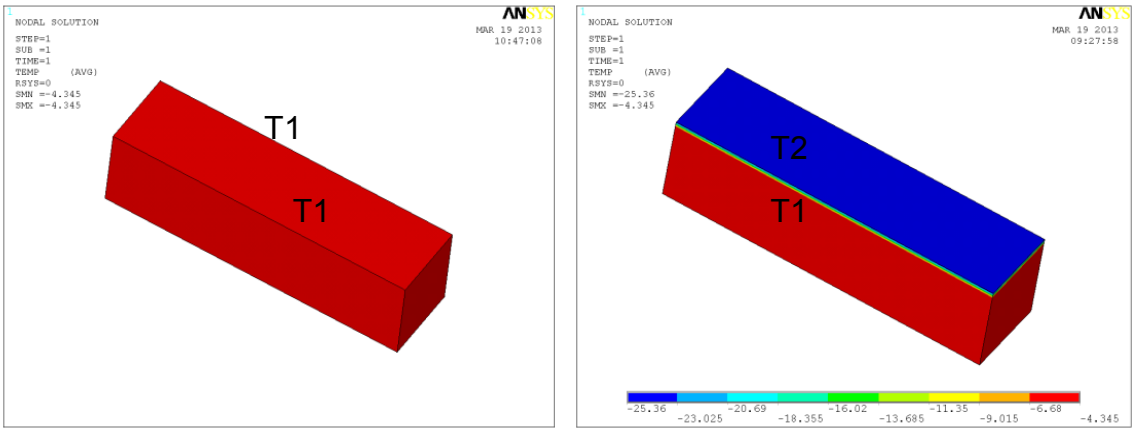

(a) Prism with all surfaces sealed (T1=-4.35°C)

(b) Prism with 1 side surface exposed (T1=-4.35°C; T2=-25.36°C)

Figure 6.5—Temperature contours of concrete prisms under different exposure conditions

As the outcome of this analysis, Figure 6.7 presents the artificial temperature field for the elliptical rings with $a \times b = 150 \times 75 mm^2$. It should be noted here, that the assumption aforementioned is different with the think rings. The shrinkage of prism is not based on one temperature field but two temperature fields. In Figure 6.6 a & b, the temperature field applied is the one acting on the exposed surfaces. Therefore, the value of this temperature drop will not reflect the magnitude of the actual shrinkage of prism from test results.

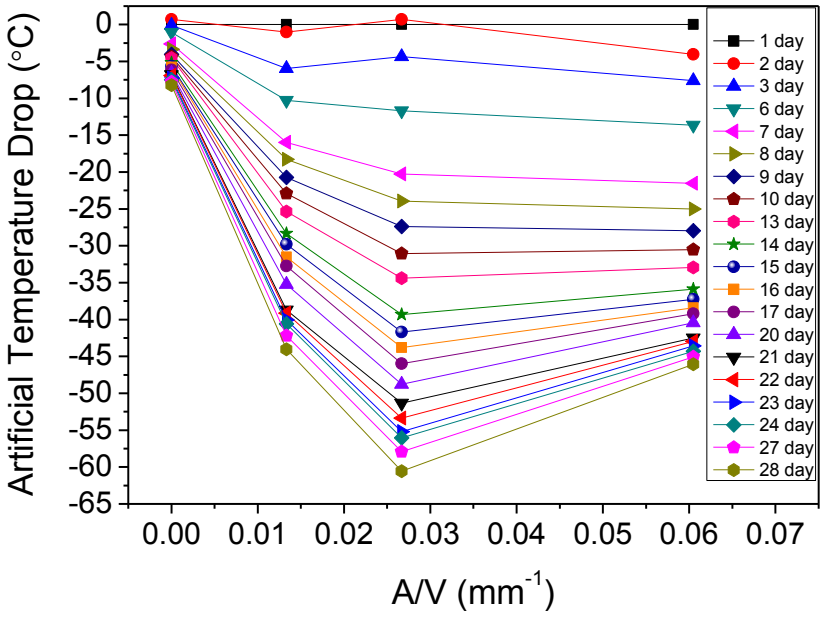

(a)

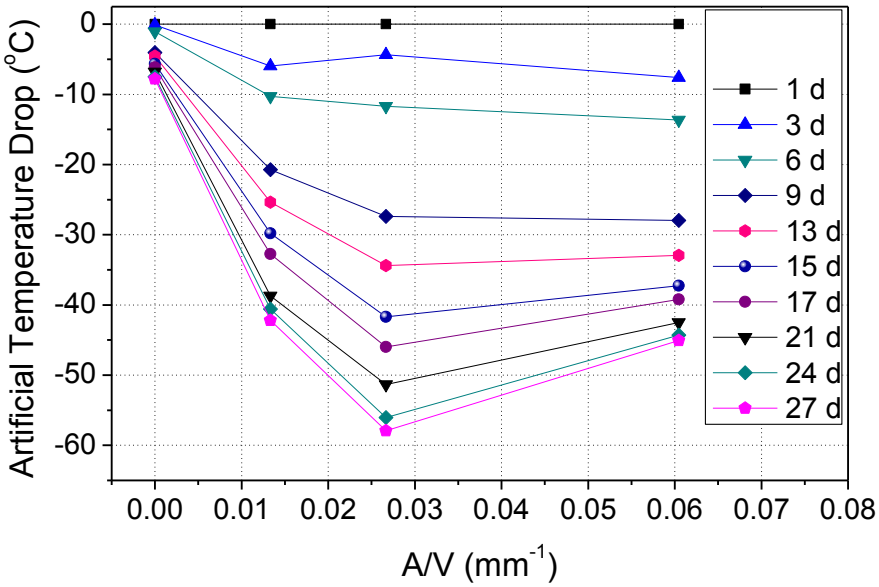

(b)

Figure 6.6—Artificial temperature drop vs. A/V ratio for thick rings at (a) 1-Day interval and (b) 3-Day interval

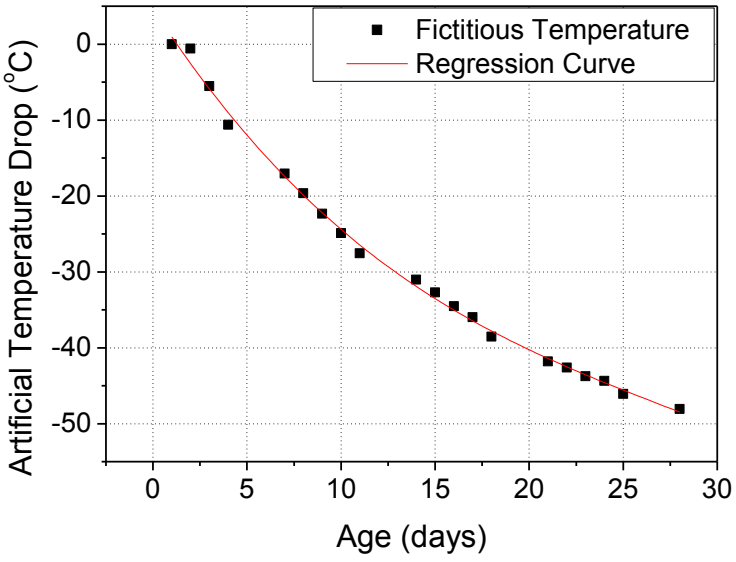

Figure 6.7—Artificial temperature drop for a thick elliptical ring (with $a \times b$=150×75mm^2)

Regression analysis was conducted to obtain continuous functions that can represent the age-dependent artificial temperature drop applied to the exposed surface of a ring specimen with the same effects as shrinkage does.

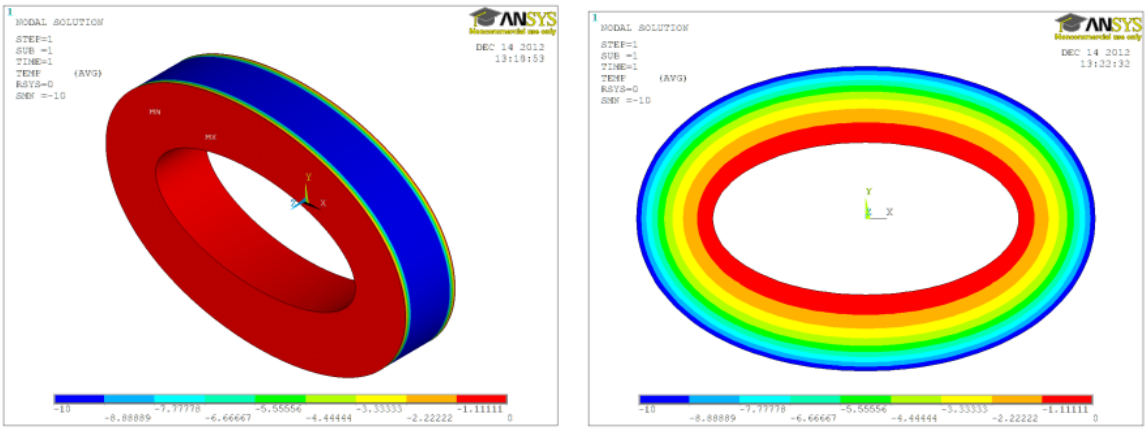

(a) 3D model (b) Mid-height cross section

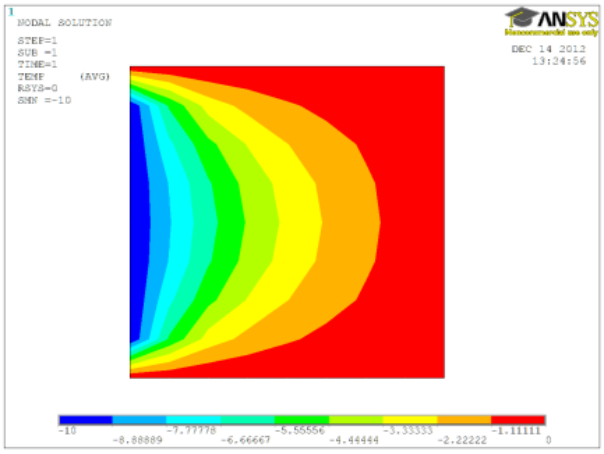

(c) Radian cross section along the major axis

Figure 6.8—Temperature contour in a concrete ring

Figure 6.8 presented the temperature contour, from numerical analyses, in an elliptical concrete ring with top and bottom surfaces sealed, in which Figure 6.8(a) is a three-dimensional model of the concrete ring; Figure 6.8(b) is a cross section at mid-height of the ring; and Figure 6.8(c) is a radian cross section along the major axis of the ring. Here, the temperatures acting on the sealed and exposed surfaces were assumed as T_1=0°C and T_2=-10°C, respectively.

6.5 Cracking age

The artificial temperature field derived in Section 6.4.1 was applied on the ring specimen in numerical analyses which causes concrete shrinking as shrinkage does. Once the shrinkage

caused by the artificial temperature field is restrained by the inner steel ring, tensile stress will be developed in the concrete ring surrounding it. In this chapter, same as the last (Chapter 5), a maximum circumferential tensile stress cracking criterion was adopted for determining crack initiation in concrete rings, i.e., when the maximum circumferential tensile stress caused by the artificial temperature field exceeds the tensile strength of concrete at the same age, cracks will initiate in concrete.

Modelling the Thick Rings

Numerical analyses were carried out on a series of ring specimens with various geometries to study stress development in concrete rings subject to restrained shrinkage. The concrete ring specimens investigated in this study all had a depth of 75 mm with the inner steel ring having a wall thickness of 12.5mm. To investigate the effect of concrete wall thickness on cracking, a wall thicknesses of 75mm, was examined. Three-dimension 20-nodes solid elements (SOLID 90) were used for simulating concrete and steel rings. In order to eliminate the effect of friction between concrete and steel, the outer circumferential surface of the steel ring, which contacts the inner circumferential surface of the concrete ring, was coated with a release agent as suggested by AASHTO PP34-99 and ASTM C1581/C1581M-09a when preparing ring tests.

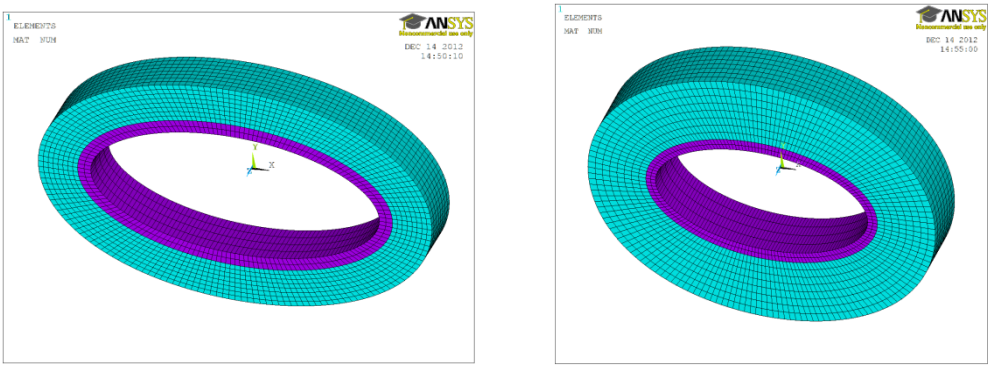

(a) FE mesh for thin rings (b) FE mesh for thick rings

Figure 6.9—Typical FE mesh for simulating thin and thick rings under restrained shrinkage

Accordingly, in numerical analyses, contact element with zero friction between the contact pair was utilised to simulate this measure in conducting concrete ring tests. Typical FE

meshes are shown for both thin and thick rings in Figure. 6.9. In this case, the inner purple elements and outer green element represent steel and concrete, respectively.

In numerical analyses, concrete shrinkage effect was replaced by an artificial temperature fields applying on ring specimens. For thin rings with a 37.5mm-thick wall, a uniform temperature field with zero gradient across concrete ring wall thickness was adopted, which is already derived/developed in Chapter 5, while for thick ring specimens with a 75mm-thick wall, considering the effect of humidity gradient across the wall, different artificial temperature drops were applied on the sealed and exposed concrete surfaces, respectively, when analysing behaviour of thick concrete rings under restrained condition. The two temperature fields can be derived using the approach described in Section 6.4.2. Taking these parameters into finite element analysis, the time-dependent circumferential stress in concrete rings can be obtained.

6.6 Cracking age and stress development

To verify the numerical approach developed in this chapter, a series of circular and elliptical ring specimens with various geometries subject to restrained shrinkage were analysed using the numerical model developed in Chapters 3 and 5. Figure 6.10 presents the maximum circumferential tensile stress developed in various concrete ring specimens both thin and thick obtained from numerical analyses. The maximum circumferential tensile stress was chosen from the mid-height section of a concrete ring specimen, same as efforts from Hossain and Weiss (2004). When the maximum circumferential tensile stress that developed in the concrete ring reaches the tensile strength of concrete, crack initiates at the point of intersection. At this point, the cracking age is determined (see Figure. 6.10).

It can be reasonably concluded from experimental results that ring geometry has a significant effect on cracking sensitivity of ring specimens subject to restrained shrinkage. For both thick and thin rings, cracking age depends on the degree of stress concentration in a concrete ring, which further depends on the geometry factor a/b of an elliptical ring. At the same time, it is acknowledged that, with the increase of concrete wall thickness, the influence of elliptical geometry on crack sensitivity decreases. For instance, compared with circular rings, cracking ages of thin and thick elliptical rings with $a \times b = 150 \times 75 mm^2$ are shortened by 33.3% (i.e. reduced from 15 to 10 days for thin rings) and 18.2% (i.e. reduced from 22 to 18 days for thick rings), respectively, as indicated in Table 6.3. In fact, when concrete wall thickness increases from 37.5 to 7 mm, the stiffness of the concrete ring increases while the stiffness of

the central restraining steel ring does not change as the wall thickness of the central restraining steel ring remained the same as 12.5mm in the course of the test.

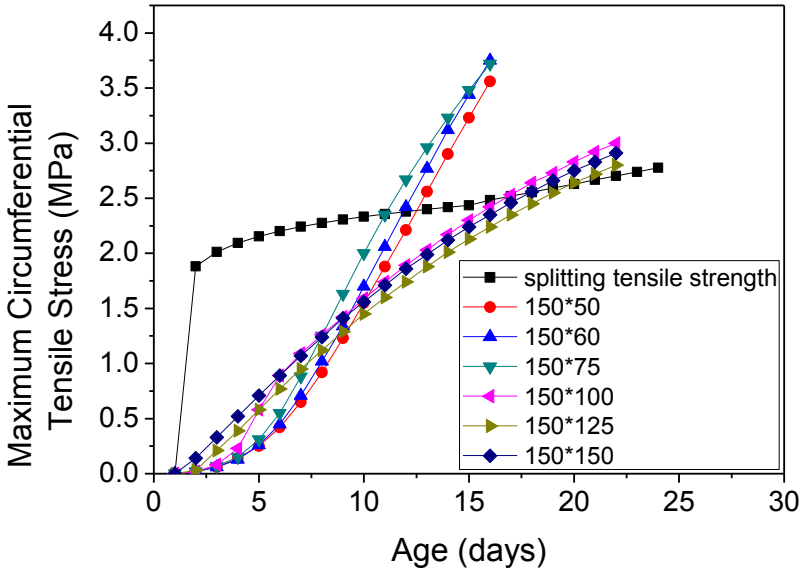

(a) Thin rings

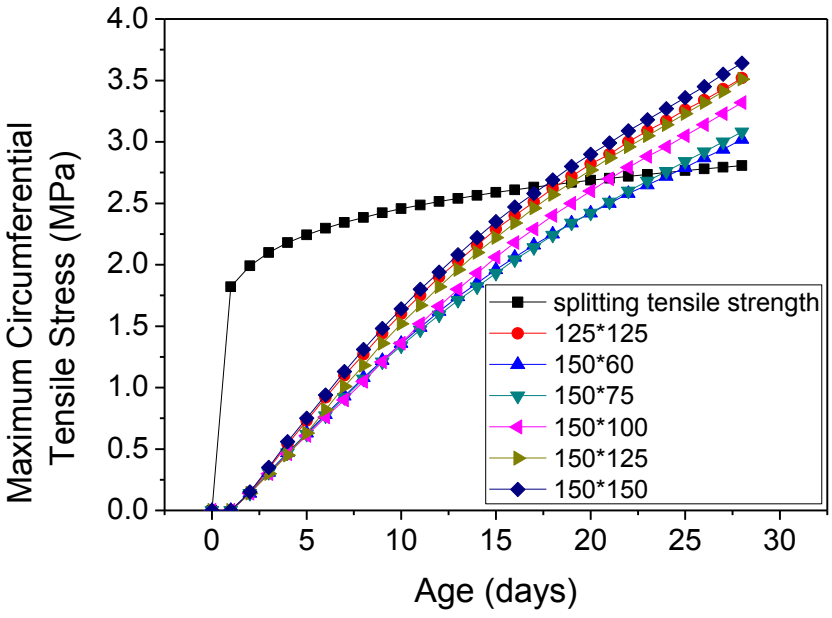

(b) Thick rings

Figure 6.10—Evolution of maximal circumferential tensile stress in restrained concrete rings with age

Therefore, the restraint effect provided by the inner steel ring becomes relatively weaker resulting in the thick rings cracking later than thin ones. In addition, according to the simulated results employed using numerical analysis, the maximum circumferential tensile stress developed in thin and thick concrete rings significantly exhibits different features. In thin rings, the stress development experiences different stages depending on concrete age, i.e. the degree of restraint is dependent on both the geometric factor a/b and the age of concrete. Comparing both the circular and elliptical rings with $a/b<2$ at early ages (i.e. between ages 0 and 10), the elliptical ring with $a/b>2$ does not significantly increase the degree of restraint (see Figure. 6.10(a)).

However, with the increase of concrete age, the degree of restraint provided by the central elliptical steel ring with b=75, 60, or 50 mm were enhanced significantly. Nonetheless things are different in thick rings; it can be seen from Figure 6.10(b) that the development trend of the maximum circumferential tensile stress in concrete is consistent with the trend of concrete tensile strength respect to concrete age. Additionally, the thick ring specimens in this case with a wall thickness of 75mm, the same as that recommended by AASHTO PP34-99, exhibited a different cracking behaviour. Most thick ring specimens cracked at the age on or older than 20 days with the exception of the elliptical one with $a \times b$=150×75mm^2 which cracked at an age of 18 days on average as shown in Table 6.2 and 6.3 also see Figure 6.11 which illustrates the strain measurement taken in the course of the ring test.

The circular thick ring specimens with a=125mm cracked at about an age of 21.5 days. For elliptical ring specimens, with the increase of the geometrical factor a/b, i.e. minor semi-axis b decreased from 125, 100, 75 to 60mm, average cracking ages are around 20.5, 21.5, 18, and 20 days, respectively, as observed from experiment. It seems that the influence of elliptical shape on shortening cracking age in thick elliptical rings is not as significant when compared with the thin elliptical ones as well as the circular ring. Comparing cracking ages in Tables 6.2 and 6.3, it can be seen that ring specimens with a thicker concrete wall cracked on average at an age of 20 days as compared with those with a thinner wall showing crack initiation on average at an age of 13.3 days under the same exposure condition (See table 6.2 and 6.3), in this case the outer circumferential surface exposed for drying but the top and bottom sealed. This indicates however that, as the wall thickness of the ring increases, the potential for

cracking is consequently reduced owing to the fact that all specimens should have almost the same free shrinkage because of their closely identical exposed surface area-to-volume ratio (A/V).

Table 6.2—Cracking ages for thick ring specimens obtained from numerical analyses and experiment

Ring Geometry: $a \times b$ (mm×mm)	Drying condition (exposed Surface)	Crack Age (days) Experimental	Average (days)	Crack Age (days) Numerical
150×150	Outer Circumferential Surface	—	—	17
125×125	Outer Circumferential Surface	19 25	21.5	18
150×125	Outer Circumferential Surface	20 21	20.5	19
150×100	Outer Circumferential Surface	21 22	21.5	20
150×75	Outer Circumferential Surface	18 18	18	23
150×60	Outer Circumferential Surface	21 19	20	24

Table 6.3—Comparison between Cracking ages for thin and thick ring specimens obtained from numerical analyses and experiment

Ring Geometry: $a \times b$ (mm×mm)	Thin (37.5mm)			Thick (75mm)		
	Num.	Exp.		Num.	Exp.	
150 × 150	18	15	14	17	—	—
125 × 125	—	—	—	18	19	25
150 × 125	20	15	14	19	20	21
150 × 100	17	15	14	20	21	22
150 × 75	11	10	10	23	18	18
150 × 60	12	11	15	24	21	19

Furthermore, thicker specimens are less sensitive to the development of a similar sized initial crack (Weiss et al, 2000), implying that the crack driving energy (i.e. the energy required for

crack growth) is lower for thicker specimens which require a higher stress to cause a crack to propagate after it initiated. This further indicates that ring wall thickness influences the behaviour of concrete under restrained condition.

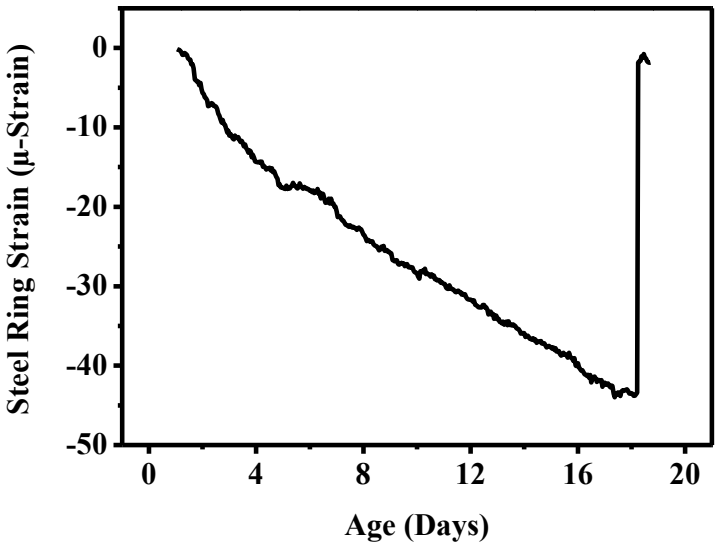

(a) $a \times b$=150×75mm^2

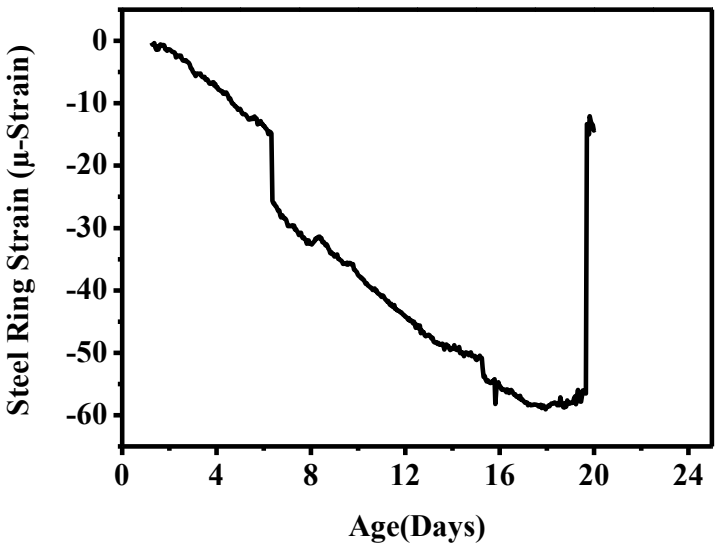

(b) $a \times b$=150×125mm^2

Figure 6.11—Steel strain measured in thick elliptical ring tests

6.7 Crack Position

For a ring test, it is desirable if the position of cracking can be predicted in advance so that the resource required for detecting crack initiation and tracking crack propagation can be minimized during experiment. For circular rings, it is impossible to predict the position of initial cracking due to the equal opportunity of cracking along their circumference. However, due to geometrical effect, stress concentration may take place at a specified position for elliptical ring specimens, which is usually assumed to be close to the two vertices on the major axis of the elliptical circumference. Experimental results of some thin ring specimens support this assumption (see Figure 6.12(a) and (b)).

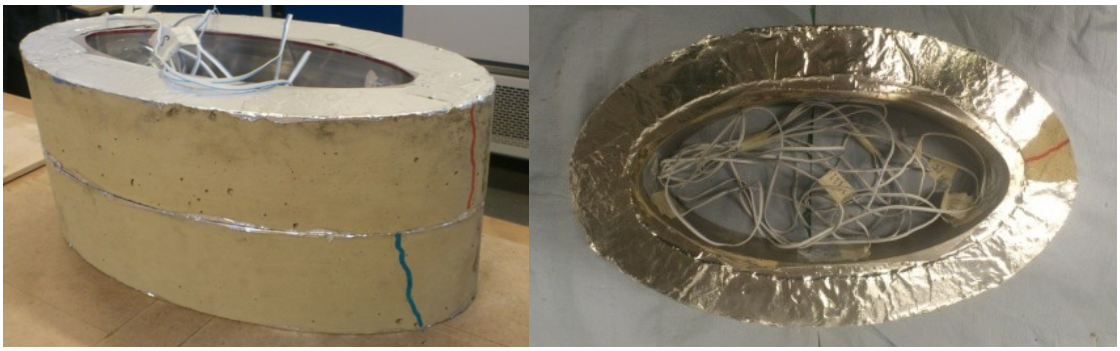

(a) $a \times b = 150 \times 60 mm^2$ (b) $a \times b = 150 \times 75 mm^2$

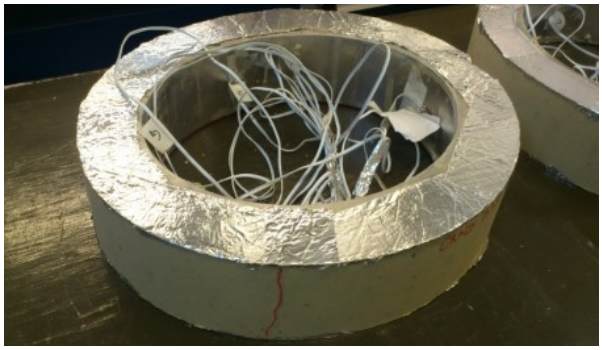

(c) $a \times b = 150 \times 125 mm^2$

Figure 6.12—Cracks in various thin ring specimens observed from experiment

In order to show crack position clearly, all cracks were highlighted by red or blue pens after testing when the pictures shown in Figure 6.12 were taken. According to experimental results, for elliptical rings with $a \times b = 150 \times 60 mm^2$ (see Figure. 6.12(a)) and $a \times b = 150 \times 75 mm^2$ (see Figure. 6.12(b)), cracks initiated close to the vertices on the major axis of the inner elliptical circumference; for rings with $a \times b = 150 \times 125 mm^2$ (see Figure 6.12(c)), crack occurred close to

the minor axis. It can be seen from the circumferential stress contour (see Figure. 6.13 (a) and (b)) that the stress concentration is more conspicuous in elliptical concrete rings with $a \times b$=150×60mm^2, and 150×75mm^2.

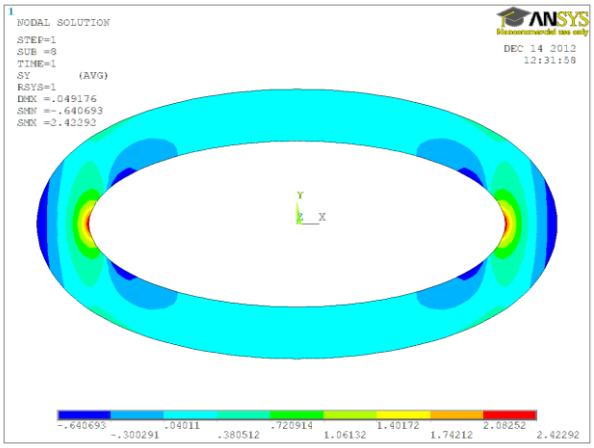

(a) $a \times b$=150×60mm^2

(12 days)

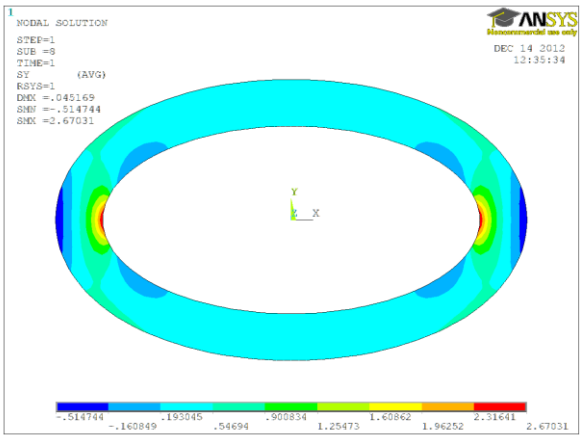

(b) $a \times b$=150×75mm^2

(11 days)

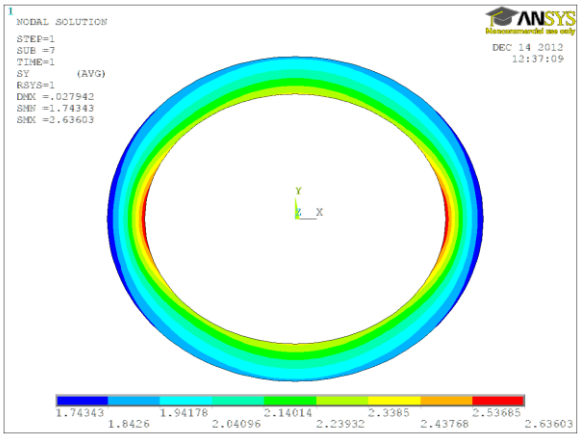

(c) $a \times b$=150×125mm^2

(20 days)

Figure 6.13—Circumferential stress contour in thin ring specimens at the age of crack initiation

The maximum stress at the two vertices on the major axis of the inner elliptical circumference is much greater than those in other zones. On the other hand, according to the circumferential stress contour shown in Figure 6.13(c), variation of tensile stress along the circumferential

direction is not as sharp and the stress concentration is not as obvious either. Similar to the circular ring specimen, the actual crack position observed from experiment may be mainly depended on defects of concrete, which results in the randomness of crack position along the ring circumference. Figure 6.14 presents crack positions in three thick ring specimens observed from experiment. It can be seen that, different from the scenario observed from thin ring specimens, some cracks (see Figure 6.14) occurred between the major and minor axes and they were not in the vertices on the major or minor axis of the outer elliptical circumference.

Conversely, as a result of the increased stress in thicker specimens which was believed to be developed in the radial direction of the ring due to the presence of moisture gradient, Weiss and Shah (2002) proposed that crack may actually initiate at the outer circumferential surface and propagate towards the inner one in thick rings which was confirmed in this study by the results of thick elliptical rings with $a \times b$= 150×75mm^2, 150×100mm^2 and 150×125mm^2 as shown in Figure 6.14. The rings were observed to crack at two opposite positions either side of the outer circumferential surface along the minor axes and/or major axes and extended slightly to the top and bottom surfaces (i.e. surfaces sealed during test) as shown in Figure 6.14(c)

(a) $a \times b$=150×60mm^2

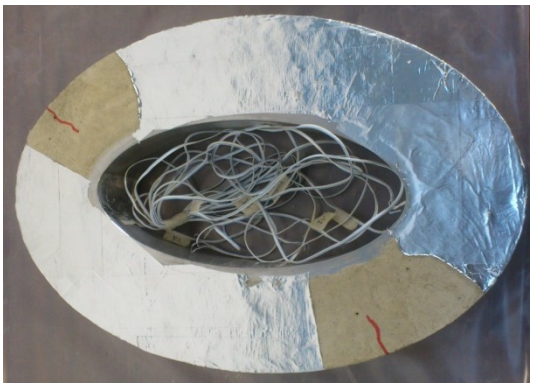

(b) $a \times b$=150×75mm^2

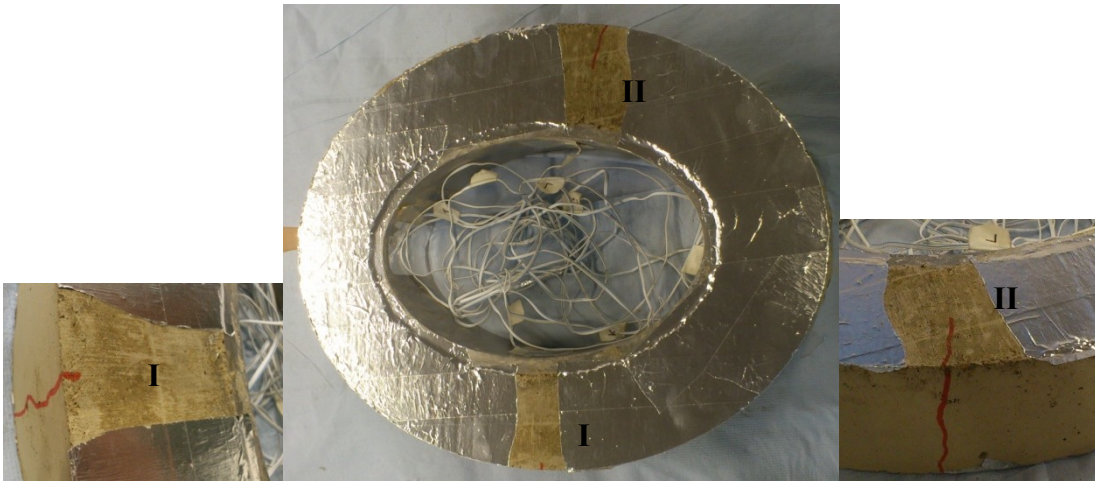

(c) $a \times b = 150 \times 100 mm^2$

Figure 6.14—Positions of cracking in thick elliptical rings

This fact can be further explained based on numerical results obtained from simulation. According to the circumferential stress contour (see Figure 6.15), the variation of circumferential stress along the radial direction is not sharp and stress concentration is not significant either. The thick elliptical geometry cannot provide higher degree of restraint to concrete surrounding it and thus enhance the circumferential tensile stress developed in thick ring specimens as it did in thin ones.

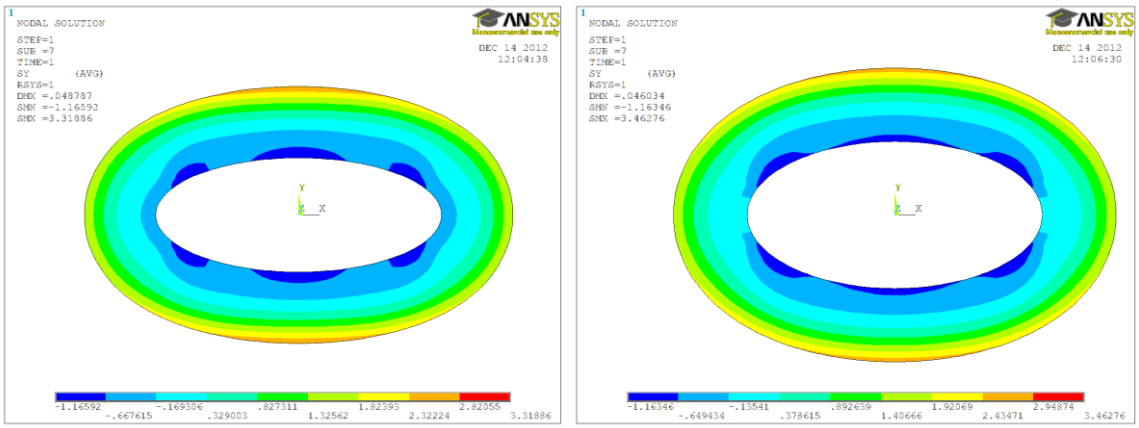

(a) $a \times b = 150 \times 60 mm^2$ (24 days)

(b) $a \times b = 150 \times 75 mm^2$ (23 days)

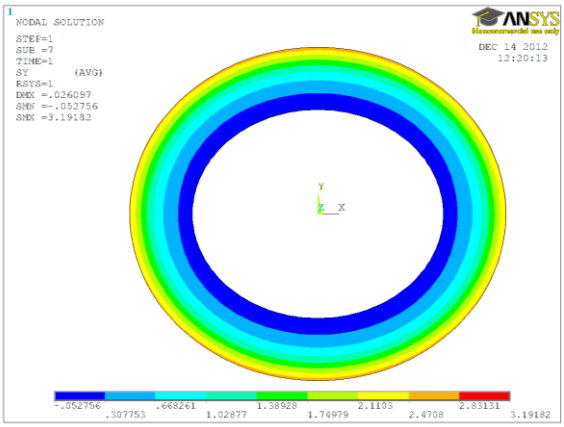

(c) $a \times b$=150×125mm^2

(19 days)

Figure 6.15—Circumferential stress contour in thick ring specimens at the age of crack initiation

6.8 Crack Initiation and Propagation

Crack propagation in restrained concrete rings is also worthy of attention. Although the cracking age can be determined through strain monitoring, it does not tell whether the sudden strain drop indicates crack initiation or crack propagation throughout the ring wall after its initiation. Therefore, in this study, visual observation of cracks was conducted alongside with strain monitoring for examining crack initiation and propagation in restrained concrete rings. After the sudden strain drop was detected by the strain data acquisition system, a ring specimen was moved out of the environmental chamber and checked carefully at the naked eyes to see whether crack appeared on the exposed ring surface in this case the outer circumferential cylindrical surface. If there was no visible crack on the exposed ring surface, the ring specimen was then put back into the chamber and the experiment was continued till at least one visible crack appeared on the exposed ring surface and extended along the height of the ring. Following this effort, it was found from this study that cracks were usually noticed by visual observation two days after being detected by strain gauges for thick ring specimens. In comparison, cracks were visually observed only one day after crack initiation as detected by strain gauges for thin ring specimens. This further ascertained that the abrupt drop in measured strain detected by strain gauges indicated that crack initiated rather than it propagating throughout the ring wall because crack can only be visually observed after propagation takes place through the wall of the ring specimen and subsequently it takes time

for crack to propagate throughout the ring wall after it initiates. In this case, it took longer for crack to propagate through the wall of the thick ring and hence longer to be visually observed after initiation detected by strain gauges and represented by sudden drop in measured strain.

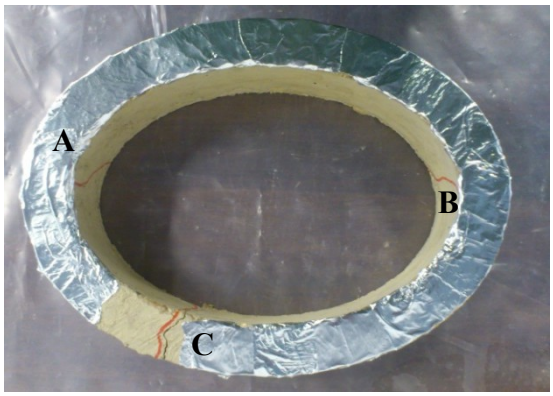

(a) Crack position

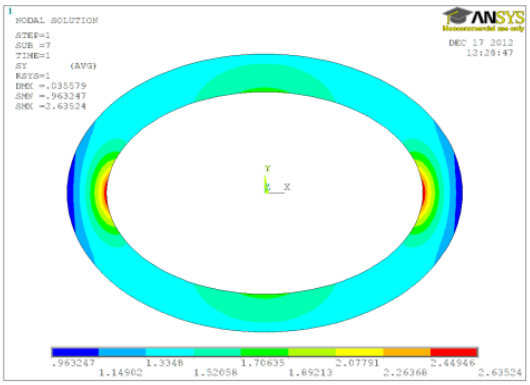

(b) Circumferential stress contour

Figure 6.16—Crack position and circumferential stress contour of a thin elliptical ring specimen with $a \times b = 150 \times 100 mm^2$

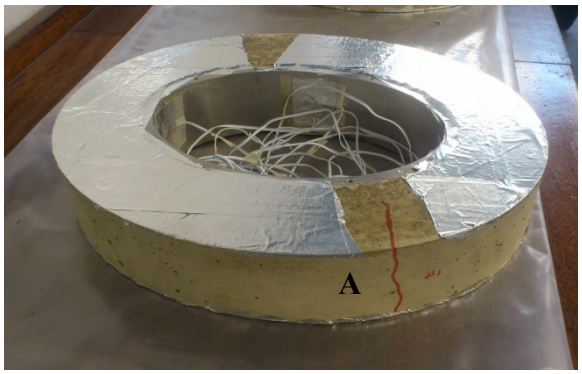

(a) Crack A

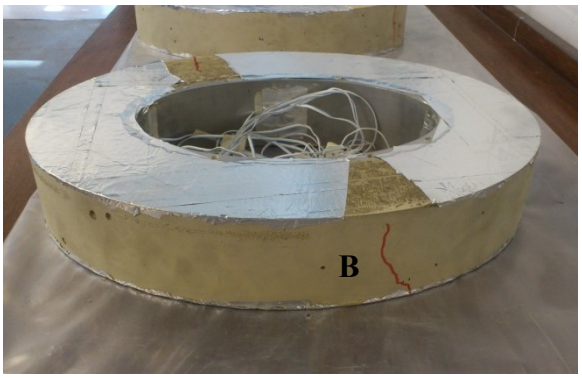

(b) Crack B

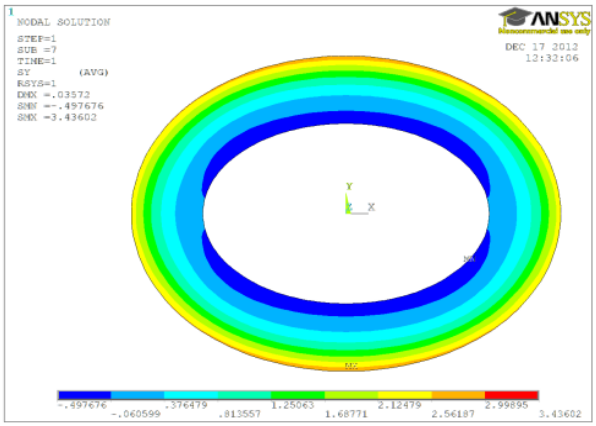

(c) Circumferential stress contour

Figure 6.17—Cracks and circumferential stress contour of a thick elliptical ring specimen with $a \times b = 150 \times 100 mm^2$

Following this effort, Figures 6.16 and 6.17 show the final crack patterns of the thin and thick ring specimens with $a \times b = 150 \times 100 mm^2$, respectively, observed from experiment. For thick rings showed in Figure 6.17(a) and (b), there are two cracks, marked as Crack A and B, respectively. These cracks are close to the vertices on the minor axis, and none of them managed to propagate throughout the ring wall from the outer circumference to the inner circumference after crack initiation. This results further strengthens findings throughout this study, in this case, the numerical results are at par with those obtained from experiment. Compared with thin rings, there is another obvious difference in crack initiation in thick rings, i.e., cracks propagated from the outer circumferential surface towards the inner circumferential surface (see Figure 6.17 (a) and (b)) while in thin rings, crack initiated at the inner circumferential surface and propagated towards the outer circumferential surface (see Figure 6.16(a)), details are expounded in chapters 4 and 5. Circumferential stress contour of a thick elliptical ring obtained from numerical analysis is presented in Figure 6.17 (c).

It can be seen that the maximum circumferential tensile stress occurred at the two vertices on the minor axis of the outer elliptical circumference, which supports the findings from experiment that crack initiated from the outer circumferential surface and propagates towards the inner surface in case of thick rings. Moreover, since the specimen loses the majority of its moisture at the outer circumferential surface, the stresses are highest at that face according to Moon and Weiss 2006. If this is case (i.e. crack extending from the outside circumferential surface to the inside), it negates the conventional stress analysis stipulating that stresses are

highest at the inner surface. Then again, in this case, experimental and numerical outcome agrees that the stresses are highest at the outer circumferential surface and hence cracks are more likely to initiate at that end.

6.9 Summary

In summary, a numerical model for thick rings was developed by introducing artificial temperature fields to represent the mechanical effect of shrinkage of concrete for the purpose of predicting stress development and cracking initiation in concrete rings subject to restrained shrinkage. In order to achieve this, different temperature fields were derived to take into account the effect of concrete wall thickness on moisture gradient, thus shrinkage strain across a ring wall. Numerical results were effectively compared with experimental ones for both thin and thick rings. Based on the efforts outlined above, the following conclusions can be drawn:

(a) Cracking age and stress development in concrete rings under restrained shrinkage can be predicted by introducing appropriate artificial temperature fields to simulate concrete shrinkage.
(b) For thick rings with wall thickness of 75 mm as recommended by AASHTO PP34-99, an artificial temperature field with a linear gradient, consisting of different temperature drops at sealed and exposed surfaces, across the concrete ring wall is more appropriate by comparing cracking ages and positions obtained from numerical analyses and experiment.
(c) On the other hand, thin rings with a wall thickness of 37.5 mm as recommended by ASTM C1581/C1581M-09a, employed a uniform temperature field with zero gradient across the concrete ring wall is accurate enough for simulating the effect of shrinkage of concrete.
(d) Thin and thick rings demonstrate different cracking behaviour when subject to restrained shrinkage. In the thick rings crack initiated from the outer circumferential surface and propagated towards the inner one. Similarly, in thick elliptical rings, the maximum circumferential tensile stress occurred in the two vertices on the minor axis of the outer elliptical circumference resulting in that crack initiated in these zones first and propagated towards the inner circumference.

(e) In comparison with thick rings, crack initiated from the inner circumferential surface and propagated towards the outer one for thin rings. Conversely, the maximum circumferential tensile stress occurred at the two vertices on the major axis in thin elliptical rings of the inner circumference, meaning that in this case, cracks initiated at these zones first and subsequently propagated towards the outer circumference, albeit with further emphasis when the geometrical factor a/b is greater than 2.

(f) Based on experimental results, the elliptical thin ring with the geometrical factor a/b between 2 to 3 is recommended to replace traditional circular rings for restrained shrinkage test, which can increase cracking sensibility and consequently shorten the restrained ring test period for faster and reliable assessment of the tendency of cracking of concrete and other cement-based materials.

(g) With the increase of concrete ring wall thickness, the restraining effect provided by the inner steel ring on surrounding concrete decreases, which marks down the advantage of using thick elliptical ring specimens to replace circular ring specimens in shortening restrained shrinkage ring test period.

CHAPTER 7: CONCLUSION AND FUTURE RESEARCH

7.1 Summary

Over the last half century, extensive investigations by researchers have been undertaken in assessing cracking potential of concrete and other cement-based materials under restrained condition including experimental, theoretical and numerical approaches. In this light, this phenomenon (i.e. cracking potential of concrete and other cement-based materials under restrained condition) have been found to depend on many factors such as, shrinkage, mechanical properties and fracture resistance of concrete as well as restrained conditions exerted on concrete making it a complex problem frustrating the engineering community. This research utilised procedures, in this case restrained shrinkage tests using circular and elliptical rings, for the investigating shrinkage cracking of concrete. Both thin and thick concrete rings harmonise well with the ring thickness recommended by ASTM C1581/C1581M-09a and AASHTO PP34-99 respectively, were tested under restrained condition till cracks initiated and propagated throughout the ring wall. In addition, both traditional circular and the newly proposed elliptical rings were tested in pairs for exploring the possibility of replacing traditional circular ring test with the new elliptical ring test as an improved method. Cracking age, cracking features and final cracking patterns of a series of elliptical and circular, thin and thick rings were examined for discovering the mechanism of using elliptical ring specimens for assessing cracking potential of concrete to replace the traditional circular ring test in order to overcome time consumption and difficulties in detecting cracking initiation and tracing crack propagation in concrete rings. Besides, various material tests were conducted to compliment the restrained shrinkage test in this research to obtain mechanical properties such as compressive strength, tensile strength and elastic modulus as well as volumetric properties such as free shrinkage of concrete at early ages for establishing a numerical model for simulating shrinkage cracking of concrete. The approach presented for the ring test in essence, can be extended for determining the effects of concrete variations and the degree of restraint on cracking tendency of concrete. Moreover, the effects of the ring geometry and concrete wall thickness on stress development in concrete rings were explored through testing a series of circular and elliptical, both thin and thick, concrete rings under restrained shrinkage. A numerical model, by introducing artificial temperature fields to represent the mechanical effect of shrinkage of concrete, was developed for predicting stress development and cracking initiation in concrete rings subjected to restrained shrinkage.

Different temperature fields were derived to take into account the effects of exposed concrete surface area-to-volume ratio and concrete wall thickness on moisture gradient, thus shrinkage strain, across a concrete ring wall. Cracking age, position and stress development were predicted for a wide range of circular and elliptical concrete rings under restrained shrinkage. The effects of ring geometry (for both circular and elliptical specimens), degree of restraint (for thin steel rings), and drying direction (for thin concrete rings) on the cracking behaviour of a concrete ring specimen under restrained condition were explored through numerical analyses. Finally a parametric study was carried out by using the numerical model to analyse several other ring specimens and their drying direction in order to further investigate the mechanism of the elliptical ring test and its influence on crack initiation and eventual propagation.

7.2 Conclusions

Based on experimental and numerical studies on exploring the mechanism of using elliptical geometry for assessing cracking potential of concrete conducted in this research, the following conclusions can be drawn:

1. The abrupt drop observed from steel strain recorded during restrained ring test indicated crack initiation rather than crack propagation through the concrete ring wall and was usually one day for thin ring specimens and two days for thick rings before visible cracking was observed.

2. By comparing experimental and numerical results, it can be seen that cracking time and crack position in the elliptical concrete rings can be predicted well by introducing the artificial temperature fields to simulate the mechanical effect of concrete shrinkage. For thin ring specimens, a uniform temperature field across the concrete wall was good enough for simulating the shrinkage of concrete. On the other hand, for thick concrete ring specimens, the temperature field with gradient, in this case linear gradient, across a concrete wall was more effective in simulating the effect across the thick concrete element under restrained condition.

3. Both experimental and numerical results showed different cracking behaviour in thin and thick concrete ring specimens under restrained condition. For thin concrete rings, crack initiated from the inner circumferential surface and propagated to the outer one with the maximum of circumferential stress occurring at the two vertices on the major axis of the inner

elliptical circumference, resulting in the crack initiation in this region for elliptical rings with the geometry factor a/b greater than 2.

4. Thin elliptical rings were observed to have cracks on the inside surface of the concrete ring along the major principal axis as would have been expected but without propagating through the concrete ring wall. Rather some other cracks initiated later at other position but do not necessarily propagate fully through the concrete ring wall. On the other hand, for thick concrete rings, crack initiated from the outer circumferential surface and propagated to the inner one with the maximum circumferential stress occurring at the two vertices on the minor axis of the outer elliptical circumference.

5. The increased stress in thicker ring specimens developed in the radial direction was attributed to the moisture distribution in the ring specimen. Besides, the effect of the geometry of ring specimens on cracking sensitivity was significant in the aforesaid test results. In the case of specimens with a thin concrete wall, the elliptical ring with a/b=2 is recommended to be used in restrained shrinkage test, which can increase cracking sensitivity so that concrete ring can crack in a shorter period. However, for thick concrete rings, the elliptical shape did not give much promise in demonstrating the advantage for shortening restrained ring test with the relative thin central restraining steel ring.

6. For thin concrete rings, the drying direction was noteworthy. Thin concrete ring specimens exposed to drying from the top and the bottom surfaces as well as outer circumferential surface in general cracked much earlier than the two other cases (i.e. top and bottom surfaces exposed for drying but outer circumferential surface sealed; and outer circumferential surface exposed for drying but the top and bottom surfaces sealed). Similarly, thin ring specimens drying from the outer circumferential surface experienced crack initiation earlier than the ring specimens exposed to drying at the top and bottom surfaces. This behaviour can be attributed to the exposed A/V of the concrete ring specimen, and so the influence of the drying path is likewise evident in the crack age when all the different ring series are employed in numerical analyses. With the increase in concrete ring wall thickness, the restraining effect provided by the inner steel ring, assuming its thickness remaining constant, on the surrounding concrete decreases, which minimises the advantage of using thick elliptical ring specimens to replace circular ones in shortening restrained shrinkage ring test period.

7. Overall, this research explores the possibility of using elliptical ring geometry to replace the traditional circular one, for faster and more reliable assessment of cracking tendency of

concrete and other cement-based materials under restrained condition. With appropriate geometry, the elliptical shape can enable concrete to crack earlier with cracking position at a certain region which could be predicted by the numerical model established in this study considerably well. The findings of this research also provides guidance in choosing appropriate concrete and steel ring geometries for simulating restrained concrete in the field, so that the elliptical ring test proposed in this research can be used to determine the behaviour in variations of the concrete properties as it relates to cracking time when restrained, and subsequently aiding in the selection of concrete mixtures that are less likely to crack.

7.3 Future Research and Recommendation

The findings of this research will pave way to provide guidance in choosing appropriate ring geometry for simulating restrained concrete in the field. In this case, the elliptical ring with a/b=2 (i.e. a=150 mm, b=75 mm, concrete thickness=37.5mm) has already been recommended to be used in restrained shrinkage test. This geometry specification selected can increase cracking sensitivity so that concrete ring can crack in a shorter period, in addition it can be used for the following;

(1) With further research, the fictitious temperature field can be used to simulate the shrinkage of concrete and this can be applied to different structures.

(2) The elliptical ring test can be explored further for determining the behaviour in variations of concrete properties as it relates to cracking time when restrained. It can subsequently be extended for aiding in the selection of concrete mixtures that are less likely to crack before they are used for construction projects.

(3) Future research is recommended to investigate thicker restraining thick steel rings to further assess the impact the thicker elliptical steel rings will have on the cracking performance of the concrete.

(4) Extended research is recommended to focus on predicting the performance of concrete repairs materials using the elliptical ring test.

(5) Likewise, additional experimental tests can be performed to investigate the effect of drying direction on the cracking behaviour when certain surfaces of the rings (thin and thick) are sealed and others exposed.

Bibliography

AASHTO PP34-98, 1998. *Standard Practice for Estimating the Crack Tendency of Concrete*. AASHTO Provisional Standards.

Altoubat, S.A., and Lange, D., 2002. Grip-Specimen Interaction in Uniaxial Restained Test., 2002. ACI – Special Publication.

ASTM C 157-04, 2003. *Standard Test Method for Length Change of Hardened Hydraulic-Cement, Mortar, and Concrete*. West Conshohocken, PA: American Society for Testing and Materials.

ASTM C 1581-04, 2004. *Standard Test Method for Determining Age at Cracking and Induced Tensile Stress Characteristics of Mortar and Concrete under Restrained*. West Conshohocken, PA: ASTM International.

Attiogbe, E. K. SHT., Milterberger, M. A., 2003. Cracking potential of concrete under restrained shrinkage." Proceedings, advances in cement and concrete: Volume Changes, Cracking, and Durability. Copper Mountain, Colorado, 2003. Engineering Conferences International.

Attiogbe, E. K., Weiss, W. J., and See, H. T., 2004. A Look at the Stress Rate Versus Time of Cracking Relationship Observed in The Restrained Ring Test. *Advances in Concrete Through Science and Engineering*, p.14.

Babaei, K. and Purvis, R. L, 1996. *Prevention of Cracks in Concrete Bridge Decks*. Summary Report– Research Project. Falls Church, VA: Wilbur Smith Associates.

Bazant Z P, Planas J, 1997. *Fracture and size effect in concrete and other quasibrittle materials*. Boca, Baton: CRC Press.

Bazant Z. P and Planas J, 1998. *Fracture and Size Effect in Concrete and Other Quasi-Brittle Materials*. Boca Raton: CRC Press.

Bazant ZP, Kazemi MT, 1990. Determination of fracture energy, process zone length, and brittleness number from size effect with application to rock and concrete. *International Journal of Fracture*, 44(2), p.111–31.

Bazant ZP, Oh BH, 1983. Crack band theory for fracture concrete. *Materials and Structures (RELIM)*, 16(93), p.155–177.

Bazant ZP, 1984. Size effect in blunt fracture: concrete, rock, metal. *Journal of Engineering Mechanics ASCE*, 110, p.518–35.

Bazant, Z. P., and Chern, J, 1985. Concrete at Variable Humidity: Constitutive Law and Mechanisms. *Materials and Structures, RILEM*, 18, pp.1-20.

Bentur A and Kovler K, 2003. Evaluation of early age cracking characteristics in cementitious systems. *Materials and Structures*, Vol 36(1359-5997/03 © RILEM), pp.183-90.

Berke N. S, Dallaire, M. C., Hicks, M. C., and Kerkar A, 1997. New Developments in Shrinkage-Reducing Admixtures", Superplasticizers and Other Chemical Admixtures in Concrete. Rome, Italy, 1997. Proceedings Fifth CANMET/ACI International Conference.

Bloom, R and Bentur, A, 1995. Free and Restrained Shrinkage for Normal and High Strength Concretes. *ACI Materials Journal*, 92(2), pp.211-17.

Branch, J., Rawling, A., Hannant, D. J, 2002. The effects of fibres on the plastic shrinkage cracking of high strength concrete. *Materials and Structures*, 35(4), pp.189-94.

British Standards Institute, -. *BS EN 196-6: Methods of testing cement –Part 6: determination of fineness*. 2010: BSI.

British Standards Institute, -. *BS EN 197-1:2000 cement – Part 1: composition,specifications and conformity criteria for common cements*. 2000: BSI.

British Standards Institute, n.d. *BS EN 12390-2:2009 testing hardened concrete Part 2: making and curing specimens for strength tests*. 2009: BSI.

British Standards Institute, n.d. *BS EN 12390-3:2009 testing hardened concrete Part 3: compressive strength of test specimens*. 2009: BSI.

British Standards Institute, n.d. *BS EN 12390-6: 2009: testing hardened concrete Part 6: tensile splitting strength of test specimens*. 2009: BSI.

British Standards Institute, n.d. *BS EN 12620:2002+A1:2008 aggregates for concrete*. 2002 : BSI.

British Standards Institute, n.d. *BS EN 196-1: 2005: methods of testing cement – Part 1: determination of strength*. 2005: BSI.

Brooks, J. J. and Neville, A., 1992. Creep and Shrinkage of Concrete as Affected by Admixtures and Cement Replacement Materials. *ACI SP*, 135, pp.19-36.

Burrows, R. W, 1998. The Visible and Invisible Cracking of Concrete. *ACI Monograph*, 11, p.78.

Byfors, J., 1980. *Plain Concrete at Early Ages*. Swedish Cement and Concrete Research Institute.

Carlson R. W and Reading T.J, 1988. Model Of Studying Shrinkage Cracking in Concrete Building Walls. *ACI Structures Journal*, 85(4), pp.395-404.

CCAA, 2005. *Plastic Shrinkage Cracking*. Cement Concrete and Aggregate Australia.

Chariton, T. and Weiss, W. J., 2002. Using Acoustic Emission to Monitor Damage Development in Mortars Restrained from Volumetric Changes. *ACI SP*, 206, pp.205-18.

D'Ambrosia M.D, Lange D.A, and Grasley Z.C, 2004. Measurement and Modeling of Concrete Tensile Creep and Shrinkage at Early Age. *ACI Materials*, 220, pp.99-112.

Folliard, K. J. and Berke, N. S., 1997. Properties of High-Performance Concrete Containing Shrinkage-reducing Admixture. *Cement and Concrete Research*, 27(9), pp.pp. 1357-1364.

Folliard. K, Smith.C, Sellers. G, Brown. M, Breen. E.J, 2004. *Evaluation of Alternative Materials to Control Drying-Shrinkage Cracking in Concrete Bridge Decks*. Red River, Austin: Center for Transportation Research The University of Texas.

Grysbowski, M., 1989. *Determination of Crack Arresting Properties of Fiber Reinforced Cementitious Composites*. Stockholm, Sweden: Ph.D. Thesis, Royal Institute of.

Grzybowski.M and Shah S.P, 1990. Shrinkage Cracking of Fiber Reinforced Concrete. *ACI Materials Journal*, 87(2), pp.138-48.

He. Z.J. Li. M. Z. Chen. W. Q. Liang, 2006. Properties of shrinkage-reducing admixture-modified pastes and mortar. *Materials and Structures*, 39, pp.445-53.

Hedlund, H., 1996. *Stresses in High Performance Concrete Due to Temperature and Moisture Variations at Early Ages*. Luleå, Sweden: Luleå University of Technology.

Hewlett, P.C., 1998. *Lea's Chemistry of Cement and Concrete*. 4th ed. Oxford, UK: Elsevier Ltd.

Hillerborg A, Modeer M, Petersson P-E., 1976. Analysis of crack formation and crack growth in concrete by means of fracture mechanics and finite elements. *Cement and Concrete Composites*, 6, p.773–82.

Holt, E., 2001. *Early Age Autogenous Shrinkage of Concrete*. Doctoral dissertation ed. Seatle: University of Washington.

Holt, Erika E., 2001. *Early age autogenous shrinkage of concrete*. Technical Research Centre of Finland: VVT Publications 446.

Holt, E.E., 2001. *Early age autogenous shrinkage of concrete*. Technical research centre Finland: VVT PUBLICATIONS.

Hossain, A. B., Pease, B., and Weiss, J., 2003. Quantifying Early-Age Stress Development and Cracking in Low Water-to-Cement Concrete: Restrained-Ring Test with Acoustic Emission. *Transportation Research Record*, 1834, pp.24-32.

Hossain, A. B., 2003. *Assessing residual stress development and stress relaxation in restrained concrete ring specimens*. Ph.D Disseratation. Purdue University.

Hossain, A.B., Weiss, J., 2002. Assessing Residual Stress Development and Stress Relaxation in Restrained Concrete Ring Specimens. *Cement and Concrete Composites*.

Janz, M., 2000. *Moisture Transport and Fixation in Porous Materials at High Moisture Levels*. Lund: Lund Institute of Technology.

Japan, C.I., 1999. *Autogenous Shrinkage of Concrete*. Committee Report. London: Japanese Concrete Institute.

Jenq YS, Shah SP., 1985. Two parameter fracture model for concrete. *Journal of Engineering Mechanics ASCE*, 111(10), p.1227–41.

Jenq, Y. S., and Shah, S. P., 1991. Features of Mechanics of Quasi-Brittle Crack Propagation in Concrete. *International Journal of Fracture*, 51, pp.103-20.

Justnes, H., Van Gemert, A., Verboven, F., and Sellevold, E.J., 1996. Total and External Chemical Shrinkage of Low W/C Ratio Cement Pastes. *Advances in Cement Research, Vol. 8, No. 31, July 1996, pp. 121 - 126*, 8(21), pp.121-26.

Kaplan, M. F., 1961. Crack Propagation and the Fracture of Concrete. *Journal of the American Concrete Institute*, 58(5), pp.591-610.

Karaguler, M. E. and Shah, S. P., 1990. Test Method to Evaluate Shrinkage Cracking in Concrete., 1990. Proceedings of the First Materials Engineering Conference.

Karihaloo, B. L., and Nallthambi, P., 1981. An Improved Effective Crack Model for the Determination of Fracture Toughness of Concrete. *Cement and Concrete Research*, 19, pp.603-10.

Karson I. D. & Jirsa J. O, 1969. Behaviour of concrete under compressive loadings. *Journal Struture Division, ASCE*, 95, pp.2543-63.

Kesler CE, Naus DJ, Lott LL., 1972. Fracture mechanics-its applicability to concrete. In: Proceedings of the int conf on the mechanical behavior of materials. *Soc Material Science*, 4, p.113–24.

Kim B and Weiss W.J, 2003. Using Acoustic Emission to Quantify Damage in Restrained Fiber Reinforced Cement Mortars. *Cement and Concrete Research*, 33(2), pp.207-14.

Koenders, E.A.B., 1997. *Simulation of Volume Changes in Hardened Cement-Based Materials*. Delft University Press.

Kovler K and Zhutovsky S, 2006. Overview and future trends of shrinkage research. *Materials and Structures*, 39, p.827–847.

Kovler K, Sikuler J, Bentur A, 1993. “Restrained Shrinkage Tests of Fiber-Reinforced Concrete Ring Specimens: Effects of Core Thermal Expansion.”. *Materials and Structures*, pp.26(4), 231-237.

Kovler K. and Bentur A, 1997. Shrinkage of Early Age Steel Fiber Reinforced Concrete. *Archives of Civil Engineering*, 43(4), pp.431-39.

Kovler, K., 1994. Testing System for Determining the Mechanical Behavior of Early Age Concrete Under Restrained and Free Uniaxial Shrinkage. *Materials and Structures RELIM*, 27(170), pp.324-30.

Kraai, P.P., 1985. Proposed Test to Determine the Cracking Potential Due to Drying Shrinkage of Concrete. *Concrete Construction*, 30(9), pp.775-78.

Krenchel, H., and Shah, S. P., 1987. Restrained shrinkage tests with PP-fiber reinforced. *Fiber reinforced concrete properties and applications*, pp.SP- 105.

Li ZJ, Qi M, Li ZL, Ma BG, 1999. Crack width of high-performance concrete due to restrained shrinkage. *Journal of Materials in Civil Engineering*, 11(3), pp.214-23.

Lim Y.M, Wu H.C and Li V.C, 1999. Development of Flexural Composite Properties and Dry Shrinkage Behavior of High-Performance Fiber Reinforced Cementitious Composites at Early-Age. *Journals of Materials*, 96(1), pp.20-26.

Loser, R., Leemann, A, 2008. Shrinkage and Restrained Shrinkage Cracking of Self-Compacting Concrete Compared to Conventionally Vibrated Concrete. *Materials and Structures*.

Lura P, Jensen O.M, Ye G, and Tanaka K, 2005. Micro-crack detection in high-performance cementitious Materials, 2005. 4th Seminar on Self-Desiccation and its importance on concrete technology.

Lyman, G. C., 1934. *Growth and Movement in Portland Cement Concrete*. London, U. K: Oxford, University Press.

M.Briffaut, F. Benboudjema, J.M. Torrenti, G. Nahas, 2011. A thermal active restrained shrinkage ring test to study the early age concrete behaviour of massive structures. *Cement and Concrete Research*, 41, pp.56-63.

Ma Baoguo, Wang Xingang, Liang Wenquan, Li Xiangguo, He Zhen, 2007. Study on early-age cracking of cement-based materials with superplasticizers. *Construction and Building Materials*, 21, pp.2017-22.

Malhotra, V.M, and Zoldners, N.G, 1967. Comparison of Ring-Tensile Strength of Concrete with Compressive, Flexural, and Splitting Tensile Strengths. *Journal of Materials*, pp.160-99.

Mehta, P.K. and Monteiro, J.M., 1993. *Concrete: Structure, Properties and Materials*. 2nd ed. Prentice Hall, Inc.

Mehta, P.K, 1994. Concrete technology at the crossroads-Problems and opportunities. *American Concrete Institute*, SP-144, pp.1-30.

Mindess, S. and Young, J.F., 1981. *Concrete*. Prentice-Hall.

Modwer, M and Peterson, P. E,Hillerborg, A., 1976. Analysis of Crack Formation and Crack Growth in Concrete by Means of Fracture Mechanics and Finite Elements. *Cement and Concrete Research*, 6, pp.773-82.

Mokarem, D.W., Weyers, R.E., Lane, D.S., 2005. Development of a shrinkage performance specifications and prediction model analysis for supplemental cementitious material concrete mixtures. *Cement and Concrete Research*, 35(5), pp.918-25.

Moon J.H, 2006. *Shrinkage, Residual Stress and Cracking in Heterogenous Materials*. PhD Thesis. West Lafayette, Indiana: Purdue University.

Moon, J. H., Pease, B., Weiss, J., 2006b. Quantifying the influence of specimen geometry on the results of the restrained ring test. *Journal ASTM International*, 3(8), pp.1-14.

Moon, J.H., Weiss, J., 2006a. Estimating residual stress in the restrained ring test under circumferential drying. *Cement and Concrete Composites*, 28(5), pp.486-96.

Neville, A. M., 1996. *Properties of Concrete*. 4th ed. Essex, England: ADDISON Wesley Longman.

Neville, A.M., Dilger, W. H., and brooks, J. J., 1983. *Creep of plain and Structural Concrete*. London England: Construction Press.

Neville, A.M., 1978. *Properties of Concrete*. 2nd ed. London: Pitman Publishing.

Ödman, S. T. A., 1968. Effects of Variations in Volume, Surface Area Exposed to Drying, and Composition of Concrete on Shrinkage. *RILEM/CEMBUREAU International Colloquium on the Shrinkage of Hydraulic Concretes*.

Paillere A.M., Buil, M., Serrano, J.J., 1989. Effect of Fiber Addition on the Autogeneous Shrinkage of Silica Fume Concrete. *ACI Materials Journal*, 86(2), pp.139-44.

Passuello, A., Moriconi, G., Shah, S. P, 2009. Cracking behavior of concrete with shrinkage reducing admixtures and PVA fibers. *Cement and Concrete Composite*, 31(10), pp.699-704.

Peter H. Emmons and Douglas J. Sordyl, 2006. *The State of the Concrete repair industry, and a Vision for its future*. Michigan: ICRI.

Powers, T. C., 1959. Causes and Control of Volume Change. *Journal of the PCA Research and Development Laboratories*, 1(1), pp.29-39.

RILEM, TC89-FMT, 1991. Fracture mechanics of concrete test methods. *Materials and Journals*, 23, p.457–60.

RILEM, c., 1990. *Determination of the fracture parameters (KICS and CTODC) of plain concrete using three-point bend tests on notched beams*. Materials and Structures.

Roesler J, Paulino G.H, Park.K, Gaedicke. C, 2007. Concrete fracture prediction using bilinear softening. *Cement and Concrete Composites*, p.doi:10.1016/j.cemconcomp.2006.12.002.

Ropke, J.C., 1982. *Concrete problems: causes, and cures*. Illustrated ed. Michigan: McGraw-Hill Inc.

S.P. Shah, C. Ouyang, S. Marikunte, W. Yang, E. Becq-Giraudon, 1998. A method to predict shrinkage cracking of concrete. *ACI Materials* , 95, pp.339-46.

Saragaputi M., Shah S. P., and Vinson K. D, 1993. Shrinkage Cracking and Durability Characteristics of Cellulose Fiber Reinforced Concrete. *ACI Materials*, 90(4), pp.309-18.

See H. T, Attiogbe E. K and Miltenberger M. A., 2003. Shrinkage Cracking Characteristics of Concrete Using Ring Specimens. *ACI Materials Journal*, 100(3), pp.239-45.

Shah S. P. Karaguler M. E and Sarigaphuti M., 1992. Effects of Shrinkagereducing-reducing Admixtures on Restrained Shrinkage Cracking of Concrete. *ACI Materials*, 89(3), pp.291-95.

Shah S.P, Swartz S.E and Ouyang C, 1995. *Fracture Mechanics of Concrete:Application of Fracture Mechanics to Concrete Rock, and Other Quasi-Brittle Materials*. New York: John Wiley and Sons Inc.

Shah, S. P., Weiss, W. J., Yang, W., 1998a. Shrinkage Cracking – Can It Be Prevented. *Concrete International*, 20(4), pp.51-55.

Shoya, M., and Sugita M., 1976. *Application of Special Admixture to Reduce Shrinkage Cracking of Air Dried Concrete*. Hachinohe,Japan: Hachinohe Institute of Technology.

Shoya, M., 1979. II-5 *Drying Shrinkage and Moisture Loss of Super Plasticizer Admixed Concrete of Low Water Cement Ratio*. Transactions of the Japan Concrete Institute.

Simo J, Oliver J, Armero F., 1993. An analysis of strong discontinuities induced by strain softening in rate-independent inelastic solids. *Computer Mechanics*, 12, p.277–96.

Swamy, R. N., and Stavarides, H., 1979. Influence of Fiber Reinforcement on Restrained Shrinkage Cracking. *ACI Materials*, 76(3), pp.443-60.

Tada H., Paris P. C., and Irwin G. R, 1985. *The Stress Analysis of Cracks Handbook*. 2nd ed. St. Louis, USA: Paris Productions.

Tang T, Ouyang C, Shah SP, 1996. A simple method for determining material fracture parameters from peak loads. *ACI Materials*, 93, p.147–57.

Tarr, Scott M., and Farny, James A., 2008. *Concrete Floors on Ground*. 4th ed. Skokie, Illinois, USA: Portland Cement Association.

Tia. M, Subramanian. R, Brown. D, Broward. C, 2005. *Evaluation of Shrinkage Cracking Potential of Concrete used in Bridge decks in Florida*. Gainesville, Florida: Department of Civil Engineering University of Florida.

Toma, G., Pigeon, M., Marchand, J., Bissonnette, Bercelo, L., 1999. Early-Age Autogenous Restrained Shrinkage: Stress Build Up and Relaxation," Self-Desiccation and Its Importance in Concrete Technology. pp.61-72.

Tongaroonsri, S., Tangtermsirikul, S, 2009. Effect of mineral admixtures and curing periods on shrinkage and cracking age under restrained condition. *Constructions and Building Materials*, 23(2), pp.1050-56.

Tritsch.N, Darwin.D and Browning.J, 2005. *Evaluating shrinkage and cracking behavior of concrete using restrained ring and free shrinkage tests*. Lawrence kansas: Structural Engineering and Engineering Materials The University of Kansas center for research, Inc.

Troxell. G, Harmer. D, Kelly. J, 1996. *Composition and Properties of Concrete*. 2nd ed. New York: McGraw-Hill.

Turcry P, Loukili A, Haidar K, Pijaudier C. G., Belarbi A., 2006. Cracking tendency of self-compacting concrete subjected to restrained shrinkage: Experimental study and modeling. *Journal of Materials in Civil Engineering*, 18(1), pp.46-54.

Van Breugel, K., and Lokhorst, S. J., 2001. Stress-Based Crack Criterion as a Basis for the Prevention of Through Cracks in Concrete Structures at Early-Ages., 2001. RILEM International Conference on Early-Age Cracking in Cementitous Systems (EAC'01).

Victor E. Saouma, 2000. *Fracture Mechanics*. Colorado: University of Colorado.

Weigrink K, Marinkunte S, and Shah S.P, 1996. Shrinkage Cracking of High Strength Concrete. *ACI Materials*, 93(5), pp.409-15.

Weiss W. J and Shah S. P., 2002. Restrained Shrinkage Cracking : The Role of Shrinkage Reducing Admixtures and Specimen Geometry. *Materials and Structures*, 34(246), pp.85-91.

Weiss, W. J., Yang, W., and Shah, S. P., 1998. Shrinkage Cracking of Restrained Concrete Slabs. *ASCE Journal of Engineering Mechanics*, 124(7), pp.765-774.

Weiss, W. J., Yang, W., Shah, S.P., 2000. Influence of specimen size/geometry on shrinkage cracking of rings. *ASCE Journal of Engineering and Mechanics*, 126(1), pp.93-101.

Weiss, W. J., 1999. *Prediction of early-age shrinkage cracking in concrete*. Ph.D Disseratation. Northwestern University.

Weiss, W.J., and Furgeson, S., 2001. Restrained Shrinkage Testing: The Impact of Specimen Geometry on Quality Control Testing for Material Performance Assessment," Concreep 6: Creep, Shrinkage, And Curability Mechanic of Concrete and Other Quasi-Brittle Materials, ed.. *Elsevier*, pp.645-51.

Xianyu Jin, Nanguo Jin, and Yanguo Zheng, 2006. Fractural Modelling of Early-Age Concrete Beams Under Three-Point Loading. Montreal, Canada, 2006. Joint international conference on computing and decision making in civil and building engineering.

Xu S, Reinhardt HW., 1999. Determination of double-K criterion for crack propagation in quasi-brittle fracture, Part III: Compact tension specimens and wedge splitting specimens. *International Journal of Fracture*, 98(2), p.179–93.

Z. He, Z.J. Li, M.Z. Chen, W.Q. Liang, 2006. Properties of shrinkage-reduced admixture-modified pastes and mortar. *RILEM Materials and Structures*, 39, pp.445-53.

Z. He, Z.J. Li, 2005. Influence of Alkali on restrained shrinkage behavior of cement-based materials. *Cement and Concrete Research*, 35, pp.457-63.

Zhao Yanhua, Xu Shilantg, Wu Zhimin, 2007. Variation of fracture energy dissipation along evolving fracture process zones in concrete. *ASCE, Journal of Materials in Civil Engineering*, 19(8), pp.625-33.

Zhao, Yanhua, Li, Zongjin and Xu, Shilang, 2005. Brittle behaviour of high strength concrete. In *ICF XI - 11th International Conference on Fracture*. Turin, Italy, 2005. International Conference on Fracture.

Zhen He, Xiangming Zhou, Zongjin Li, 2004. New experimental method for studying early-age cracking of cement-based materials. *ACI materials*, 101(1), pp.50-56.

Zhen He, Zongjin Li, 2005. Influence of alkali on restrained shrinkage behaviour of cement-based materials. *Cement and Concrete Research*, 35, pp.457-63.

Appendix

Publications

Journal:

- Xiangming Zhou, Joel R Slater, Stuart E Wavell, and Olayinka Oladiran, "Effects of PFA and GGBS on Early-Ages Engineering Properties of Portland Cement Systems," Journal of Advanced Concrete Technology, 10(2), 2012, pp 74-85.
- Xiangming Zhou, Seyed Hamidreza Ghaffar, Wei Dong, Olayinka Oladiran and Mizi Fan, "Fracture and impact properties of short discrete jute fibre-reinforced cementitious composites," Materials and Design 49 (2013) 35–47.
- Xiangming Zhou, Wei Dong, and Olayinka Oladiran, "Assessment of Restrained Shrinkage Cracking of Concrete Using Elliptical Ring Specimens: Experimental and Numerical," ASCE Journals. Accepted December 2013.
- Wei Dong, Xiangming Zhou, Olayinka Oladiran and Zhimin Wu, "Assessment of the Effect of Specimen Size on Shrinkage Cracking of Concrete by Elliptical Rings: Thin vs. Thick," Cement and Concrete Research. Under review.

Conferences:

- Olayinka Oladiran, "Preliminary Investigation on Restrained Shrinkage Cracking of Cracking with Circular and Elliptical Ring Specimens" (Res Con 2011)
- Olayinka Oladiran, "Study on Shrinkage Cracking of Early-age Concrete Using Elliptical Rings" (Res Con 2012)
- Xiangming Zhou, Wei Dong, and Olayinka Oladiran, "A Numerical Approach for Predicting Shrinkage Cracking Age of Concrete in Elliptical Ring Tests," Proceedings of 3rd Interntional Conference on the Durability of Concrete Structures (ICDCS2012), 17-19 September 2012, Belfast, Northern Ireland.
- Xiangming Zhou, and Olayinka Oladiran, "Assessment of Restrained Shrinkage Cracking of Concrete with Elliptical Ring Specimens – Preliminary Results," RILEM International Conference on Advances in Construction Materials through Science and Engineering, 5-7 September 2011, Hong Kong.